STRATIGRAPHIC FRAMEWORK AND PROVENANCE OF THE LOWER BELT (NEWLAND FORMATION), BELT SUPERGROUP, HELENA EMBAYMENT, CENTRAL MONTANA

by

Colter James Anderson

A thesis submitted in partial fulfillment
of the requirements for the degree

of

Master of Science

in

Earth Sciences

MONTANA STATE UNIVERSITY

Bozeman, Montana

November 2017

©COPYRIGHT

by

Colter James Anderson

2017

All Rights Reserved

ACKNOWLEDGEMENTS

This thesis would not have been possible without the love and support of my Family! A special thanks to my wife, and her constant encouragement throughout this project. I'm forever grateful to her.

A special thanks to Don Winston for welcoming my classmates and I into his home and leading a Belt Basin field trip. I am thankful for my entire committee Dave Lageson, Dave Bowen, and Dave Mogk for help and encouragement through this project. I also want to thank Nicholas Fox, Thomas Poush and Kristopher Patane, Laura Kellerman, Dr. Paul Mueller of the University of Florida, and my fellow classmates for their help in the field, lab, and encouragement through this endeavor.

TABLE OF CONTENTS

1. INTRODUCTION 1

Significance 1
General Geology 2
Methods 7

2. TECTONIC FRAMEWORK 9

Phanerozoic Tectonics 14

3. SEDIMENTOLOGY AND STRATIGRAPHY 18

Introduction 18
Methods 18
Helena Embayment Stratigraphy 19
Neihart Quartzite 19
Chamberlain Formation. 20
Newland Formation 20
Lithofacies 20
Lithofacies (Gms): Intraclast Conglomerate 27
Interpretation 27
Lithofacies (Sm): Massive Sandstone 28
Interpretation 28
Lithofacies (St): Trough Cross Stratified Sandstone 29
Interpretation 29
Lithofacies (Sr): Ripple Cross Laminated Sandstone. 30
Interpretation 31
Lithofacies (Fls): Lenticular Laminated Sandy Siltstone 32
Interpretation 32
Lithofacies (Se): Erosional scours 34

TABLE OF CONTENTS CONTINUED

Interpretation....35
Lithofacies (Fl): Plane Bedded Siltstone....35
Interpretation....35
Lithofacies (Fp): Plane Laminated Mudstone....35
Interpretation....36
Lithofacies (Sgc): Graded Calcarious Sandstone....37
Interpritation....37
Lithofacies (Src): Ripple Laminated Sandstone....37
Interpretation....37
Lithofacies (Fsc): Fissile Black Shale....38
Interpritation....38
Lithofacies (Lm): Lime Mudstone....39
Interpretation....40
Lithofacies (Fcs): Calcareous Shale....42
Interpretation....43
Lithofacies (Ccl): Cross Laminated Silty Microspar....44
Interpretation....44
Lithofacies (Ccn): Microspar with Chert Nodules....45
Interpretation....46
Lithofacies (Ibs): Interbedded Microspar and Calcareous Shale....46
Interpretation....47
Lithofacies (Fsn): Fissile Shale with Microspar Nodules....47
Interpretation....47
Lithofacies (Cpl): Plane Parallel Laminated Microspar....47
Interpretation....48
Diagenesis....49

TABLE OF CONTENTS CONTINUED

4. FACIES ASSOCIATION, DEPOSITIONAL SYSTEMS, AND STRATIGRAPHIC CORRELATIONS 53

Lithofacies Association 53
FA1: 53
FA2: 54
FA 3: 55
FA 4: 55
FA 5: 56
FA 6: 59
FA 7: 59
Stratigraphic Correlations 61
North –South Interpretation 61
East-West Interpretation 64
Discussion 67
Conclusion 68

5. GEOCHRONOLOGY AND GEOCHEMISTRY 70

Introduction 70
X-RAY Fluorescence (XRF) 72
Methods 72
Harker Diagrams 73
Rare Earth Elements 77
Results 77
Detrital Zircon Geochronology 79
Methods 79
Results 81
Discussion 83
Conclusion 89

TABLE OF CONTENTS CONTINUED

6. MINERALOGY 91

Introduction 91
Bulk Mineralogy 92
Methods 92
Results 95
Clay Mineralogy 97
Illite/Smectite 97
Chlorite and Corrensite 98
Methods 98
Results 105
Conclusion 108

7. SUMMERY AND CONCLUSIONS 110

Future Work 111

REFEENCES CITED 112

APPENDICES 121

APPENDIX A: Graphic Logs 122
APPENDIX B: Bulk Mineralogy 124
APPENDIX C: Clay Mineralogy 130

LIST OF TABLES

Table Page

1. Lithofacies descriptions....22
2. Faceis association....60
3. Principle zircon ages. 90
4. Stratigraphic and geographic locations of samples 93
5. Primary mineralalogy....96
6. Position of peak reflections for estimating percent illite/smectite f....105
7. Clay Mineralogy from the east fork of Swimming Woman Canyon 107
8. Percent illite found in each sample....107
9. Clay Identification of 1S-SW....132
10. Clay identification of Ch-6-29 from checkerboard outcrop 133
11. Clay identification of Deep Creek Unit 1....134
12. Clay identification of East Fork Swimming Woman Creek....135
13. Clay identification of Miller Gulch 136
14. Clay identification of West Fork Swimming Woman Canyon....137
15. Clay Identification of Belt Creek....138
16. Clay identification for Deep creek CC1 139
17. Reflections for estimating percent illite/smectite from 140
18. Percent illite found in each sample....145

LIST OF FIGURES

Figure Page

1. Map showing the outline of Belt outcrops 5
2. Stratigraphic columns of the Belt-Purcell Supergroup..... 6
3. Field area 7
4. Modern analogue of the Belt Basin 11
5. Paleo reconstruction placing Australia as the western source. 12
6. Structural blocks of the Belt Basin. 13
7. Map of the Sevier fold-and-thrust belt 16
8. Proterozoic movement along the Buttress fault 17
9. Sm lithofacies. 30
10. Sr lithofacies 31
11. SSl lithofacies 33
12. Syneresis cracks 34
13. Fs lithofacies. 39
14. Gss lithofacies 36
15. Lm lithofacies 41
16. Domal structures characteristic of stromatolites 42
17. Outcrop of Fcs lithofacies. 43
18. Gms lithofacies 28
19. Gcs lithofacies 38

LIST OF FIGURES CONTINUED

Figure Page

20. Contact between Fcs and Ccl lithofacies....45

21. Ccl lithofacies....46

22. FS lithofacies....49

23. Ropes within in the Ccl lithofacies at Checkerboard....51

24. Small concretions on a thin Mt bed from Swimming Woman Canyon. 51

25. Walcott's Newlan Creek type section. 52

26. Sgc sandsstone bed within Fcs lithofacies 57

27. Distal turbidite....58

28. Block diagram of the northern margin of the basin....62

29. Down to the south block faulting 63

30. East-West Cross section location 65

31. East-West cross section. 66

32. Cohesive bedding of microbial mats....68

33. Harker Diagrams shown by location....75

34. SiO2 vs. K2O/Na2O abundance plot 76

35. Trace element plot of Cr vs. Ni....76

36. REE spider plot. 78

37. Showing BSE (A) and CL (B) images of detrital zircons. 81

38. Kernal density plots.....83

LIST OF FIGURES CONTINUED

Figure Page

39. Crustal events that occurred from 2.0-2.8 Ga. 85

40. Potential source areas for the Belt Basin. 87

41. Zoomed in view of the Wyoming Craton. 88

42. Bulk mineralogy of the Newland Formation. 94

43. Schematic interpretation of corrensite and chlorite pathways 101

44. Clay minerology 102

45. Ethyl glycol treated sample from Deep Creek 103

46. Ethyl glycol treated sample from Swimming Woman Canyon. 104

47. Xrd profile of Ch-6-29 125

48. Xrd profile of 1S-SW 125

49. Xrd profile of Belt Creek 126

50. Xrd profile of Deep Creek 126

51. Xrd profile of Deep Creek Unit 1 127

52. Xrd Profile of EFSW Swimming Woman Creek 128

53. Xrd Profile of Miller Gulch 128

54. Xrd profile of Sw-125 129

55. Clay mineralogy of 1s-sw from Swimming Woman Creek. 132

56. Clay mineralogy of ch-6-29 from checkerboard. 133

57. Clay mineralogy of DC-U1 from Deep Creek. 134

58. Clay mineralogy of EFSW from Swimming Woman Creek. 135

LIST OF FIGURES CONTINUED

Figure Page

59. Clay mineralogy of Lower Newland from Miller Gulch. 136

60. Clay mineralogy of the West Fork Swimming Woman Canyon..... 137

61. Clay mineralogy of Belt Creek Sample..... 138

62. Clay mineralogy of CC1..... 139

63. 1S-SW Ethyl Glycol treatment..... 141

64. Ch-6-29 Ethyl Glycol treatment..... 141

65. DC-U1 Ethyl Glycol treatment..... 142

66. EFSW Ethyl Glycol treatment..... 142

67. Miller Gulch Ethyl Glycol treatment..... 143

68. SW-125 Ethyl Glycol treatment..... 143

69. BC-ln Ethyl Glycol treatment..... 144

70. CC1 Ethyl Glycol treatment..... 144

ABSTRACT

The Belt Supergroup is exposed in western Montana where most of the unit is allochthonous due to Sevier thrusting. However, east of the Helena salient several autochthonous sections of Newland Formation pin it to central Montana. This study focuses on the stratigraphy, provenance, and structural framework of the Newland across this boundary. Measured sections in the Big Belt, Little Belt, and Big Snowy Mountains, along with previously published sections (Zieg 1981) were used to correlate the Newland and interpret its origin. Detrital zircon geochronology (U-Pb by LA-ICP-MS) was used to establish provenance. Clay mineralogy was used to determine burial depth across the embayment

Deposits of the lower Newland locally contain intraformational conglomerates suggesting basinal reorganization at the onset of Newland deposition. Core from a well south of the Volcano Valley fault demonstrate thickening of the lower Newland in the footwall and indicate down-to-the-south faulting (buttress fault). The Volcano Valley fault was reactivated as a thrust fault during Sevier shortening. Above these local units, the lower Newland is a regionally extensive parallel laminated tan calcareous shale containing thin beds of microspar, interpreted as a deep-water depositional system across the entire Helena embayment, indicating the Belt Basin extended further east than most current depictions.

Detrital zircon geochronology of the Newland Formation from the Big Belt Mountains suggests diverse sources. The primary source of ~2.45-2.61 Ga, may correspond to the Medicine Hat Block and/or crystalline basement in the western part of the basin. A younger Paleoproterozoic source (~1.79-1.98 Ga) matches the Great Falls Tectonic Zone, and two less prominent Archean sources of ~2.61-2.8 GA and ~3.0-3.2 Ga may reflect contributions from intra-basinal crystalline basement. Elemental analyses complement the detrital zircon geochronology, but do not distinguish distal Archean contributions (e.g., Canadian Shield) from a more proximal Wyoming Province. Xrd analysis of clays reveals the Helena embayment experienced a minimum burial depth of 3,300 m

It has been proposed that the Belt Supergroup is an allochthonous block that translated 1300 km north (Hildebrand, 2013). However, this study suggests the Lower Belt in the Helena embayment has not undergone significant latitudinal translation relative to cratonic North America.

INTRODUCTION

Significance

An investigation of the Mesoproterozoic Newland Formation along the northern margin of the Helena embayment in central Montana provides insight into the paleogeography of western Laurentia and, in particular, the Mesoproterozoic Belt-Purcell Basin (Belt Basin). The Newland Formation is stratigraphically low (older) within the Belt Basin, has experienced very little or no metamorphism, and interfingers with the southern LaHood Formation of the Helena embayment (Fox, 2017). This laterally continuous unit allows comparison of allochthonous parts of the Belt Basin that have been translated during the Sevier orogeny to the west, and autochthonous parts of the basin to the east.

Prior research in the Helena embayment has not resolved the tectonic setting and depositional environments during the initial stages of Belt Basin evolution, or its influence on Phanerozoic tectonic events. Several key points should be addressed: 1) interpretations of the depositional environment of the Newland Formation vary from shallow, microbial-influenced carbonate shelf and slope (Schieber, 1989), to sub-wave base, deep water (Zieg, 1981), but these studies have not been conclusive. Refining the depositional environments interpretation of the Newland Formation through lithofacies and facies associations would greatly facilitate the interpretation of basin margins and lateral extent of the basin. 2) Whole rock geochemistry and detrital zircon geochronology of Belt rocks within the Helena embayment has been done (Winston et al., 1992; Ross and Villeneuve 2003) and suggest multiple possible source areas, but more work needs to

be done. 3) Subsidence history of Belt rocks has been studied through clay mineralogy transects (E-W) across the Belt Basin (Ryan, 1991), but further investigation within the same stratigraphic unit (e.g., Newland) spanning the Helena salient will add to the subsidence story of the embayment. 4) Several contrasting interpretations of displacement during the Sevier and Laramide orogenic events exist (Sears, 2007; Hildebrand, 2013), yet have not included the para-autochthonous Belt rocks east of the thrust front, which has significant implications on our understanding of the tectonic evolution of the Cordillera.

This project is an integrated study of field observations, stratigraphic measurements, lithofacies and facies association, mineralogy, geochemical and geochronological analysis of the Mesoproterozoic Newland Formation to contribute to our understanding of basin development and its influence on Phanerozoic tectonism.

General Geology

The Belt Supergroup is currently exposed as a northwest-southeast trending succession of rocks covering ~200,000 km^2 of Washington, Idaho, Montana, British Colombia, and western Alberta (Figure 1) (Lydon, 2005). Within this area, the Belt Supergroup can be subdivided into two segments: The main Belt Supergroup basin with a ~750 km NNW trending orientation, and the Helena embayment extending eastward from the main basin (Graham et al., 2012; Sears, 2007)

Initial deposition within the Belt Basin can be bracketed by the youngest zircons from the crystalline basement of the Little Belt Mountains at 1.79 Ga (Paul A. Mueller et al. 2002) and the 1.45 Ga intrusive Moyie Sills within the Lower Belt Aldridge

Formation, or the 1.46 Ga Perma Sills of the Prichard Formation. Final stages of deposition within the Belt Basin occurred prior to the late Proterozoic Windermere group between 780 and 550 Ma based on continental rift facies and (Sears, 2007).

The western portion of the Belt Supergroup has a stratigraphic thickness of 15-20km (Sears, 2007), thinning to the east in the Helena embayment to a thickness of 2.5 km (Chandler, 2000). The western limit of the Belt rocks is unclear due to the Late Proterozoic Windermere Group, accreted terranes, granitic complexes and extensional core complexes (Winston, 1986b) and coincides with the Sr 0.706 line, demarcating the western edge of the craton (Ross and Villeneuve, 2003).

The Helena embayment is an eastern extending arm of the Belt Basin bounded on the north by the Little Belt Mountains and to the south by the Perry Line (McMannis 1963). The easternmost exposed outcrops of Belt rocks are located in the Big Snowy Mountains of Central Montana. These outcrops have been described by Reeves (1931) and Lindesy (1980) as Newland shale. The western margin of the Helena embayment is not correlative to the main Belt Basin due to obstruction from Late Cretaceous Elkhorn Volcanics and the Boulder batholith (Lageson et al., 2002).

Stratigraphy within the lower Helena embayment includes the Neihart, LaHood, Chamberlain, Newland, and Greyson Formations (Figure 2). These formations are composed of mature quartzite of the Neihart Formation, conglomerate arkose carbonates and shale of the LaHood Formation, dark black to gray shale of the Chamberlain Formation, carbonate and calcareous shale and sandstone of the Newland Formation, and dark brown silty shale and conglomerate of the Greyson Formation. The lower Belt rocks

of the Helena embayment unconformably rest on crystalline basement and are capped by an angular unconformity with the overlying Cambrian Flathead Formation.

The study area focuses on the northeast margin of the Helena embayment and includes four mountain ranges spanning over 160 km. From west to east, these are: The Big Belt Mountains, Little Belt Mountains, Castle Mountains and the Big Snowy Mountains (Figure 3). Structurally the field area crosses the leading edge of the Sevier fold-and-thrust belt within the Helena embayment (known as the Helena salient) and Laramide basement involved thrusts to the north and east in the Little Belt Mountains and Big Snowy Mountains.

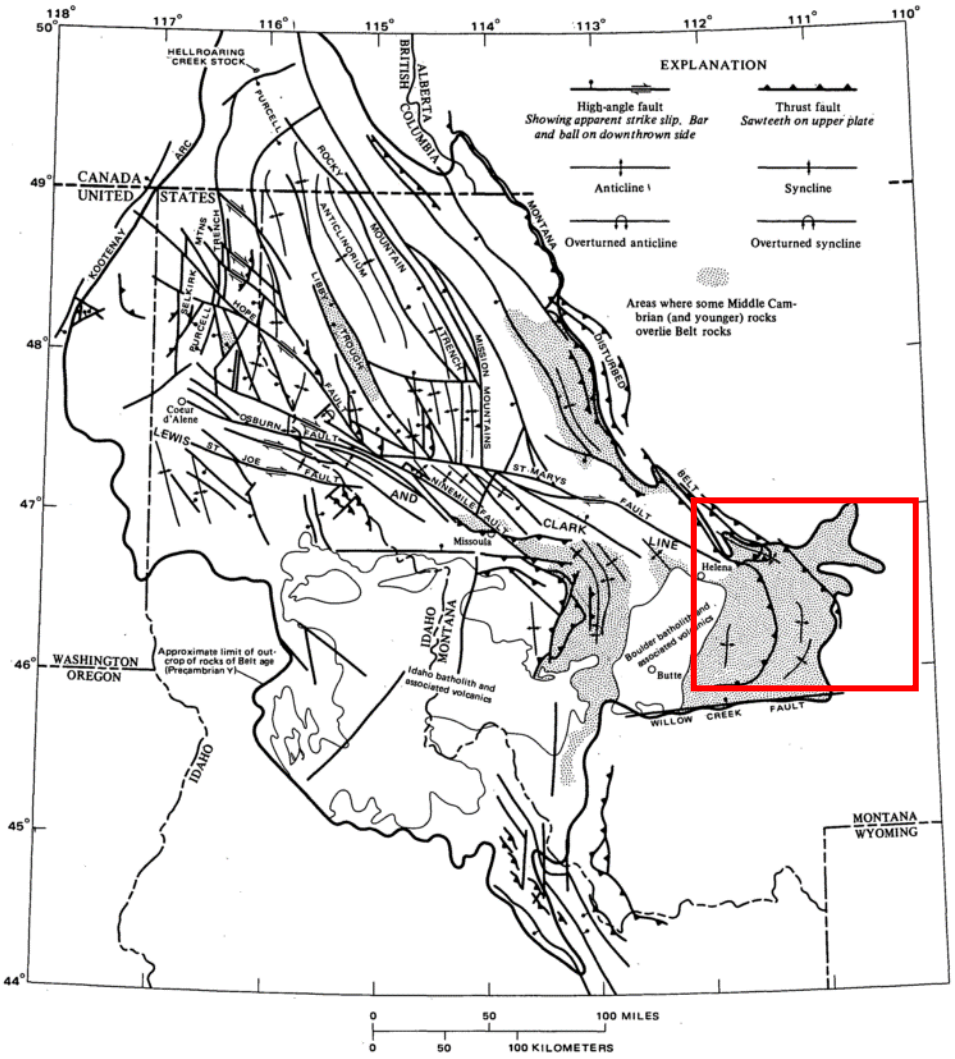


Figure 1. Map showing the outline of Belt outcrops and major folds and faults within the Belt Basin. Field area is outlined in red and spans the Helena salient. The Boulder batholith can be seen to the left of the field area. Modified from Harrison et al., (1974)

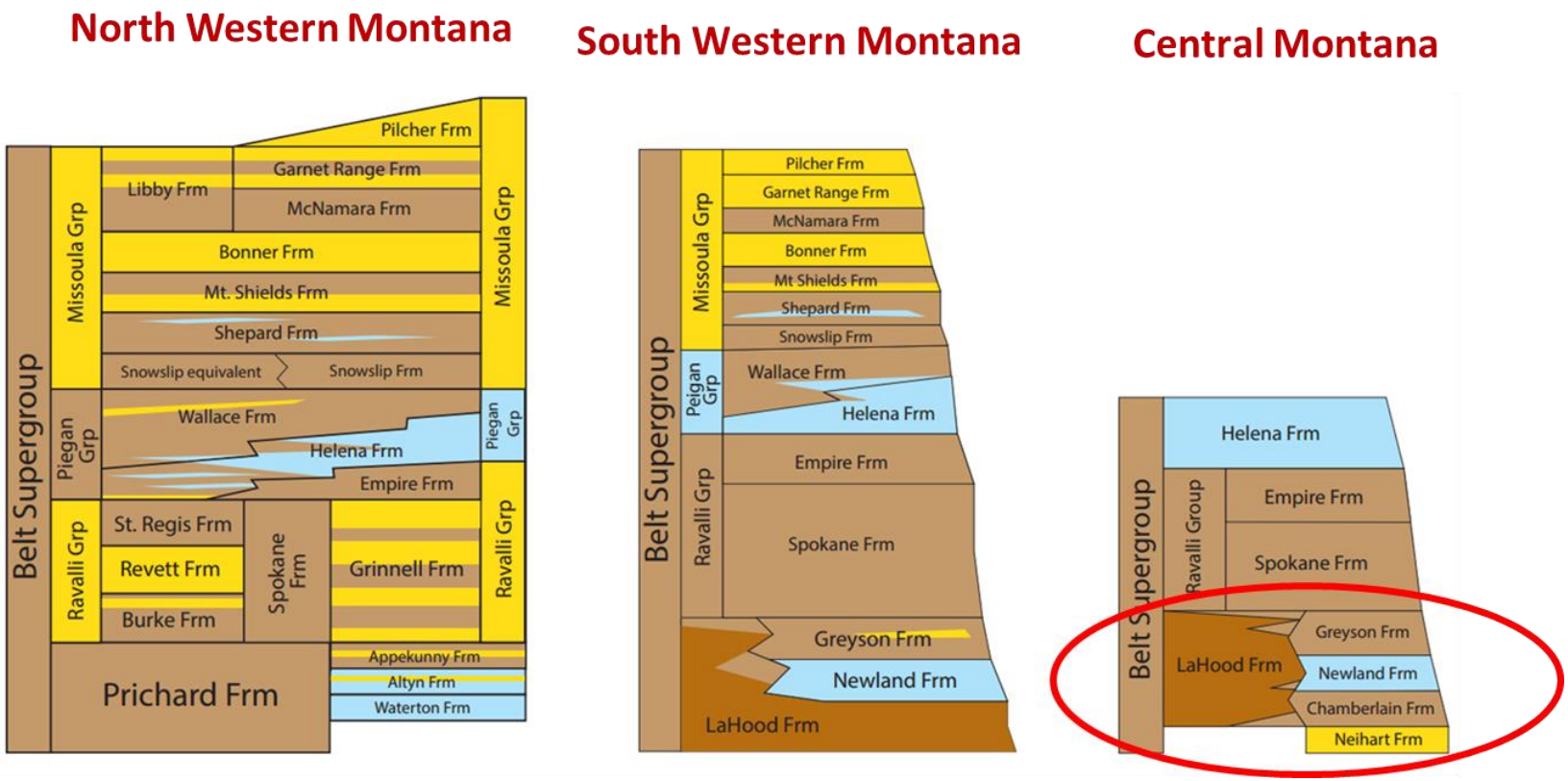


Figure 2. Stratigraphic columns of the Belt-Purcell Supergroup from several locations in Montana. Stratigraphy within the field area circled in red. Modified from (Vuke et al., 2009)

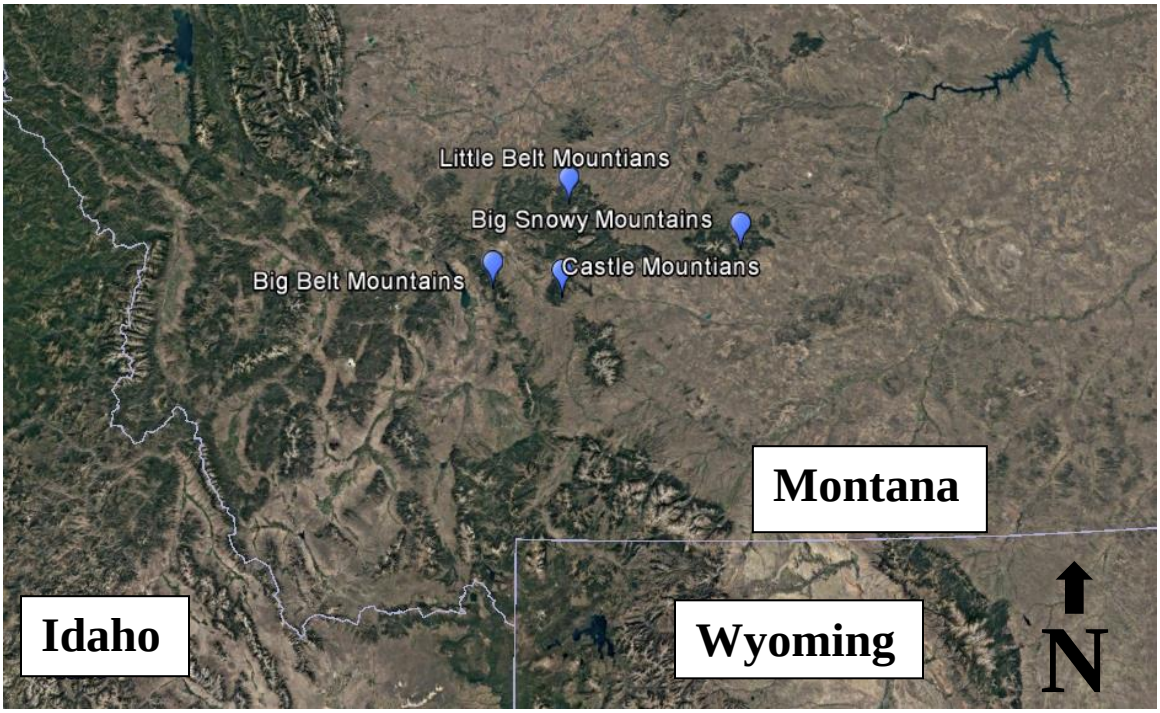


Figure 3. Map of Montana showing the location of the four ranges involved in this study. Distance from the Big Belt Mountains to the Big Snowy Mountains is ~160 kilometers

Methods

This project utilized previously published description and measured sections at five locations to identify lithofacies of the lower Belt Supergroup and correlate them to newly measured section east of the Helena salient. Previously published stratigraphic sections were field-checked and graphic logs created from previous work from Zieg (1981) and Feedback (1997) to correlate across the Helena salient. Core analysis was also done to further understand the northern margin of the Helena embayment. Lithological characteristics were described and correlated across the Helena salient, which allowed depositional environments to be determined and basin margins inferred. Sample

preparation and analytical methodology differed greatly for each analysis in this study and are summarized in each section and in the appendices.

Samples were analyzed using X-ray fluorescence (XRF) elemental analysis and X-ray Powder Diffraction (XRD) mineralogy and clay identification. Detrital zircon geochronology was done through laser ablation at the University of Florida Geology Department isotope geoscience research facility. XRF of the Newland Formation was done to measure the whole rock geochemistry and compare major and trace element abundances and determine the composition of the provenance. XRD analysis was used to determine both bulk mineralogy of the Newland Formation as well as clay mineralogy and detect any alteration of clay minerals and diagenesis across the Helena salient. Finally, these attributes were combined to correlate the allochthonous Belt rocks in the western portion of the study area to the autochthonous Belt rocks in the eastern portion of the study area.

TECTONIC FRAMEWORK

The tectonic framework of the Belt Supergroup was influenced by basement structures prior to Belt Basin deposition and is still being affected by extension (Sears, 2007). The hypothesis that Precambrian structures have controlled Phanerozoic structures in the Belt Basin has been discussed for over a century (e.g. Peale, 1896). This chapter will address the multiple tectonic events that have influenced the Belt Basin, prior to, during and after formation of the Basin.

Prior to Belt Basin deposition, subduction of the Medicine Hat block beneath the Wyoming block formed the Great Falls Tectonic Zone (GFTZ), a suture zone occurring around 1.80-1.86 Ga, (Mueller et al. 2002; Gifford et al. 2014). The GFTZ is a NE-trending zone greater than 650 km in length characterized by high angle faults and shear zones (O'Neill and Lopez, 1985) (Sims et al., 2004). The lithospheric boundary between these two blocks is seen as long linear faults and Mesozoic and Tertiary dike swarms (Gifford, 2013). The Perry Line is one of these liner faults and marks the southern boundary of the Dillon block and southern margin of Belt deposition within the Helena embayment (Fox, 2017).

Consensus on the tectonic setting and basin development of the Belt Basin remains unresolved with multiple hypotheses: rift basin (Hoy, 1992), intra-cratonic lake basin (Winston, 1986a), continental margin delta basin (Price, 1964), impact basin (Sears and Alt, 1989), trapped ocean basin(Shepard, 1987) (Hoffman, 1988), and even an aulacogen (Shepard, 1987). Ross and Villeneuve (2003) proposed the basin formed as an

extensional domain based on mafic volcanic rocks, rapid rates of sedimentation, and intra basinal syn-depositional fault system similar to the Cretaceous Caspian Sea.

Anderson et al. (2015) looked at the stratigraphic thickness across the Belt Basin and determined the basin had shifting depocenters. Characteristics of a transtensional basins include: lateral displacement of depocenters, lateral offset of matched source areas and sediment, presence of course grained alluvial fans or fan deltas, thick sedimentary packages from rapid deposition and increase in accommodation, abundant slumping and syn sedimentary deposition (Nilson and Sylvester, 1995). Evidence of shifting depo-center, and compartmentalization of sub basins interpreted by (Fox, 2017) along the Perry Line supports the transtensional-rift model of (Wu et al., 2009) for the formation of the Belt Basin (Anderson et al., 2015). Modern analogues for this model include transtensional rifting of the Sinai block and the Arabian plate forming the Dead Sea fault system (Wu et al, 2009) (Figure 4).

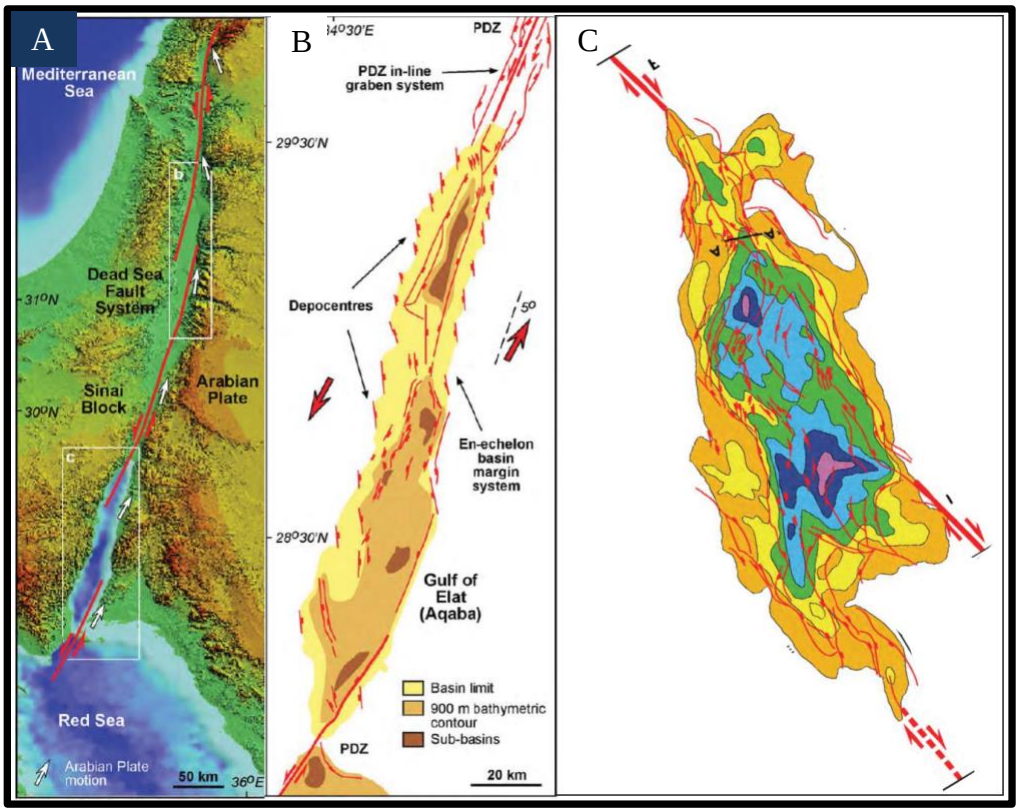


Figure 4. Modern analogue of the Belt Basin. A) The Dead Sea fault system. B) Large scale of the Gulf of Elat. Note the two depo-centers and the en-echelon marginal fault system. C) The Vienna Basin that has been rotated 180 degrees. Note the two depo-centers similar to the Belt Basin (Anderson et al., 2015) Modified from (Wu et al., 2009)

Many hypothesis regarding a western craton as a sedimentary source area have been proposed and include: Australia (Ross and Villeneuve, 2003), Siberia (Sears and Price, 2000), Baltica (Patchett et al., 1978), a combination of Baltica-Australia-Western United States - AUSWUS and southwest United States-East Antarctic - SWEAT (Karlstrom et al., 1999), Antarctica (Goodge et al., 2008) or the MAWSON craton (Halpin et al., 2014). Based on data from the North American magmatic gap (1.61-1.49 Ga) the aforementioned western cratons are all possible. However, further evidence supporting Australia as the western craton include Mesoproterozoic Arcitarch

assemblages within the Roper Group Australia (1429-1492 Ma), which have the strongest correlation to the Belt Basin (Adam, 2014), and alternating assemblages in the Sheep Creek copper deposit recently renamed the Black Butte Copper Project that are similar to the Mount Isa deposit of Australia (Graham et al., 2012) (Figure 5).

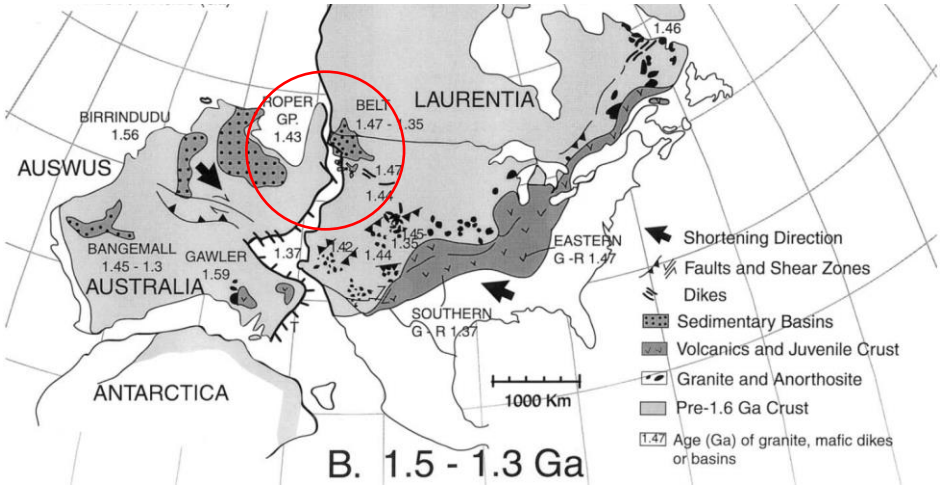


Figure 5. Paleo reconstruction of placing Australia as the western source. Note the correlation of the Roper group and Belt Basin circled in red. Modified from Karlstrom et al., (2001)

Extension within the basin formed a series of normal fault systems resulting in structural blocks trending east-west (Sears, 2007), these structural blocks controlled the main depo-centers within the basin. Winston et al., (1989) conceptualized a series of lineaments to delineate the boundaries of the main structural blocks within the basin. The primary lineament or structural zones influencing the Helena embayment include the Lewis and Clark Lineament and the Perry Line. The Lewis and Clark Lineament is an east-west trending structural zone marking the northern edge of Newland Formation exposures (Graham et al., 2012), and the Perry Line is the southern lineament marking the edge of LaHood deposition into the basin (Figure 6).

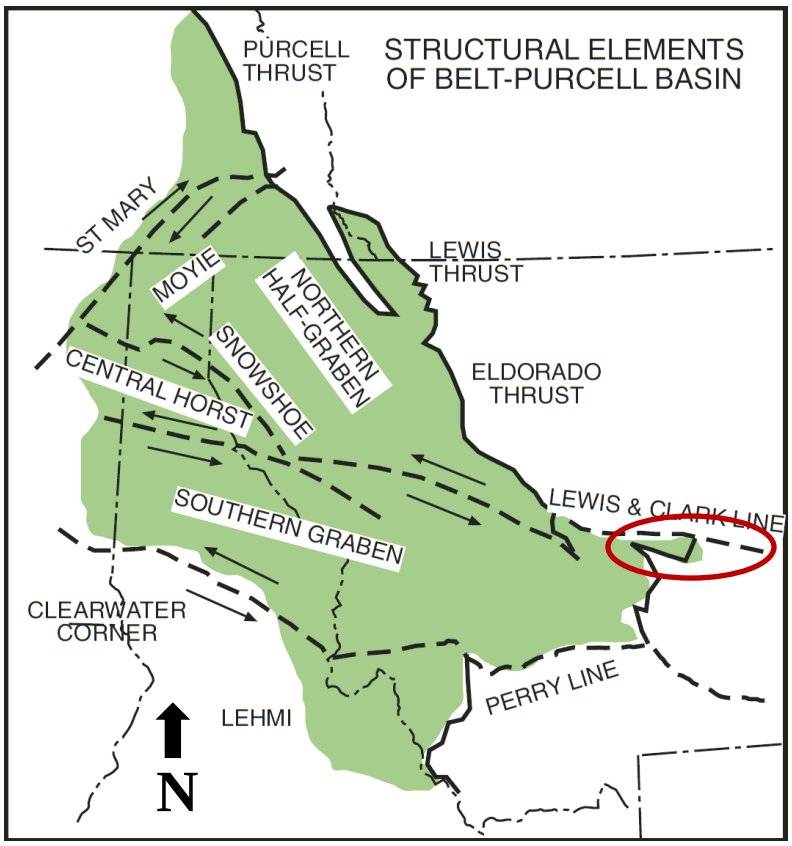


Figure 6. Structural blocks of the Belt Basin. Red oval indicates field area. Arrows along fault lines show inferred direction of movement. Modified from Sears (2007).

During Proterozoic time, a half-graben along the Perry Line received course conglomerates of the LaHood formation (McMannis, 1963). Along the northern portion of the Helena embayment, the basin underwent down-to-the-south block faulting along the northern Buttress fault at the onset of Newland Formation deposition, resulting in an increase of accommodation and the formation of an east-west trending graben (Graham, et al., 2012 ; Feedback, 1993). Structural inversion during the Proterozoic and early Cambrian is evident through an angular unconformity between Belt rocks and the Flathead Formation in eastern outcrops and well logs (Nelson, 1993)

Phanerozoic Tectonics

Two major Phanerozoic orogenic events, the Sevier and Laramide orogenies, heavily influenced the nature of the study area. The Sevier orogeny, which is characterized as thin-skinned-fold-and-thrust belt, began in the early Cretaceous ended in the Helena salient by the middle to late Paleocene (Lageson et al., 2002). The Laramide orogeny, which is characterized by basement-involved thrusting, coincided with the end of the Sevier orogeny in the late Tertiary (Nelson, 1993).

Several contrasting interpretations of Phanerozoic tectonism on western Laurentia have been proposed by Sears (2007) and Hildebrand (2013). Sears (2007) proposed that during Cretaceous deformation events the Belt-Purcell Basin sediments underwent clockwise rotation with a translation of ~250 km in the Calgary area, and as little as a few km in the Helena area (Sears, 2007). Hildebrand (2013) proposed that upwards of 1300 km of right-lateral displacement from Baja to British Colombia occurred during the Laramide orogeny. Both Hildebrand (2013) and Sears (2007) consider exposed Belt rocks to be one continuous allochthon, yet autochthonous Belt rocks are known in outcrops and the subsurface within the Helena embayment and extend well into the craton (Winston, 1986b)

The field area within the Helena embayment crosses the leading edge of the Sevier fold and thrust belt or Helena salient (Figure 7). The Big Belt Mountains, eastern portion of the Little Belt Mountains and Checkerboard area are to the west of the Helena salient. Thrust faults within the Helena embayment include the Lombard-Eldorado thrust, the Willow Creek thrust and the Volcano Valley thrust (Lageson et al., 2002). Schmidt et

al., (2014) purposed the Helena salient formed by primarily west-east transport modified by lateral ramps along is margins. Within the northern Helena salient these thrust faults were left lateral ramps along the reactivated Lewis and Clark Line, and right lateral ramps along the Perry line (Figure 6).

The Volcano Valley fault (VVF) is the primary structural feature within the field area, and is the result of Cretaceous reactivation of the Buttress fault during shortening of the Sevier orogeny (Figure 8). VVF has also been shown to have approximately 1.6 km (1 mile) of left- lateral offset in the Black Butte area and has thrust Proterozoic Belt rocks over Paleozoic strata (Zieg et al., 2013). Being the leading edge of the Helena salient, the VVF directly separates allochthonous Belt rocks from autochthonous Belt rocks on the Wyoming craton further east.

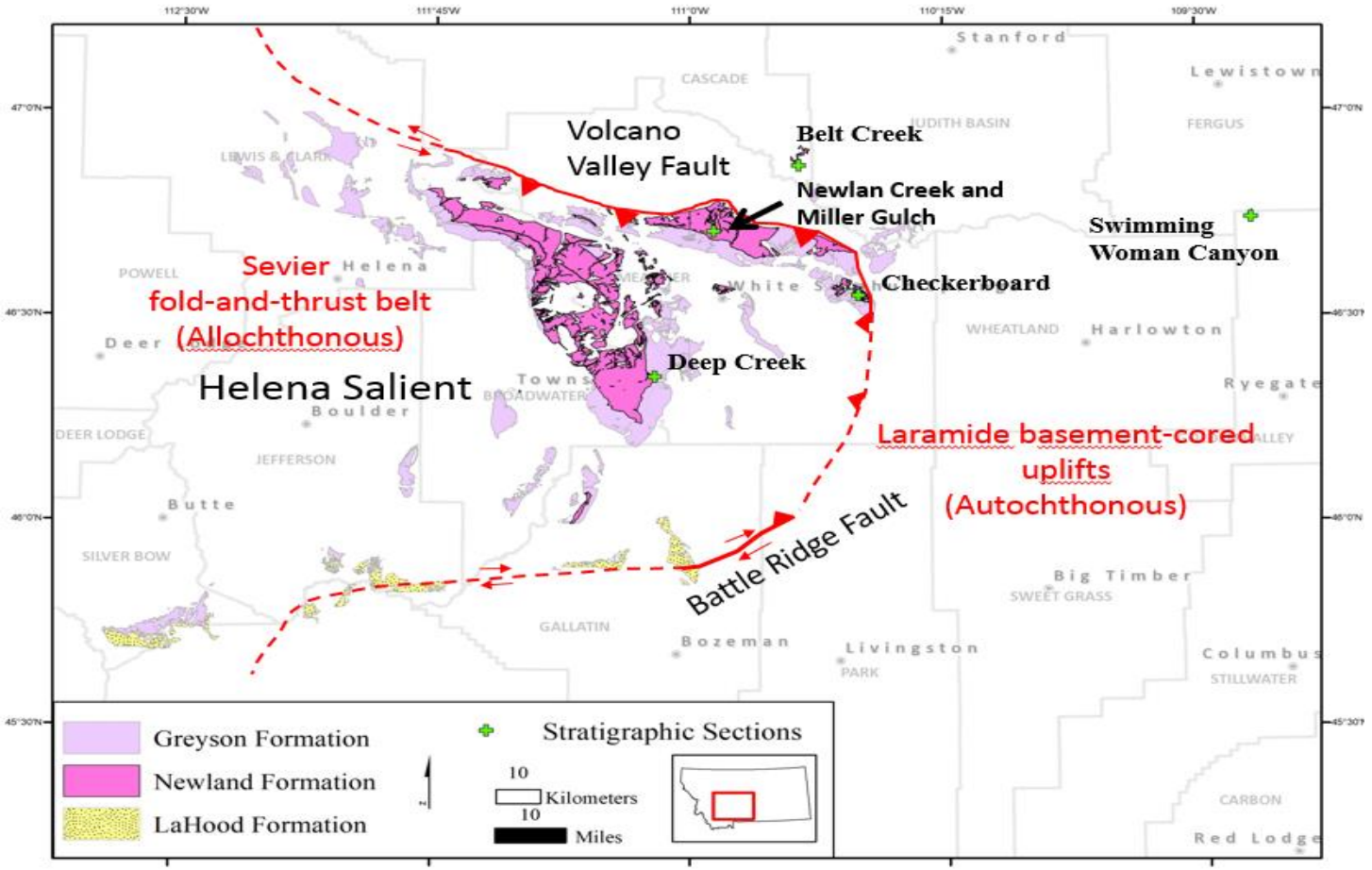


Figure 7. Map of the field area showing the leading edge of the Sevier fold-and-thrust belt and Laramide basement-involved thrust faults. Allochthonous rocks lie to the west of the Helena Salient, while autochthonous or para-autochthonous rocks lie is to the east

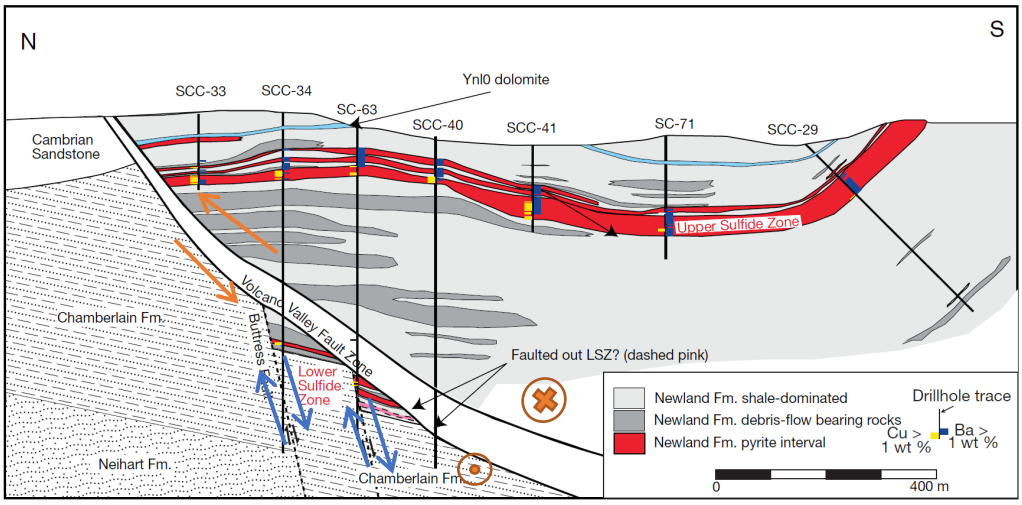


Figure 8. Showing Proterozoic movement along the Buttress fault (blue arrows) and Phanerozoic left-lateral ramp thrusting of the VVF, orange arrows show direction of movement during the Sevier orogeny with the hanging wall moving into the page. Modified from (Graham et al., 2012)

SEDIMENTOLOGY AND STRATIGRAPHY

Introduction

The stratigraphic framework of the Helena embayment has been studied in detail by Weed (1896), Walcott (1916), McMannis (1963), Schieber (1986), Zieg (1981), Fox (2017) and others. Though detailed analysis of the northern and southern margins of the Helena embayment has been done, correlation of the allochthonous Belt rocks west of the Helena salient to the autochthonous Belt rocks to the east has not been done prior to this study. Stratigraphic correlation across the Helena salient provides insight into the tectonic framework and depositional environments within the Helena embayment during the Mesoproterozoic and provides evidence of the tectonic evolution of western Laurentia throughout the Phanerozoic. Due to the overall lack of sedimentary structures within the Newland Formation, the scope of this study includes the Neihart, and Chamberlain Formations to determine the depositional environment, and interpret the lateral shifts of facies within these units along the northern margin of the Helena embayment. Depositional environments and stratigraphic correlations will be presented in chapter 3. This chapter will focus on the physical characteristics and the inferred processes by which they were deposited.

Methods

Stratigraphic sections were measured using a Jacob staff, tape measure, I-pad, and field notebook for images and data recording. In the summer of 2015 and 2016 previously published sections and newly measured sections were done in the Big Belt

Mountains (Deep Creek), Little Belt Mountains (Decker Gulch, Miller Gulch, Belt Creek, Chamberlain Creek), Castle Mountains, the Big Snowy Mountains, and analysis of the Sc12-112 core provided by Tintina Resources INC. Sc12-112 is a vertical well from the Sheep Creek area spanning the VVF, and contains the Neihart, Chamberlain and Newland Formations. Samples were taken throughout measured and field checked sections and processed for appropriate analysis.

Helena Embayment Stratigraphy

The stratigraphy within the eastern portion of the Belt Basin is composed of the Neihart, Chamberlain, Newland, and Greyson Formations. The following description of the stratigraphy are from previously published research and will be discussed beginning with the basal Neihart Formation.

Neihart Quartzite

The base of Belt stratigraphy or potentially pre-belt in the Helena embayment begins with the Neihart Quartzite (Mueller et al., 2002). The Neihart Formation unconformably overlies the Paleoproterozoic crystalline rocks in the Neihart area, informally called the "red gneiss", "gray gneiss" and Pinto Diorite (Schafer, 1935; dated at 1867-64 Ma by Mueller et al., 2002). Weed (1896) estimated the thickness of the Neihart formation by the town of Neihart to be ~213.3 m (700 ft). This is the only outcrop of the Neihart Formation and was named by Weed due to its proximity to Neihart Mountain (Zieg, 1981). The Neihart Formation is composed of massive, pink-gray frosted well-rounded quartz arenite, with cross beds and a basal conglomerate(Walcott,

1899). In the Sheep Creek area, the Neihart is ~ 250 m (820 ft) thick (Graham et al.,2012).

Chamberlain Formation.

The Chamberlain shale is dark siliceous and arenaceous shale with ripple marks, mudflows, occasional mudcracks, and carbonate-rich beds near the top (Walcott, 1899). Walcott's type section is located Chamberlain Creek south of Neihart, where he estimated the thickness of ~457.2 m (1500 ft) along Belt Creek. The Chamberlain is ~ 460 to 945 m (1509 to 3100 ft) thick in the Sheep Creek area(Graham et al., 2012).

Newland Formation

The Newland Formation was first described by Walcott (1899) as thin-bedded limestone with shale partitions. Two type sections were identified, one was in Newlan Creek, formerly Newland creek, north of White Sulfur Springs and the other was in Belt Creek. A small portion of the Lower Newland is found in Belt Creek directly below the Cambrian unconformity. In the Sheep Creek area, the Newland is ~1100 m (3609 ft) thick (Graham et al., 2012). The Newland Formation can be sub divided into the Lower and Upper Newland and will be discussed below.

Lithofacies

The physical characteristics of the rocks were described and classified according to lithofacies that could be correlated across the field area. The lithologies of these units are classified from observations in the field and core, and described using grains size, grain shape, mineral composition, matrix, cement, or chemical composition. Lithofacies

are determined by using the above mentioned physical properties as well as sedimentary structures to determine the environment of deposition. Characterization of each lithofacies is dependent on the overall scope of the project. Within this project, the major changes in lithology or depositional process were used to determine lithofacies. Correlating lithofacies within the Helena embayment aided in forming a hypothesis about the paleogeographic setting of the basin. 18 lithofacies were identified within the lower belt stratigraphy in the field area and are presented in Table 1. A brief description and interpretation of each lithofacies is then presented, as well as diagenetic features seen throughout the field area.

Lithofacies code	Lithology /Grain Size	Sedimentary Structures	Description	Interpretation	Formation/ Zieg's (1981) units
(Gms) Massive, matrix or clast supported conglomerate	Intraformational carbonate and laminated mudstone clasts up to 10 cm	Massive to chaotic bedding	Thickly to thinly bedded matrix and clast supported conglomerate	Subaqueous mass transport initiated by slop failure, soft sediment deformation	Newland Unit VI
(Sm) Massive sandstone	Medium- to very fine- grained, well-rounded, frosted, silica cemented sandstone	None.	Massive	???	Newland Unit IV and unit VII
(Sr) Ripple cross laminated sandstone	Fine- to very fine- sandstone with green siltstone interbeds	Trough cross stratification	Thickly to thinly bedded pink and greenish in color	Oscillatory flow, with episodic flows (currents, waves.)	Unit II and V

Table 1. Lithofacies descriptions

Lithofacies code	Lithology /Grain Size	Sedimentary Structures	Description	Interpretation	Formation/ Zieg's (1981) units
(St) Cross stratified sandstone	Medium- to very fine- grained, well-rounded, frosted, silica cemented sandstone	Tabular cross-bedding	Laminations are low angle and truncated	Unidirectional flow Straight crested dunes	Unit III
(Se)Erosional scours sandstone	Course- to fine-grained sandstone	Graded bedding scour-and-fill structures	Beds have erosional truncation vary from laterally extensive to concave upward	Scour-and-fill	Unit I
(Fls) Lenticular laminated siltstone and sandstone	Siltstone with fine-grained sandstone	Lenticular laminations, symmetrical ripple cross-laminated, Syneresis cracks,, load structures, flame structures	Thickly to thinly lenticular laminated green appearance in outcrop and green silt and grey to white sandstone 50/50	Episodic current flow followed by quiescence, and oscillatory flow, salinity changes, load structures	Lower Newland and unit VII
(Sgc) Sandstone graded	Course- to fine-grained sandstone, calcite cement	Graded bedding and plane laminated	Medium bedded. often isolated	Graded bedding is deposited in a upper flow regime, rapid deposition	Upper and Lower Newland

Table 1. Continued

Lithofacies code	Lithology /Grain Size	Sedimentary Structures	Description	Hydrodynamic Interpretation	Formation/ Zieg's (1981) units
(Src) Ripple laminated calcareous sandstone	Fine sandstone to siltstone calcareous cement	Cross-laminated	Thinly bedded to thinly laminated	Lower flow regime plane bed	Upper and Lower Newland
(Fp) Siltstone planer laminated	Siltstone	Planer laminations	Thinly bedded to thinly laminated	Suspension settling	Upper and Lower Newland
(Fsc) Mudstone and claystone	Claystone to siltstone, muscovite	Wavy to parallel laminated	Thinly laminated black, fissile in outcrop	Microbial influenced sedimentary structures, low energy environment	Chamberlain carbonate
(Fl) Plan bedded siltstone	Siltstone-claystone	Plane parallel laminated	Silt beds up to 15 cm.	Overbank deposits	Chamberlain
(Fsn) Fissile shale calcareous laminations	Fissile shale clay, silt, microspar nodules	Primarily plan parallel laminated with very few Ripple cross-laminated	Thickly to thinly laminated dark brown to gray	Increased terrigenous input and ripple cross-laminated from bottom currents upper flow regime, laminations are calcareous	Unit II and V Upper Newland

Table 1 Continued

Facies code	Lithology /Grain Size	Sedimentary Structures	Description	Interpretation	Formation/ Zieg's (1981) units
(Fcs) Calcareous shale (marl)	Calcareous to dolomitic mudstone and claystone	Plane parallel laminations	Thickly laminated tan weathered, gray to black fresh surface	Suspension settling.	Lower and Upper Newland
(Ccn) microspar chert nodules	Dolomitic microspar silt to clay	Plane parallel laminated chert nodules	Thickly to thinly bedded gray microspar and black chert,	Suspension settling	Unit III Upper Newland
(Ibs) Interbedded silty microspar and silty shale	Silty microspar and calcareous shale	Ripple laminated and secondary dissolution and precipitation of calcite.	Thinly bedded dark gray microspar and tan to dark brown calcareous shale	Upper flow regime, ripple cross-laminated and carbonate precipitation.	Newland Unit IV and unit VII
(Cpl) parallel laminated microspar	Gray microspar silty-claystone interlaminated	Plane parallel laminated, folded bedding	Thickly to thinly bedded, gray microspar and mottling (diagenetic)	Hemipelagic low terrigenous input and high carbonate precipitation	Newland Unit VI
(Ccl) silty microspar	Microspar clay –silt	Cross-laminated silt (very few) gradational laminations, load structures	Thickly to thinly bedded tan weathered, gray fresh surface	Bottom currents-traction transport. carbonate precipitation	Unit I

Table 1. Continued

Facies code	Lithology /Grain Size	Sedimentary Structures	Description	Interpretation	Formation/ Zieg's (1981) units
(Lm) calcareous mudstone	Calcareous mudstone, micrite	Domal laminations, molar tooth structures intraformational rip-up clasts	Thickly to thinly bedded tan weathered, gray to black fresh surface	Shallow water, low energy deposition, biological, infrequent storm events	Chamberlain carbonate

Table 1. Continue

Lithofacies (Gms): Intraclast Conglomerate

Gms lithofacies is composed of intraformational angular to rounded clasts up to large blocks of the Fcs facies. Conglomerates range from clast to matrix supported which can be both black organic rich shale and gray dolomite, and the matrix is also either black shale or grey dolomite from within the Newland Formation. Conglomerates do not show graded bedding. These conglomerate deposits are typically directly below chaotic liquefied flow structures (Figure 9)

Interpretation

Debris flow deposits of the Gms facies were formed by subaqueous mass transport deposits caused by slope failure. Mass movement occurs when the driving force of gravity exceeds the tensile strength of the sediment, which can be caused by over steepening, seismic loading, and cyclical storm wave loading of sediments (Arnott, 2010). Subaqueous debris flows are a form of cohesive flow, meaning the volume concentration of the solid and fluid phases are equal, and a cohesive matrix imparts a pseudoplastic rheology to the flow (Morhig et al., 1998). The liquefied flows seen directly above the conglomerate beds have been interpreted to be the result of lithified clasts settling through the flow displacing liquid upwards (Feedback, 1997) (figure 10).

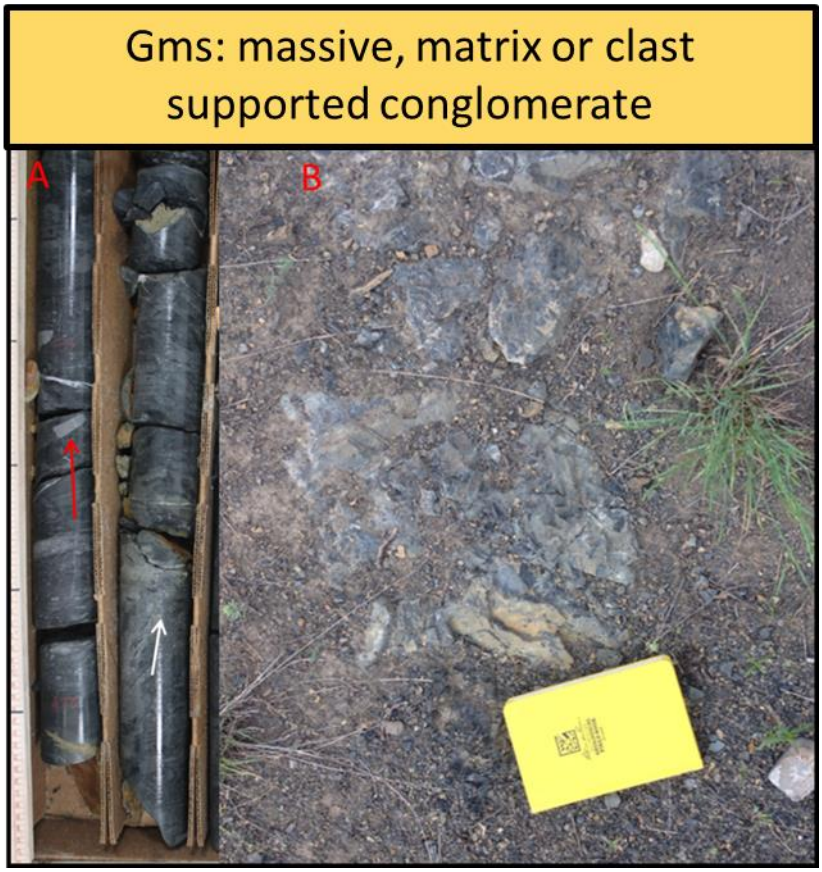


Figure 9. Gms lithofacies. A core showing Gms facies with both debris flow deposits and fluidized flow. Note the angular gray dolomicrite clast in core (red arrow) , and a fluidiezed flow chaotic bedding (white arrow). B is an outcrop near Sheep Creek of Gms facies.

Lithofacies (Sm): Massive Sandstone

A sandy (S) very mature (m) massive quartz arenite. The Sm lithofacies is a pink, course- to fine- grained quartz arenite. Individual grains are often frosted. Beds are massive with no visible sedimentary structures.

Interpretation

Massive sandstone is often deposited through rapid depositions or appears massive in outcrop, yet has noticeable sedimentary structures upon further examinations.

In Phanerozoic sandstones, sedimentary structures are often destroyed by bioturbation. However, in the Proterozoic, biota associated with this form of bioturbation were not present. Sm lithofacies is found in the lower Neihart Formation which was slightly metamorphosed and destroyed available sedimentary structures seen in outcrop.

Lithofacies (St): Trough Cross Stratified Sandstone

Trough cross stratified medium- to very fine-grained mature sandstone is present in the Sc12-112 core. Trough and tabular cross bedding can be seen and isolated lithic clasts up to pebble size were also present (Figure 10).

Interpretation

Cross bedding in Sm lithofacies was formed by the migration of either straight crested or sinus ripples or dunes forming trough to tabular cross bedding (Miall, 2010). Tangential and non-tangential (planar) forests with varying slope angles are present and are not unidirectional, indicating alternating flow directions within the lower flow regime.

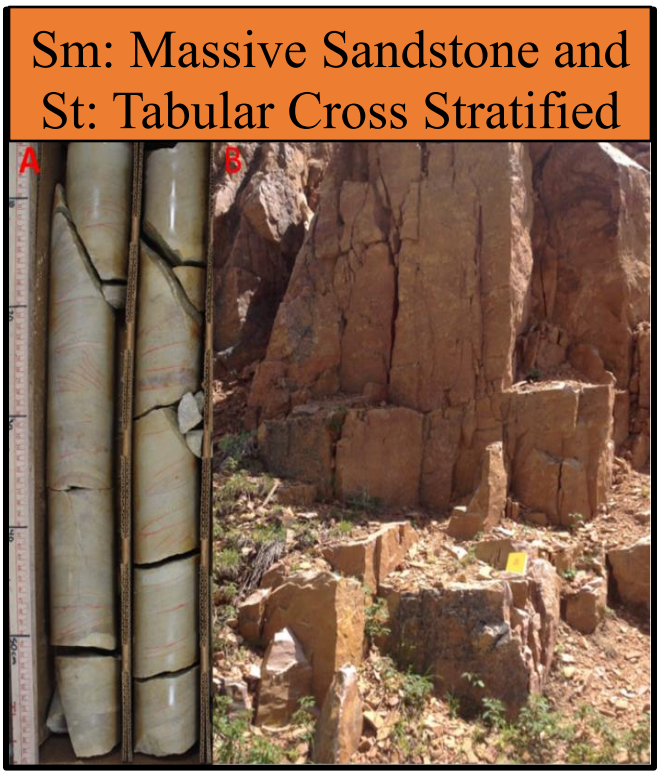


Figure 10. Sm lithofacies. A) Sc12-112 well showing cross-laminations within medium- to fine-grained sandstone. B) Outcrop of Sm lithofacies showing massive sandstone at Cathedral Falls along HW 89. Cross laminations and sedimentary structures absent in outcrop. Field notebook for scale.

Lithofacies (Sr): Ripple Cross-Laminated Sandstone.

The Sr lithofacies is composed of thick- to thin-bedded, cross stratified, fine- to very fine-grained quartz, and greenish silty claystone interbeds, macroscopically muscovite is seen within the greenish silty claystone. In outcrop at the mouth of Chamberlain Creek, in an old quarry, symmetrical ripples are seen on bedding surfaces in float. In the Sc12-112 core lenticular laminations are present (**Error! Reference source not found.**).

Interpretation

Ripple cross-lamination form under lower flow regime conditions and can form under unidirectional or oscillatory flow. Symmetrical ripples are characteristic of oscillatory flow. Sr facies in the Sc12-112 core also has wavy and lenticular laminations. Lenticular bedding is formed from the alternating deposition of mud and sand. Sand is deposited during times of current or wave activity and mud deposited during times of quiescence. (Dalrymple, 2010).

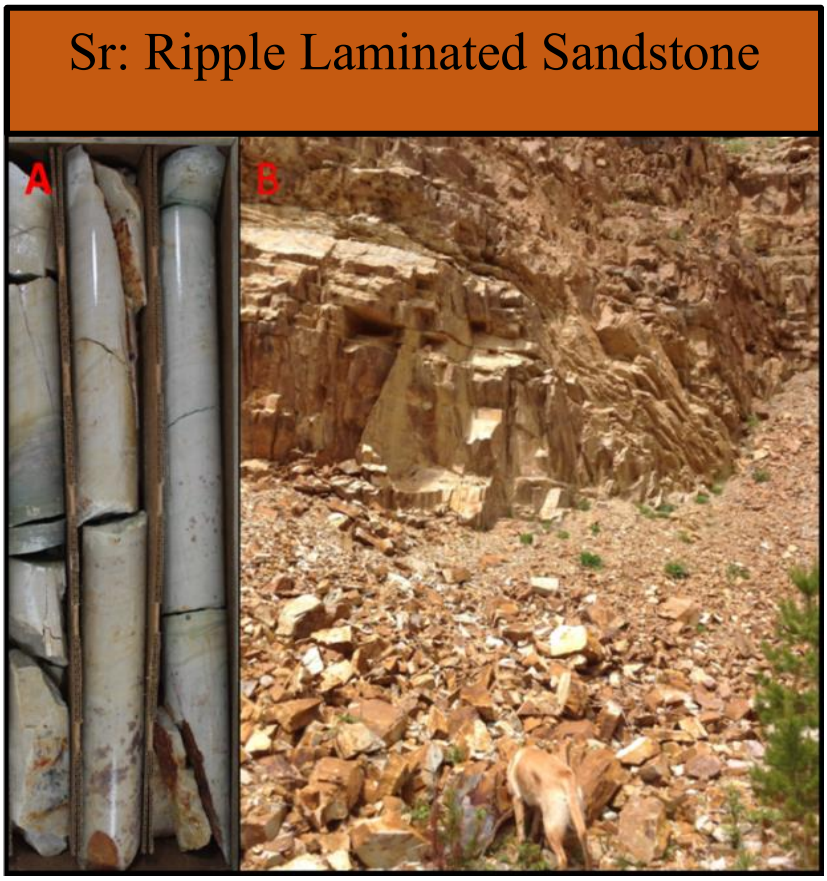


Figure 11. Thick to thin bedded, cross stratified, fine- to very fine-grained quartz, and greenish silty-claystone interbeds. A) Core Sc12-112 B) Outcrop at beginning in Chamberlain Creek

Lithofacies (Fls): Lenticular Laminated Sandy Siltstone

Fls lithofacies is composed of thin green lenticular lamina of mudstone and fine-grained well-rounded and well-sorted quartz grains. Symmetrical ripple and cross-laminations are present and were more obvious in outcrop. In core (Sc12-112) the laminations appear to be wavy or lenticular depending on the ratio of sandstone to mudstone. Syneresis cracks, flame structures, and sandstone injectites that Pratt (1997) regards as other forms of syneresis cracks are also present in Fls. (Figure 12 and Figure 13)

Interpretation

Lenticular bedding found in Fls is due to episodic current flow followed by quiescence. Ripple cross-laminations are symmetrical and support an oscillatory flow likely from wave action. Syneresis cracks were formed by changes in salinity and the deflocculating of smectite (Kinder, 1990).



Figure 12. Fls – Wavy lamina with cross stratification, syneresis cracks, flame structures, lenticular bedding and microbial wavy laminations, sparkle in hand sample indicates the presence of mica. A) Is an image of Fls in Sc12-112 core B) Shows syneresis crack within Fls lithofacies from Chamberlain Creek area.

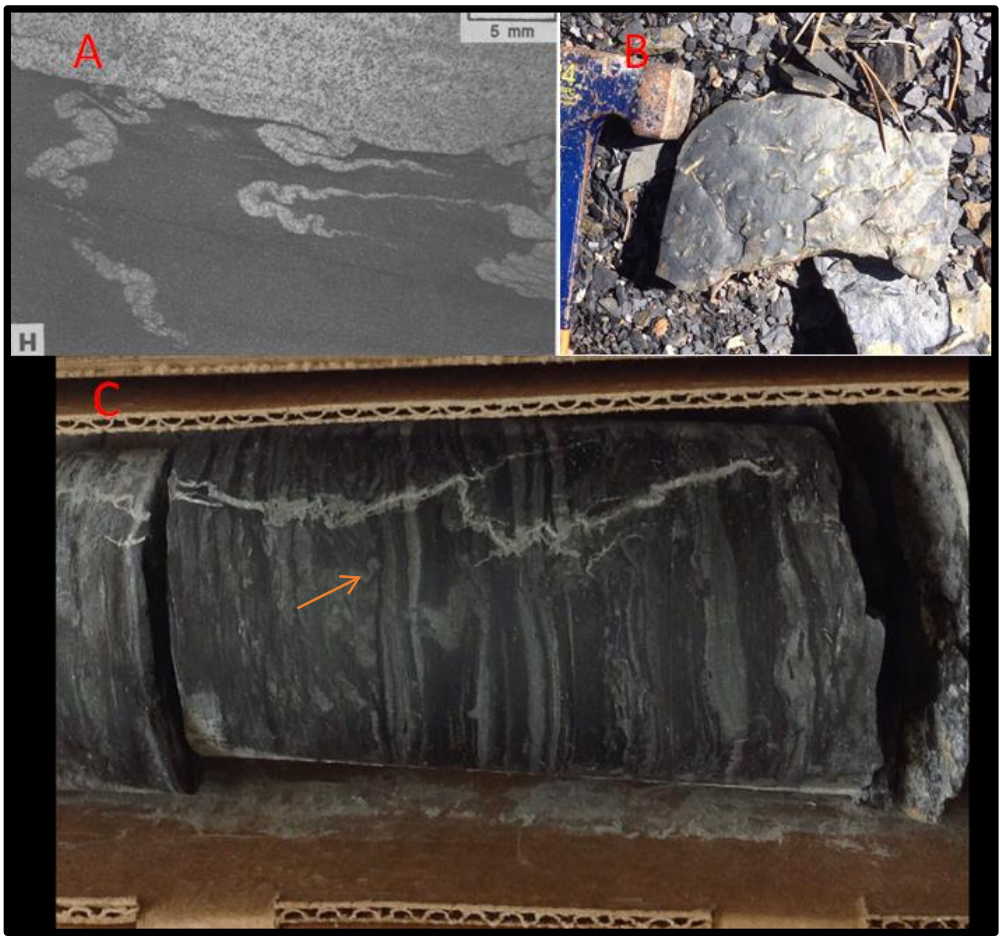


Figure 13. A) Image of syneresis cracks or "tornado" structures from Pratt 1990. B) Syneresis cracks seen in Fls lithofacies. C) Chamberlain shale from Sc12-112 well showing tornado structures (red arrow) and soft sediment deformation within the silty light beds.

Lithofacies (Se): Erosional Scours

Se lithofacies is a sandstone to siltstone composed of well-rounded to sub-rounded arkosic sandstone and sandy siltstone with beds up to 15 cm (6 in) thick that have normal grading. Bedform architecture is concave-up lenses or sheets within Fcs. Se grain size increases upward. At the first onset of the Se lithofacies in lower Chamberlain Creek, the concave-up forms are roughly 50.8 cm (20 in) thick as seen in Figure 14. Further up Belt Creek the edges of Se bedforms are not seen, and appear sheet like, with

primarily course- to fine-grained sub-rounded and moderately-sorted arkosic sandstone and siltstone.

Interpretation

Erosional truncation and channel forms with coarse-grained clasts infer a high energy environment of deposition. Channel forms and silty sheet within Se support a channelized system. The silty sheets likely represent crevasse splays which were formed by the breaching of levees within the channelized system and the finer suspended load was deposited distal to the channelized system.

Lithofacies (Fl): Plane Bedded Siltstone

Fl is a dark brown siltstone to claystone with plane parallel beds up to 10 cm thick. Fl lithofacies is found in the Chamberlain Formation along Belt Creek, but was not seen in the Sc12-112 core to the south of the VVF.

Interpretation

Plane parallel bedded siltstone beds were deposited as overbank deposits from the Es lithofacies previously discussed. As the flow transitions from confined to unconfined flow breaches the channel levee and rapid depositions occurs.

Lithofacies (Fp): Plane Laminated Mudstone

Fp lithofacies is composed of mudstone, weathers tan, and has a fresh green to dark gray surface. It is plane parallel thickly to thinly laminated and is present throughout the filed area. Fp lithofacies is the most abundant lithofacies along with Fcs lithofacies in this study within the Newland Formation.

Interpretation

Plane parallel laminations within the Fp lithofacies were formed due to the decrease in flow velocity and suspension settling of fines. Lower flow regime plane laminations are often associated with Src and Fcs lithofacies.



Figure 14. Field images of Es. A) Shows a distinct concave up bowl shape of a channel form with erosional truncation of surrounding Fcs beds. Image on the left) the bed next to field notebook is a sub-rounded course arkose. Directly below the pebble arkose bed is a bed of folded silty black shale that looks like a piece of wood. The hinge of the fold is to the right pointing towards the basin.

Lithofacies (Sgc): Graded Calcarious Sandstone

Lithofacies Sgc is a normally graded, calcarious sandstone composed of well-rounded and well-sorted, course- to fine-grained quartz grains. Laminations are not seen in outcrop, and is calcite cemented. The lower bedding plane appears to be erosional but is difficult to see due to differentail compaction and post depositional load structures.

Interpritation

Normal grading within the Sgc lithofacies was deposited through a decrease in flow velocity and settling of larger clasts. Graded bedding is the result of suspension settling from floods and storm events, or more commonly attributed to turbidity currents. The rate of settling of different clast sizes within a waning turbidity current likely accounts for normal grading (Boggs, 2012).

Lithofacies (Src): Ripple Laminated Sandstone

The ripple laminated sandstone lithofacies is composed of medium- to fine-grained quartz grains and silt grains with calcite cement. Grains appear well-sorted and mature. Src has unidirectional cross-laminations, and is typically directly above the Sgc lithofacies.

Interpretation

Src Lithofacies indicates deposition by a current within the lower flow regime. Cross-laminations indicate unidirectional flow and a decreasing velocity that deposits sediment as plane parallel laminations towards the upper bounding surface. Suggesting an episodic flow rather than a constant flow.

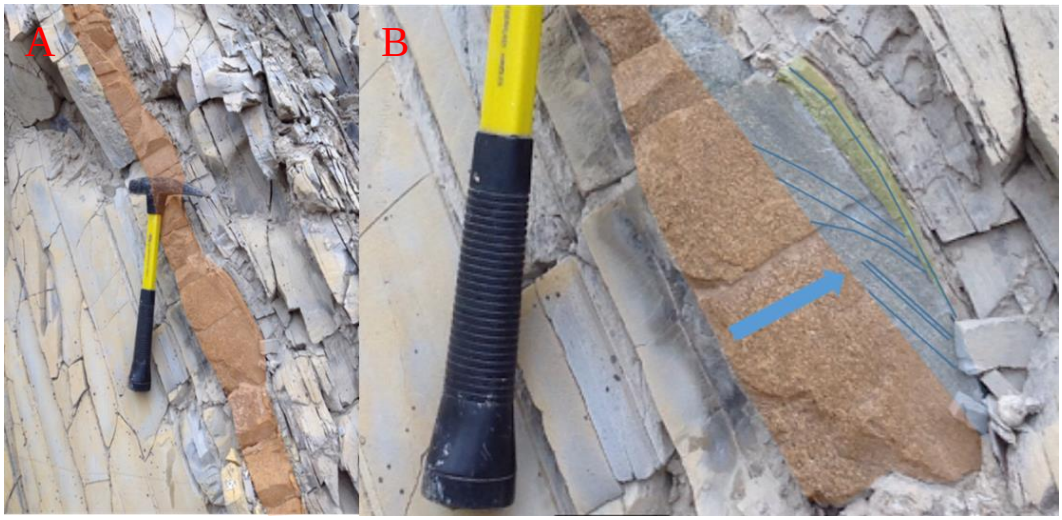


Figure 15. A) Orange bed of Sgc lithofacies within Fcs facies in Deep Creek. B) Zoomed in view of figure A showing Sgc and Src facies (blue) topped by Fcs plan parallel laminated silty shale green.

Lithofacies (Fsc): Fissile Black Shale

Fsc lithofacies is primarly black fissle shale in outcrop, and has claystone, to siltstone and very fine-grained sandstone with wavy laminations and flame structures in core. Fsc is made up of alternating wavy laminations composed of claystone with siltstone lenses. Fsc lithofacies coresponds to Feedback's (1997) clayey black shale facies. Erosional truncation within Fsc facies are present in Chamberlain Creek and Belt Creek. (Figure 16)

Interpretation

The wavy lamination within the fissile black shale is due to a higher rate of deposition of muds then silt and sand. Like Sr lithofacies, wavy laminations indicate transport from wave action bringing sand to a lower energy environment dominated by mud/clay deposition.

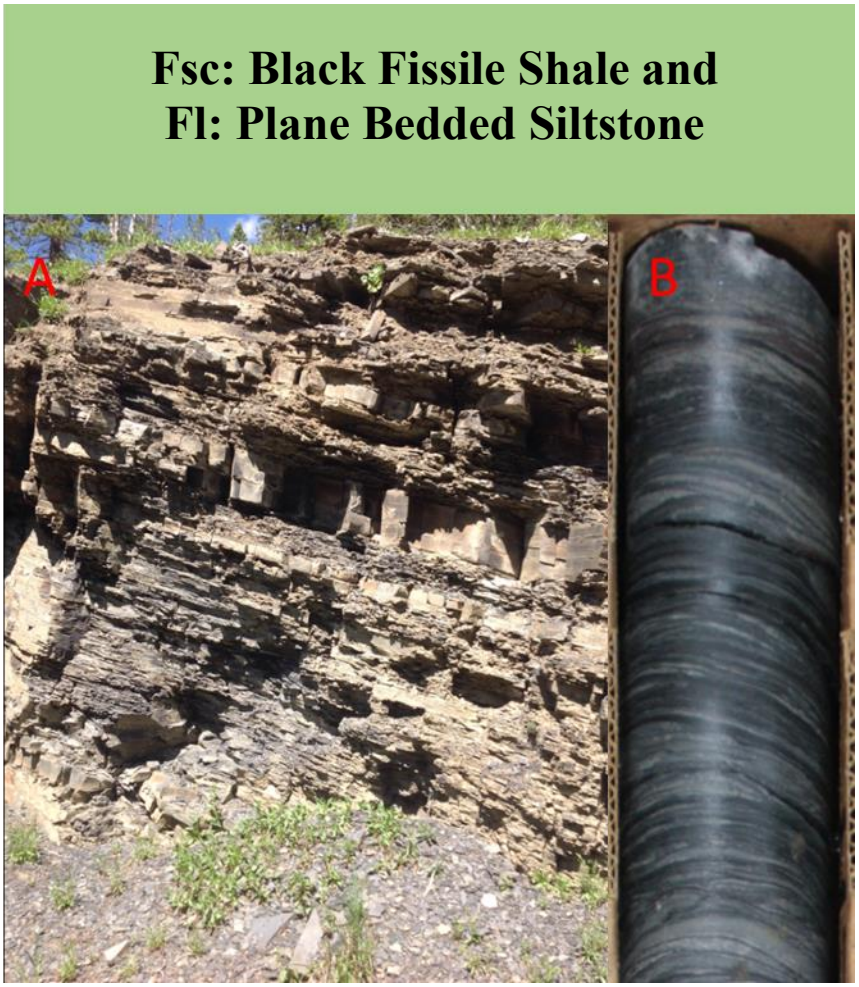


Figure 16. Fsc black silty-shale facies. A) Shows bedding of fissile black shale and sandy-silty interbeds the larger silty interbeds are Fl lithofacies. B) Shows wavy bedding within the Sc12-112 core.

Lithofacies (Lm): Lime Mudstone

Lithofacies Lm is composed of thick- to thin-bedded calcareous micrite with domal lamination, significant molar-tooth structures, and angular rip-up clasts (Figure 17). Lm in Chamberlain Creek has beds up to 2 m (6.5 ft) thick while to the south (towards the basin) in Belt Creek the micrite beds are typically < 25 cm (10 in) and domal laminations are no longer present but crinkly laminations are seen. Crinkly laminations are interpreted to indicate the presence of microbial mats (Schieber, 1989).

Interpretation

Domal laminations, rip-up clasts, and molar-tooth structures support a primarily shallow water depositional environment with occasional storm events. The rip-up clasts are made of the surrounding micrite and were likely lithified as hard ground close to the sediment water interface prior to being ripped up by storm events. Domal laminations and molar-tooth structures are characteristic of cryptal algae and further support a very low energy environment of deposition with periodic high energy storm events. Lyons (1998) determined the molar-tooth structure within the Helena Formation of the Belt Basin to be formed by the process of gas bubbles ascending through unlithified calcareous mud close the sediment water interface in a shallow primarily marine environment. Gas bubbles that flowed through the micrite mud created voids were then filled with calcium carbonate. Possible mechanisms include variations in the microbial uptake of CO_2, temperature changes, fluctuations in water depth, or salinity changes associated with cycles of evaporation and flooding, resulting in rapid precipitation of calcium carbonate into the voids (Frank and Lyons, 1998).

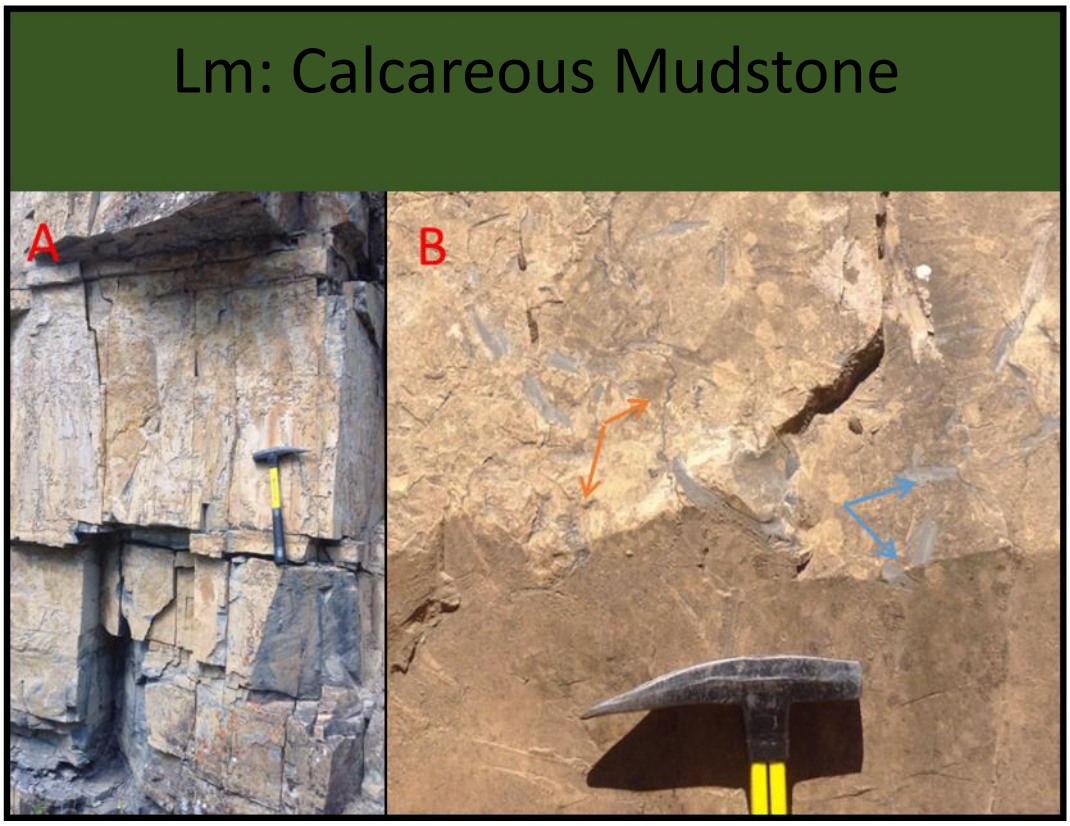


Figure 17. Images of Lm in Chamberlain Creek showing thick bedded micrite (A). Sedimentary structures include domal lamination, significant molar-tooth structures, and angular rip-up clasts within the micrite. (B) Orange arrows pointing towards molar-tooth structures and blue arrows are pointing to rip up clasts.

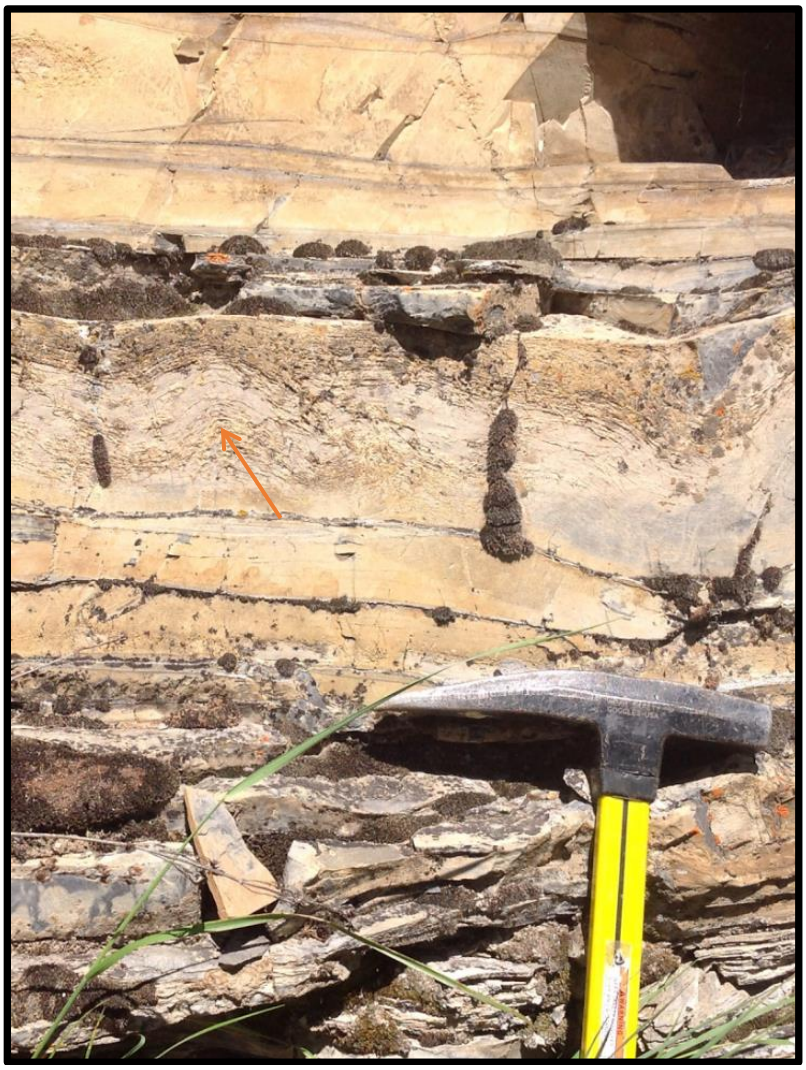


Figure 18. Domal structures characteristic of stromatolites within Lm lithofacies in the Chamberlain Formation along Chamberlain Creek indicated by the red Arrow.

Lithofacies (Fcs): Calcareous Shale

Fcs lithofacies is primarily poorly exposed tan calcareous shale that is seen as float in outcrops. When outcrops are present and in core the Fcs facies is thinly laminated gray to black calcareous shale that weathers tan and white. The gray laminations are dolomite while the black shale is primarily calcareous (Feedback, 1997). The Fcs

lithofacies is equivalent to Schieber's (1998) striped shale facies, Feedback's (1997) silty black shale and dolomitic shale facies, and Zieg's (1981) Lower Newland.

Interpretation

Abundant plane parallel lamination and the lack of other sedimentary structures within Fcs, along with a composition of primarily silty black shale and either calcite or dolomitic gray shale suggest primary deposition by suspension settling.



Figure 19. Outcrop of Fcs facies showing primarily tan weathered float. Outcrop is roughly 3.2 m (10 ft) in Miller Gulch. Core of Fcs facies showing plane parallel laminated striped shale.

Lithofacies (Ccl): Cross-Laminated Silty Microspar

Ccl lithofacies is made up of thin- to thick-bedded silty microspar up to 12.5 cm (5 in) thick in Decker Gulch and up 30 cm (12 in) in Swimming Woman Canyon. Weathered surfaces are tan and fresh surfaces are gray. Isolated silty ripple cross-laminations are present, but the primary sedimentary structure is plane parallel laminations separated by thin plane parallel laminated fissile shale. The Ccl facies is equivalent to Zieg's (1981) Unit 1.

Interpretation

Plane parallel laminations within the silty microspar were most likely deposited from settling from suspension. While the isolated cross-laminations suggest deposition by currents within the lower flow regime. Microspar precipitation is caused by the over-saturation of the basin water (Zieg, 1981). However, the diagenetic overprint within these beds is deceiving as the carbonate beds tend to pinch and swell, due to secondary diagenesis, and differential compaction.



Figure 20. Upper image showing cross-laminations in Ccl lithofacies. Lower image is the contact between Fcs and Ccl lithofacies (Miller Gulch). Red line is bounding surface with no erosional truncation seen.

Lithofacies (Ccn): Microspar

Ccn lithofacies is similar to Ccl lithofacies but contains black chert nodules (Figure 21). Ccn lithofacies is equivalent to Zieg's (1981) Unit III varies from a calcareous microspar with abundant pressure solution stylolite's, diagenetic mottling, and minimal black chert in Deep Creek Canyon to a dolomitic microspar in Decker Gulch (Godlewsk and Zieg, 1984). Ccn lithofacies has black to gray fresh surfaces and weathers tan. Along highway 12 towards the town of Checkerboard, Ccn lithofacies is a gray dolomitic microspar with very few chert nodules.

Interpretation

Ccn lithofacies with thick beds of microspar suggests a decrease in terrigenous influx, and a time of basin super-saturation, plane parallel laminations indicate deposition from suspension.

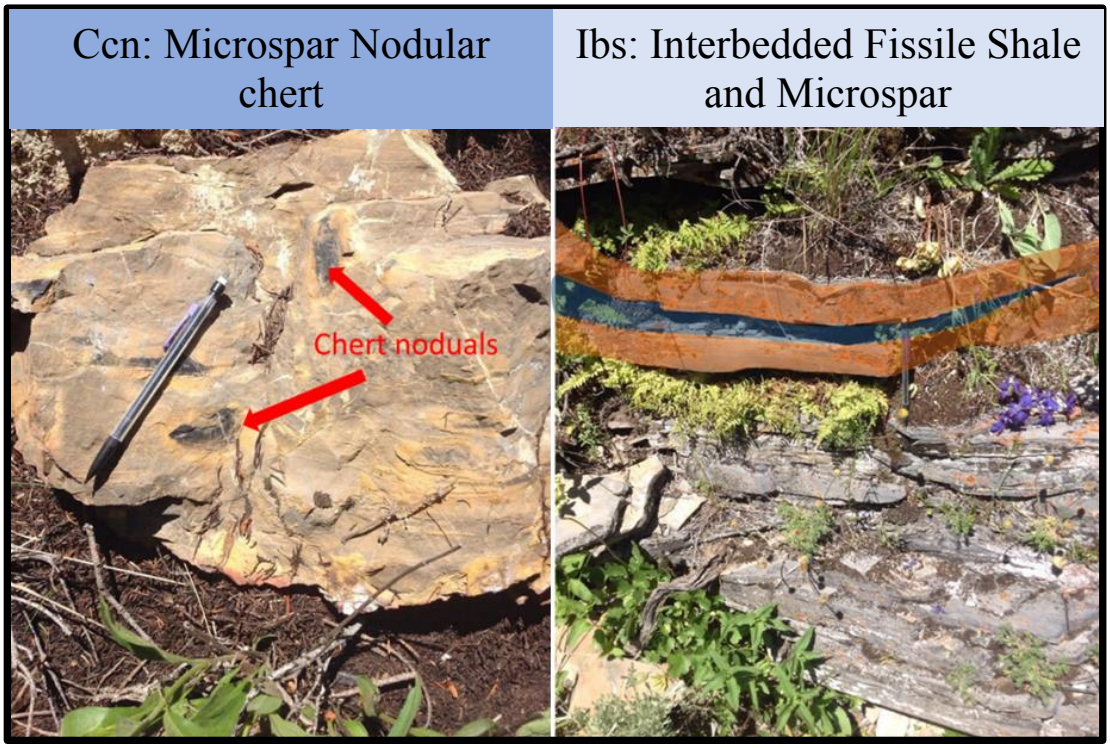


Figure 21. A) Ccn lithofacies has distinct chert nodules. B) Ibs lithofacies orange represents micrite beds and blue represents shale from Decker Gulch, Zieg's unit IV. Pencil for scale.

Lithofacies (Ibs): Interbedded Microspar and Calcareous Shale

Ibs lithofacies is composed of interbedded grey microspar and calcareous silty shale. This lithofacies has significant pinch and swell of beds due to dissolution (pinch) and precipitation (swell) of calcite. Ibs lithofacies corresponds to Zieg's unit IV and VII.

Interpretation

Plane parallel laminations of the Ibs lithofacies support a primary deposition from suspension. The alternating beds of microspar and calcareous shale indicate a balance between terrigenous deposition either by suspension settling or currents and precipitation of calcite.

Lithofacies (Fsn): Fissile Shale with Microspar Nodules

Fsn is dark brown- silty shale, fissile in outcrop, with interbedded nodular black microspar, and undulating microspar beds. Primary sedimentary structures are plane parallel lamination and asymmetrical cross-laminations. Fsn lithofacies is equivalent to Zieg's Unit II and V. (Figure 22)

Interpretation

Cross-laminations within Fsn are asymmetrical indicating a unidirectional flow. Because the majority of the laminations and bedding are plane parallel these are interpreted as bottom currents in a deep water depositional environment (Zieg, 1981). The undulating bedding planes of the calcareous beds and shale interbeds are due to early diagenesis in the burial process. This is evident through laminations passing through the concretions.

Lithofacies (Cpl): Plane Parallel Laminated Microspar

Cpl lithofacies is composed of thin to thick beds of gray dolomitic microspar (M) with thin to thick plane parallel laminated shale interbeds. Cpl lithofacies is equivalent to Zieg's unit VI which is often referred to as the contorted carbonate (personal

communication with Zieg) due to it being more faulted and folded than the other units. The gray microspar often shows diagenetic mottling and pressure solution stylolites. Cpl lithofacies is a major ridge forming unit (Figure 22)

Interpretation

Plane parallel lamination within the Cpl lithofacies was deposited through suspension settling. The presence of thick beds of microspar support a decrease in terrigenous influx, and a time of basin super saturation that allowed for carbonate precipitation.

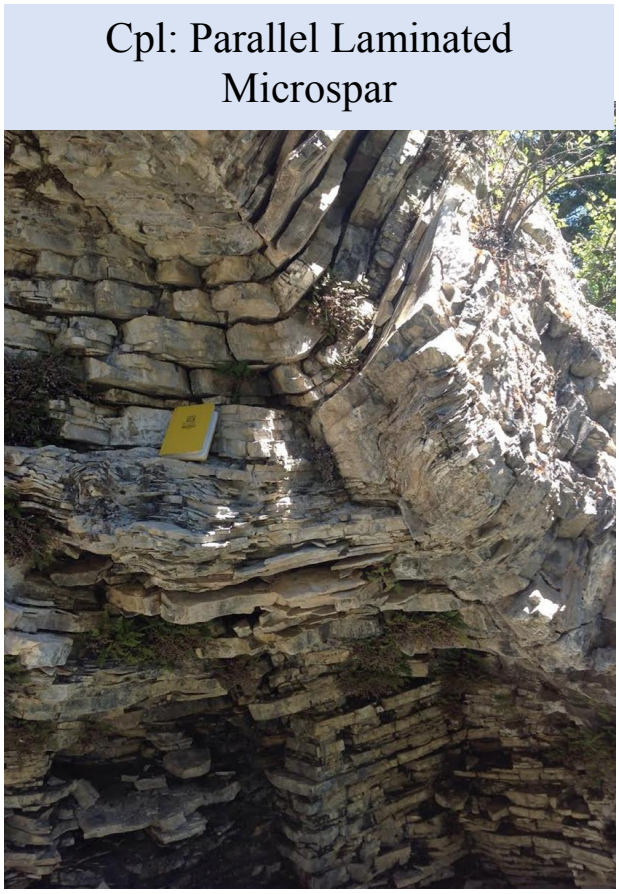


Figure 22. A) Concretion within the FS lithofacies, image taken from Decker Gulch. B "contorted carbonate" of the Cpl lithofacies and Zieg's unit VI from Decker Gulch. Field notebook for scale

Diagenesis

Diagenesis within the Newland Formation as well as LaHood Formation has been well-documented by Zieg (1981), Schieber (1990), and Fox (2017). A detailed description of diagenetic features within the Newland Formation can be found in Zieg (1981). Two diagenetic structures were seen across the field area will be discussed: mottling, and concretions.

Mottling fabric was seen in microspar across the field area. This texture was first described by Walcott (1899) as "Newlandia" and originally thought the evidence for

microbial life. Mottling texture is the result of pressure solution within the silty clay beds of the primarily calcareous lithofacies (Ccl, Ccn, and Cpl). Zieg (1981) and suggests that pressure solution initiated along stylolites, and continued into microspar beds to form the mottling texture (Figure 23).

Concretions were found in the Chamberlain, and Newland Formation along Belt Creek, Deep Creek and Swimming Woman Canyon (Figure 24). Concretions occur isolated within silty shale beds (Figure 22) or as bedding that pinch out laterally. These concretionary beds are abundant along Newlan Creek and without close investigation looked like scour and fill structures. However, upon close examination, the thin laminations are seen to continue through the concretion and the thin laminations within the shale interbeds are seen wrapping around the concretions. These concretions were likely formed due to over burden of calcareous beds within the primarily silty shale beds. (Figure 25). This digenetic feature was seen throughout the field area and were not diagnostic.



Figure 23. Mottling within in the Ccn lithofacies at Checkerboard location quarter for scale



Figure 24. Small concretions on the sole of a thin Ccl bed from Swimming Woman Canyon.



Figure 25. Walcott's Newlan Creek type section and Zieg's unit VII, A) Orange represents calcareous beds that pinch a swell but are not laterally extensive along Newlan Creek. Blue area represents the shale interbeds. B) Is an outcrop also within Walcott's Newlan Creek type section without any calcareous beds?

FACIES ASSOCIATIONS, DEPOSITIONAL SYSTEMS, AND STRATIGRAPHIC CORRELATIONS

Lithofacies Associations

This project recognized 18 lithofacies within the Neihart, Chamberlain, and Newland Formations. These lithofacies were grouped into 7 lithofacies associations based on similarities of grain size and hydrodynamic processes during deposition. Facies associations are presented below with decreasing energy based on hydrodynamic interpretations from the previous chapter.

FA1:

Lithofacies association 1 is composed of lithofacies Sm Sr, St. The Sm lithofacies as described above is primarily a mature course- to fine-grained arenite with tabular to trough cross-laminations. Winston (1989) described what this study defined as the Sm lithofacies as a continental sand sheet composed of eolian and fluvial environments. Schieber (1989) described the Neihart as a fluvial system that was a shallow (~2 m), broad (ten to hundreds of meters) braided system, and also reported seeing reverse graded lamina with low angular truncation associated with foreshore deposition.

Sr lithofacies is composed of fine sand to clay size grains ripple laminations and lenticular lamination. The lenticular bedding suggests an environment that's influenced by currents. Though common in tidal environments, nothing in outcrop or core suggests these sediments were tidally influenced (e.g. herringbone cross stratification). Lenticular

bedding can be the result of episodic flooding or weak storm events(Dalrymple, 2010) and is consistent with the interpretations of this study .

Symmetrical ripples within the Sr facies suggests an oscillatory flow most likely produced from waves in a shallow water environment. FA1 was likely deposited in a beachfront with lagoon areas where the greenish claystone was deposited.

FA2:

Lithofacies association 2 is made up of Se, Fl, Sfl, and Fsc lithofacies. Fsc has predominantly wavy–lenticular bedding with far less mature quartz arenite than the fluvial to beach front of FA1. The abundance of silty claystone and black shale suggests a relatively low energy environment. Lenticular bedding supports a depositional environment above wave base, and the smaller fine-grained sandstone to siltstone interbeds indicate less input from potential beachfront or longshore drift. This is indicative of a more distal facies than the FA1. Sfl is likely a mud flat which corresponds to previous interpretations (Godlewsk and Zieg, 1984). Syneresis cracks are present and formed sub aqueously from changes in salinity and deflocculating of swelling clays, further supporting the mud flat environment proposed by Godloski (1984).

Sfl within FA2 is primarily black fissile shale within outcrop, and has wavy silty laminations in core indicative of a wave action. The alternating sandstone and claystone laminations to thin bedding supports an above wave base environment of deposition. Flame structures seen in Sc12-112 indicate rapid deposition of sandstone onto mudstone likely caused by storm events. Se has erosional bedding planes within the Fsc lithofacies.

This is a basinward shift of facies and could be attributed to lowering of base level or increased sediment supplied to the basin.

FA 3:

Lithofacies association 3 is composed of Lm lithofacies with it's thick- to thin-bedded micrite which was likely deposited in an isolated (low energy) lagoonal setting with little to no terrigenous input. The formation of microbial mats and domal stromatolites has been linked to intertidal or subtidal environments (Buerke., 1987). Tidal influence is not a precursor to domal structures or microbial mat growth and many from in lacustrine environments. The main characteristic for microbial mat growth is within the photic zone. Based on the frequency of molar-tooth structures, and micrite ripup clasts, FA3 was likely deposited in a shallow water isolated lagoon or lacustrine environment with abundant microbial life and infrequent storm events.

FA 4:

Lithofacies association 4 is made of lithofacies Gsm. Gsm is characterized by thick bedded conglomerates and chaotic bedding, Gsm lithofacies represents the basin slope and slope failure. Major slumping along the northern margin occured after the onset of Newland deposition caused by down to the south movement along the Buttress Fault during Lower Newland time as seen in the Gsm lithofacies .

FA 5:

Lithofacies association 5 is made up Sgc, Src, Fp, and Fsc lithofacies . Theses Lithofacies also represent the basin slope to basin floor and are interpreted as turbidite and distal turbidite deposits (Figure 26 and

Figure 27). McMannis (1963) characterized the distal turbidites, that only contain the Src lithofacies in this study, as being sourced from the north and west and the larger grained turbididty flows as being deposited from the south. Detrital zircon geochronology has supplied evidence that Sgc lithofacies was sourced from the south or east of the Helena embayment (Chapter 5). Src and Fsc lithofacies show amalgamated packages of Bouma sequences (Figure 26).

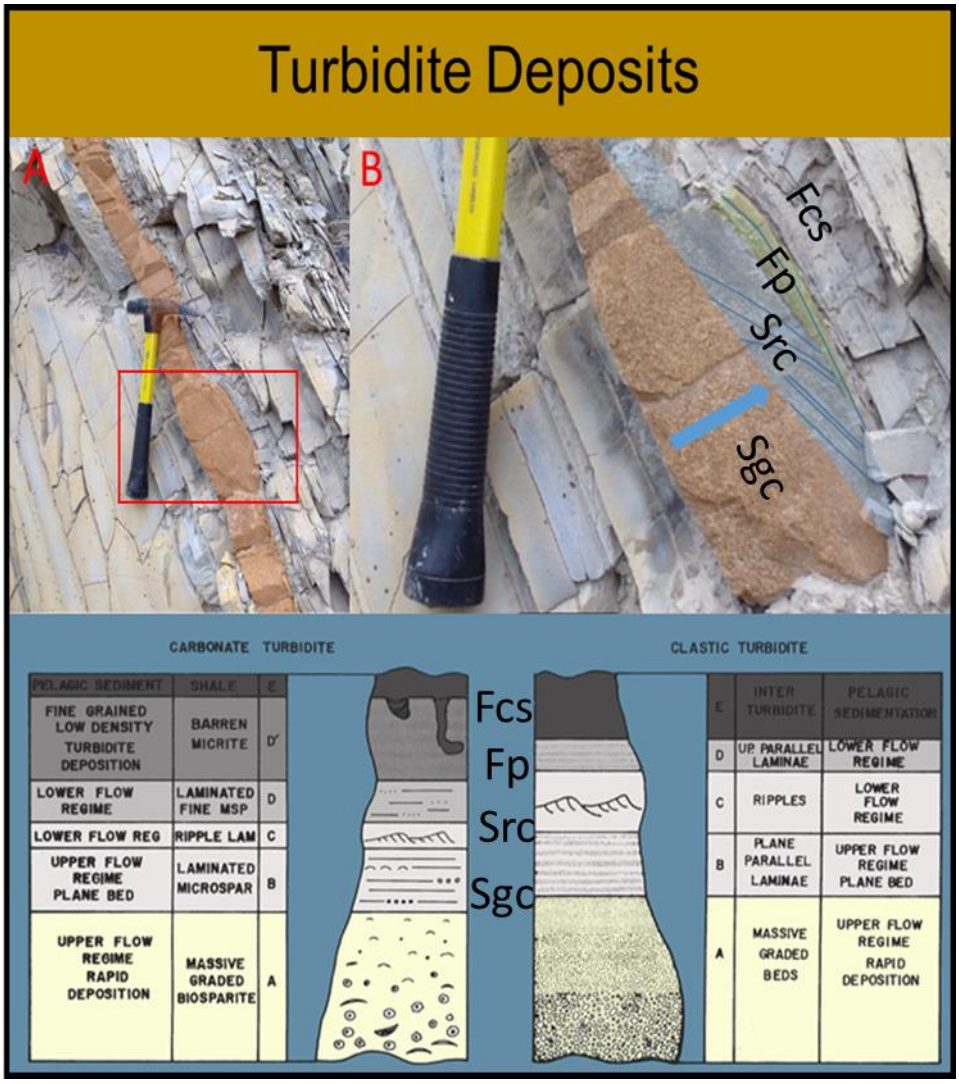


Figure 26. A). Orange shaded area is a Gcs sand bed within the Fcs lithofacies of the Lower Newland. The wavy top (to the right) is due to differential compaction which likely altered the bedding. B). Zoomed in view of A) Orange unit is medium to coarse grained Gcs lithofacies or A –B unit of the Bouma sequence, blue arrow shows the direction of fining upwards. The Blue bed with cross-laminations is equivalent to the C unit of the Bouma sequence. The bottom figure shows sedimentary structures associated with clastic and carbonate turbidite deposits and associated flow regime. (mcz.harvard.edu) modified from Mehrtens 1992

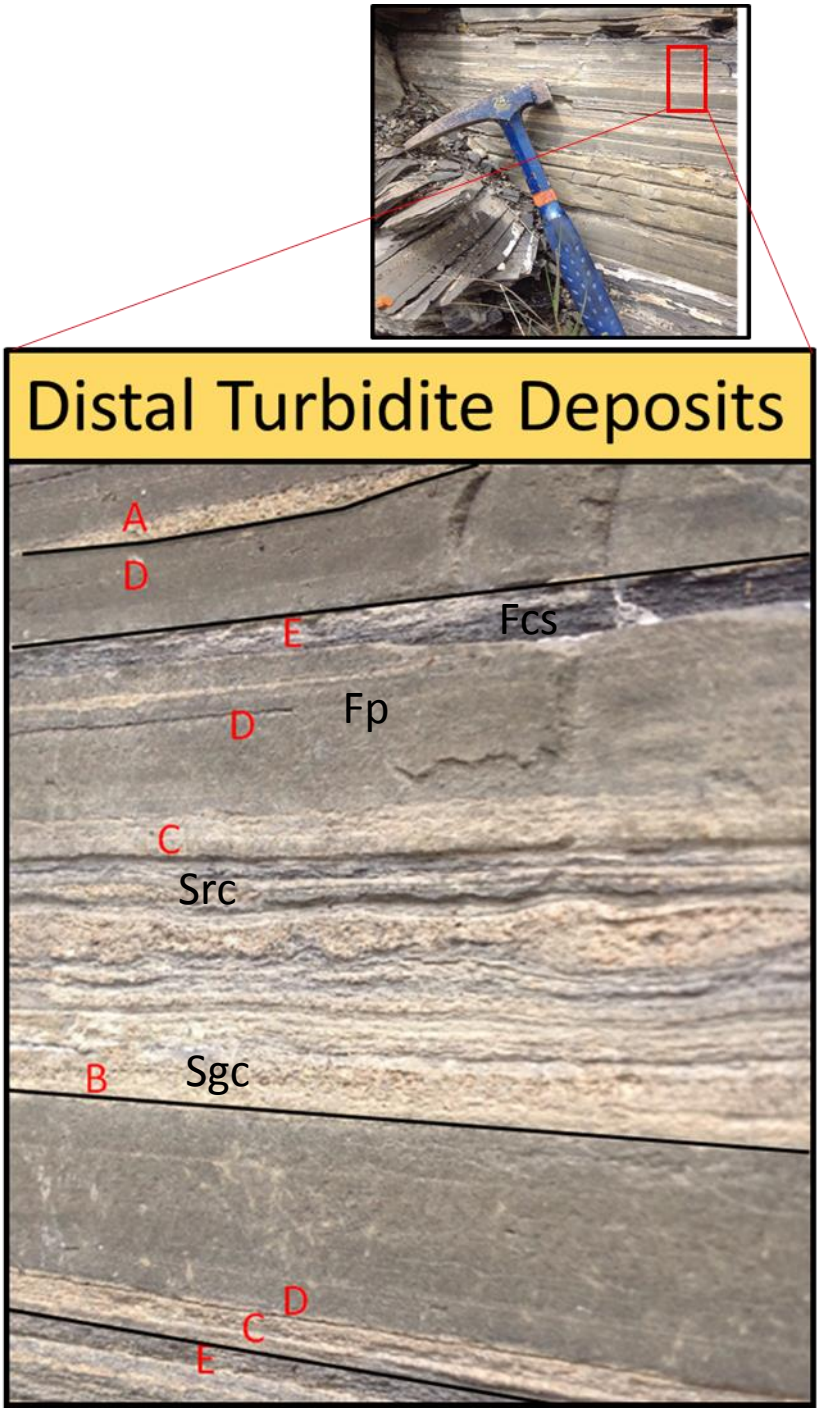


Figure 27. Lithofacies – Distal turbidite – Bouma sequence stacking is seen within Sgc and Fcs silty shale units. Unit A of the Bouma sequence is not always present. Also, notice that each sequence is not complete. Newlan Creek

FA 6:

Lithofacies association 6 is represented by Ccl, Ccn, and Cpl. These units are made of thick to thin microspar beds that were deposited during super saturation and low sediment supply to the basin. Though several characteristics differentiate these units such as black chert nodules in Mnc, they all represent a decrease in sediment supply to the basin and an increase of carbonate production Zeig (1981).

FA 7:

Lithofacies 7 is composed of Fsn and Ibs lithofacies. These lithofacies are adjacent stratigraphically with the FSn facies being directly above the Ibs facies. These are again deepwater depositional through traction transport as first described by Zieg (1981). The Ibs lithofacies marks the transition from primary precipitation of carbonate to terrigenous deposition.

Facies Association	**Lithofacies**	**Depositional environment**	**Formation**
FA1	Sm, Sr, St	Upper shoreface	Neihart
FA2	Fl, Fls, Se, Fsc	Mudflat to shelf distributary channels	Chamberlain
FA3	Lm	Lagoonal – mudflats (carbonate)	Chamberlain
FA4	Gsm	Fault margin / basin slope	Lower Newland
FA5	Sgc, Src, Fp, Fcs	Basin slope, floor	Upper and lower Newland
FA6	Ccl, Ccn, Cpl	Slope/ floor	Upper Newland
FA7	Fsn, Ibs	Slope/ floor	Upper Newland

Table 2. Faceis association

Stratigraphic Correlations

An east-west cross section was done to correlate the easternmost outcrops of the Belt Supergroup to those well documented outcrops within the Helena salient. Below is a brief description of a north-south and an east-west interpretation. Graphic logs can be found in Appendix A

North –South Interpretation

North-south interpretation was done using previously published data (Feedback, 1991) and field observations by the author along Belt Creek and the Sc12-112 core. The transition of the FA1(foreshore) to FA2 is a correlative shift of facies landward. Two carbonate-terrigenous cycles are seen in the Chamberlain Formation from FA2 to FA3 in Belt Creek, and suggests several transgressive regressive events. The transition from above wave base Chamberlain Formation (FA 2 and 3) to below wave base Newland Formation (FA 5, 6, 7), suggests a deepening event occurred at the onset of Newland deposition. As seen in Sc12-112 and described by (Graham, 2012). The Lower Newland is present in the Foot Wall of the Buttress fault as well as north of the present day Volcano Valley Fault in Belt Creek. This suggests the major deepening event occurred prior to faulting along the Buttress fault.

The thickness of the Chamberlain Formation in the allocthonous Belt Creek is 360 m (1181 ft) thick (Feedback, 1997). The thickness of the autochthonous Chamberlain formation within the Sc12-112 well is only 110 m (360.9 ft) at most. Lm and Gcs are not present in Sc12-112, but are in

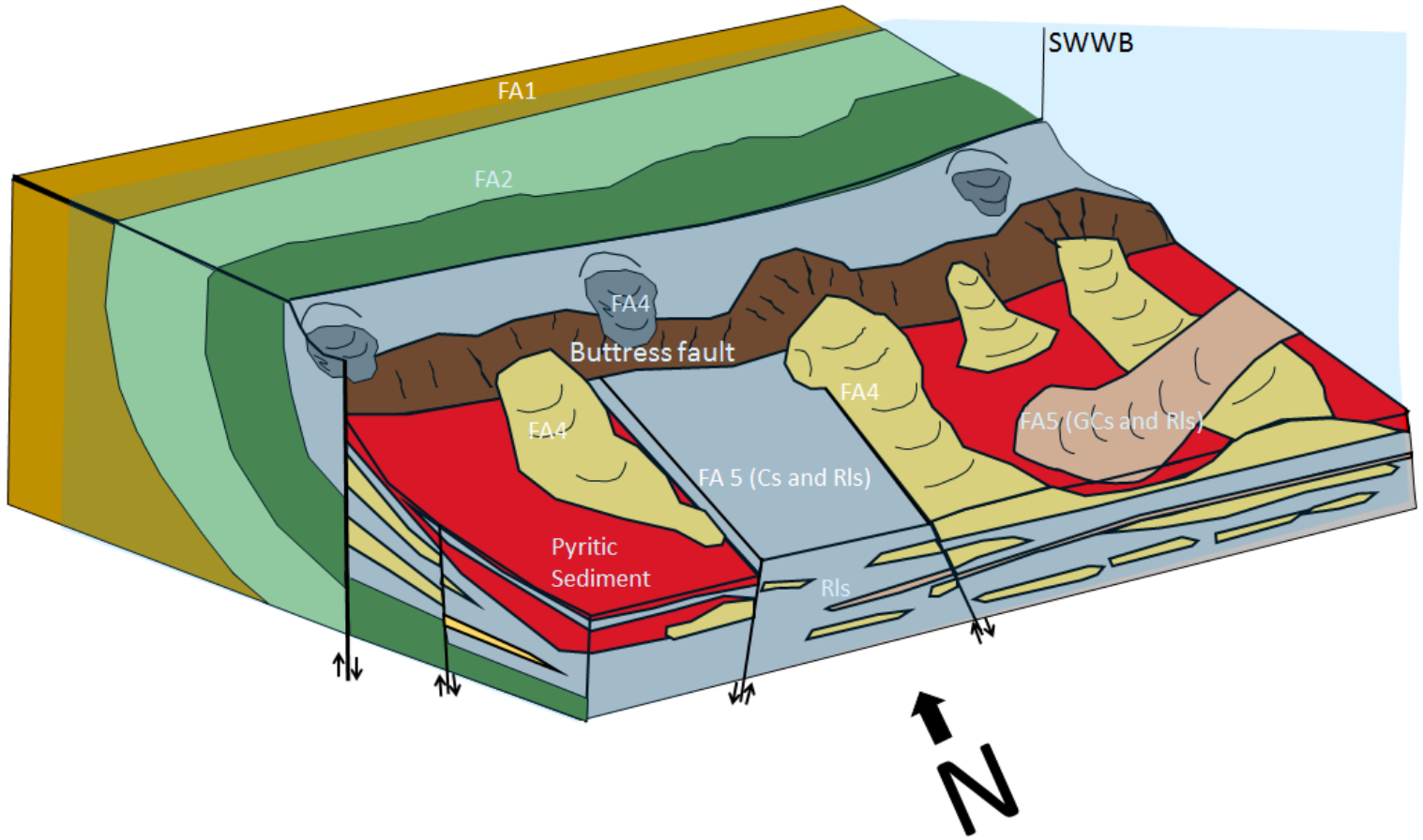


Figure 28. Block diagram of the northern margin of the basin. Labels represent facies association and storm weather wave base (SWWB) is shown at the transition from the Chamberlain and Newland contact. Modified form Graham, (2012)

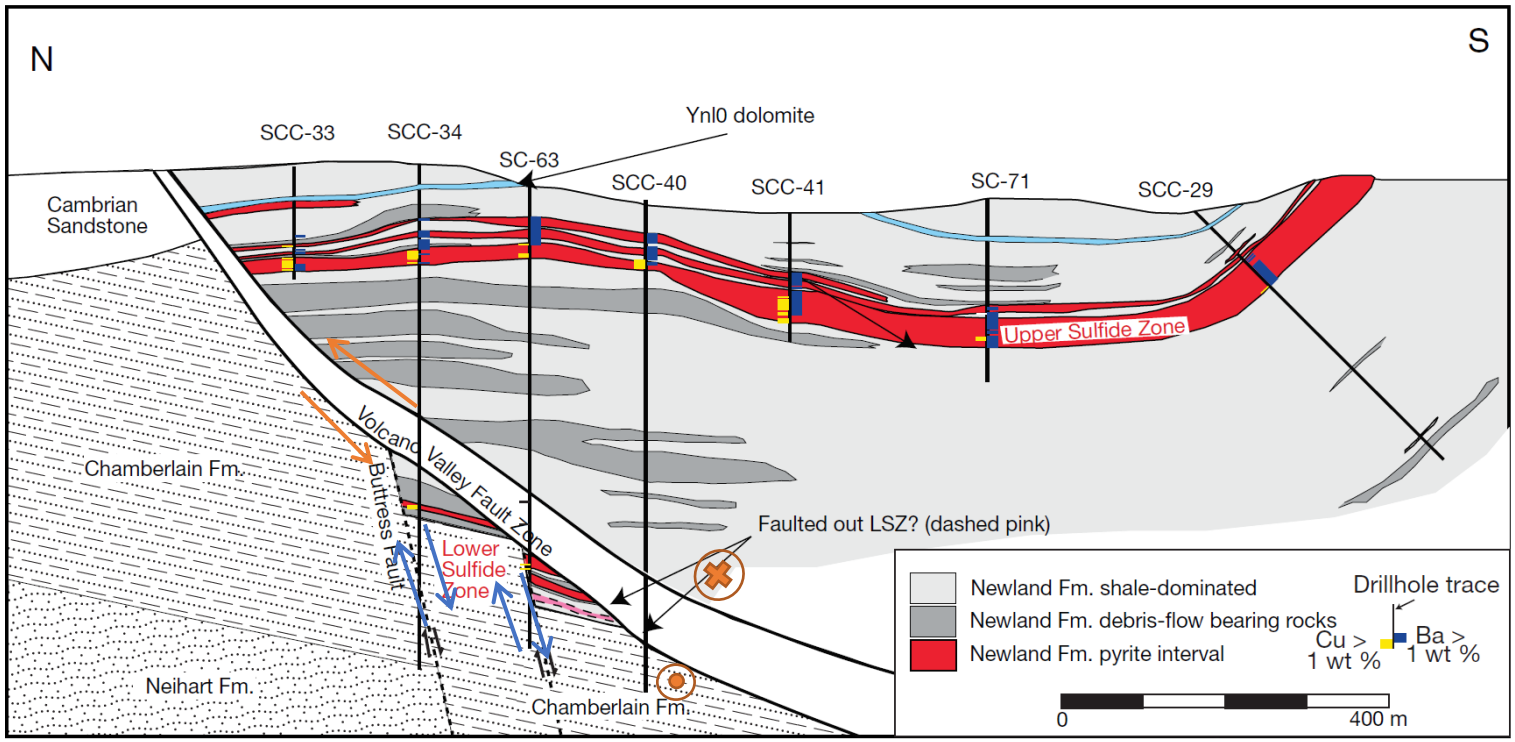


Figure 29. Showing down to the south block faulting at the onset of Newland deposition by thickening of the sediment on the down dropped blocks. Blue represents Proterozoic movement, and orange represents displacement during the Sevier orogeny (modified for Graham et al., 2012).

Belt Creek. The boundry between the Chamberlain-Newland Formations appears gradational in the Sc12-112 core, but is heavily disturbed due to faulting and slumping within the core.

East-West Interpretation

The east-west cross section includes: Deep Creek, Decker Gulch, Newlan Creek, Checkerboard, and Swimming Woman Canyon (Figure 30 and Figure 31). The total thickness of the Newland Formation is not seen in Deep Creek as the measured section cuts through the main N-S trending anticline forming the Big Belt Mountains. Beginning in the Lower Newland the Deep Creek section is made up of primarily FA 5, 6 and 7, however, the FA 4 is not present indicating a distal relationship the basin slope and basin bounding faults. Schieber and Ellwood, (1993) used AMS (anisotropy of magnetic susceptibility) to determine a paleo flow direction for the upper Newland shales to be primarily from the Northwest and south. Moving northeast to Decker Gulch, Newland Creek and significant outcrops in the Sheep Creek area, debris flow deposits of the Gms lithofacies are present, due to the close proximity to the northern Buttress fault. Graham and Zieg (2012) reported debris flow deposits in the hanging wall and foot wall of the Volcano Valley Fault throughout the Sheep Creek area (Figure 8). Moving south east to Checkerboard Ccn and Fsc are present. Dark micrite rip up clasts are seen directly below a Gcs bed with fining upward grading indicative turbidite deposit.

Spanning the Helena salient the easternmost outcrop in Swimming Woman Canyon has FA 5, 6, 7. Three sections were measured in Swimming Woman Canyon for a total thickness of 107 m (351 ft). The onset and thickening of the Ccn lithofacies within

Swimming Woman Canyon supports the interpretation of Lindsey (1990) as being middle Newland.

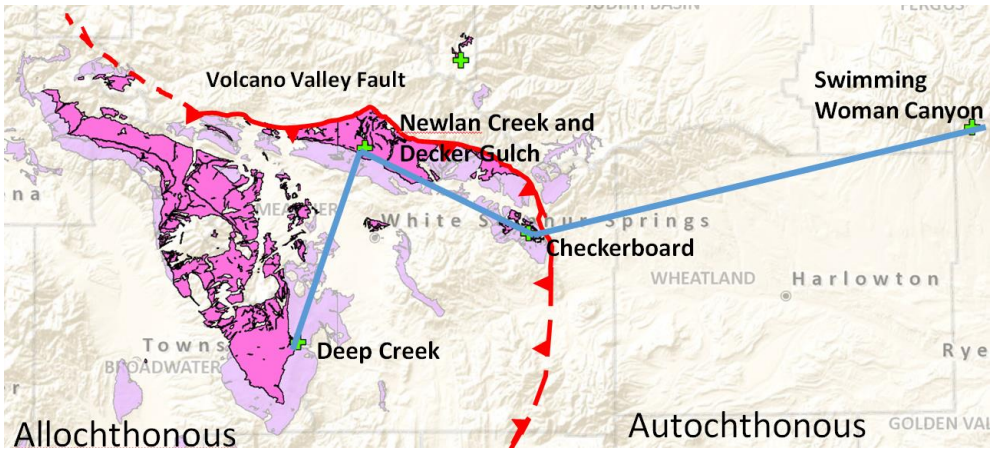


Figure 30. E-W Cross section including Deep Creek, Newlan Creek and Decker gulch, Checkerboard, and Swimming Woman Canyon

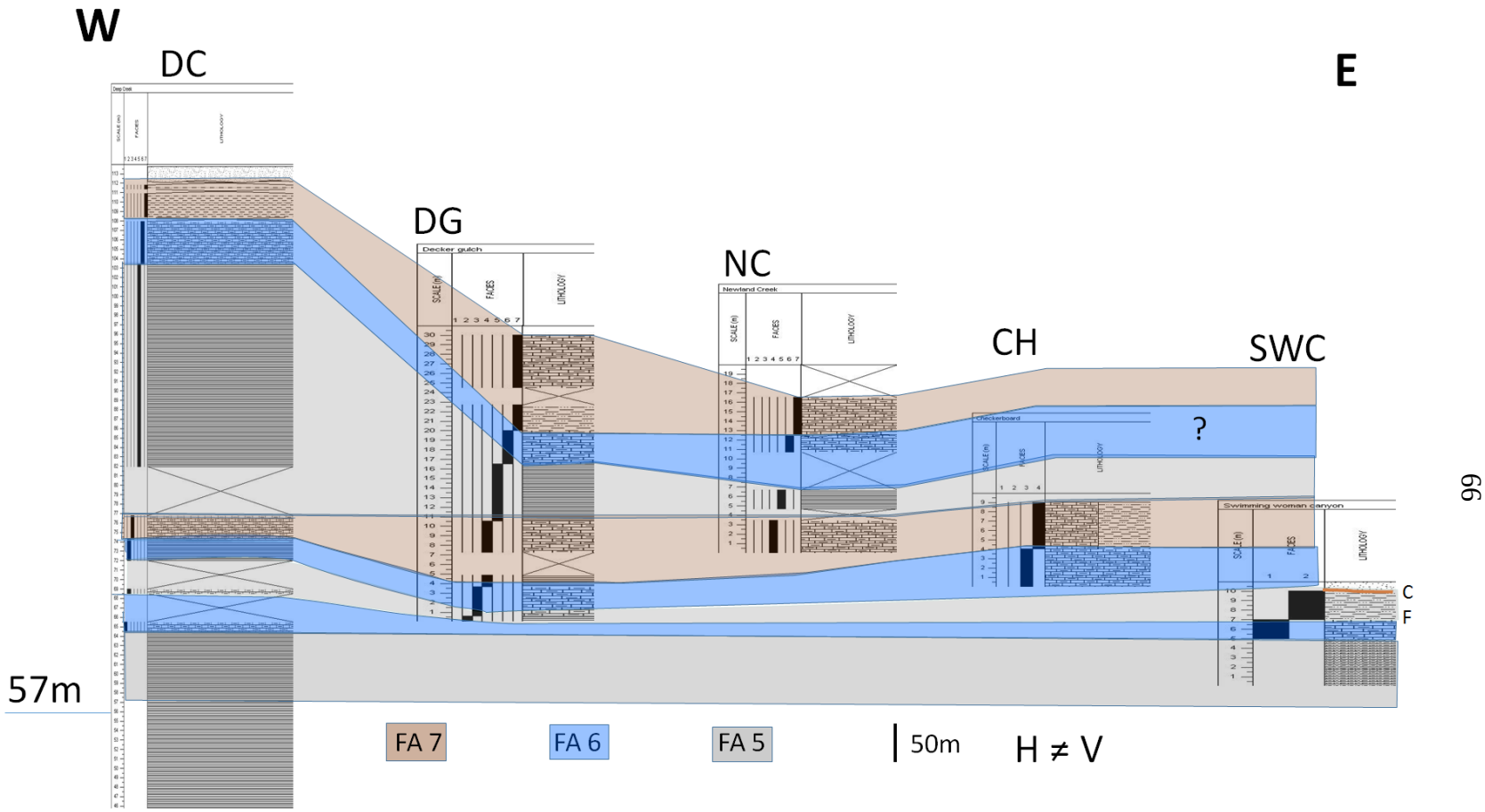


Figure 31. East-West cross section. Dc = Deep Creek, DG = Decker Gulch, NC = Newlan Creek, Ch= Checkerboard, SWC, Swimming Woman Canyon. Due to the size of these measured sections the above stratigraphic columns have been reduced. The scale is 1m/10m horizontal and vertical scales are not equal. Zieg's units and lithofacies from this study are presented.

Discussion

Several depositional environments and facies have been proposed for the Newland Formation. Zieg (1981) proposed the Lower Newland to be the deepest depositional environment within the Helena embayment. Alternatively, Schieber (1989) interpreted the Newland Formation as being deposited in a primarily shallow water environment, though still subtidal. He based his interpretation on the presence of benthic microbial mats. Several supporting features for this interpretation are the presence of wavy-crinkly texture, cohesive behavior during erosion, transport, and deformation, (Schieber, 1998). Although several of these features were seen in outcrop, there was also supporting evidence that the microbial mats or fragments of the mats were transported into the basin. Cohesive bedding interpreted to be a rolled up microbial mat was deposited in Ccl lithofacies bed within Swimming Woman Canyon (Figure 32).

Facies of the Newland Formation found in this study support a below wave base or deep water depositional environment. Supporting evidence for the deposition of the Newland Formation below wave base includes; the abundance of plane parallel laminations and turbidity flows, and Himes and Peterson (1990) used fluid inclusions from diagenetic barite within the Sheep Creek area to determine a water depth of >850 m (2788.7 ft) for the Lower Newland. Hummocky cross stratification was not seen in core or outcrop which would differentiate above wave base deposition from below wave base deposition. Scheiber (1987), reported seeing hummocky cross-stratification within the shales of the Newland Formation. In a petrographic study of the Newland Formation (Ambrose 2005) reported one sample having isolated hummocky cross-stratification from

the Newlan Creek. Feedback (1997) reported seeing hummocky cross-stratification within the black shales of the Chamberlain Formation south of the Volcano Valley Fault.

Based on the absence of hummocky cross-stratification and primarily plane parallel lamina within the Newland Formation, this study agrees with Feedback (1997) placing storm wave base withing the FA2 and Fs lithofacies of the Chamberlain Formation.



Figure 32. Cohesive bedding of microbial mats that ripped up and rolled during transport into the basin.

Conclusion

Expanding the lithofacies description of the northern margin of the Helena embayment allowed for this study to view lateral shifts in facies. Based on the above descriptions and field observations, the Helena embayment has undergone several

transgressive regressive pulses and one major transgressive regressive cycle. Transgression within the basin begins with the onset of the Chamberlain up through the Lower Newland lithofacies (Fcs). Zieg (1981) classified the onset of carbonate beds as a shoaling upward sequence of the Upper Newland and identified 2 shoaling upward cycles.

Lithofacies within Swimming Woman Canyon were identified as the Fcs and Ccl lithofacies. Gms lithofacies was not seen in Swimming Woman Canyon or sections south of Miller Gulch. A distal relationship to the basin margin or slope can be assumed. Fcs and Ccl are the primary lithofacies present in Swimming Woman indicating a very low energy depositional environment (basin floor) during Belt deposition. Based on this interpretation the Belt Basin was much larger then outcrop extent suggests, and likely extended well to the East.

GEOCHRONOLOGY AND GEOCHEMISTRY

Introduction

Geochronological studies, particularly U/Pb dating of detrital zircons have placed important temporal constraints on the depositional history of the Belt Basin. Studies by Frost and Winston (1987), Hall and Veizer (1996), Ross and Villeneuve (2003), Evans (2013), Guerrero et al., (2016), and Fox (2017) have put age constraints on both time of deposition as well as provenance of the Belt Basin. Detrital zircon geochronology in the southern margin of the Helena embayment, particularly of the LaHood Formation, suggests multiple sources and a series of compartmentalized basins rather than a simple down to the north block faulting (Fox, 2017).

Rare Earth Elements (REE) patterns and trace metal abundance of basin shale can provide critical insight into the source area (Taylor and McLellan, 1985). Source rocks are subject to many weathering processes such as erosion, meteoric fluids, transport and deposition, and diagenesis prior to lithification. Chemical fractionation that occurs within sediments during the weathering processes distinguishes sedimentary rock from the source (Schieber, 1990), although many elements (e.g., REEs) are treated as being "immobile" or refractory and therefore represent the original composition of the source area. Based on the elemental partitioning into natural waters and residence time, Taylor and McLennan (1985) determined that Ti, Zr, Hf, Al, Ga, REE, Y, Th, Sc and Co, can quantitatively be used to determine source rocks.

Schieber (1992) conducted a geochemical provenance study on the Newland Formation and determined source rock to be primarily granitic, based on relatively high

Hf content, small La/Th ratios, small contents of Cr, Co, and Ni and a low TiO_2/Al_2O_3 ratio. Ross and Villeneuve (2003) used detrital zircon geochronology within the Belt Basin to further support the paleographic connections of the Mawson craton or Australia as the western source. In their study Ross and Villeneuve (2003) looked at three formations from the Helena Embayment: LaHood, Neihart, and Newland Formations (what they termed the turbidite facies). Schieber (1990) suggests that the source area of the Newland Formation within the Big Belt and Little Belt Mountains are similar if not the same but experienced a greater degree of weathering within the Lower Newland based on depleted REE patterns. The underlying basement within the Helena embayment was determined to consist of Paleoproterozoic granitoid gneisses and migmatites (Mueller et al., 1982). The presence of Archean basement of the Wyoming Province south of the LaHood Formation with distinct ages provides a reliable source for the southern LaHood Formation (Guerrero et al.,2016). Fox (2017) showed detrital zircon ages changed significantly both spatially and temporally up section in the LaHood Formation. Primary older 3.5 Ga zircons from the Wyoming Craton were found in the basal conglomerate facies in Jefferson Canyon and north of Jefferson Canyon, and decreased to 3.2 2.8 and 1.8 Ga to the east within the Horseshoe Hills. In the Bridger Range the primary detrital age is 3.2 Ga. Increased detrital ages of 2.8 and 1.8 Ga are seen moving north within LaHood lithic arkose facies of the Bridger Range. The paucity of provenance data on the Newland Formation necessitated the need for additional data to provide insight on the Newland Formation's role in the complex depositional history of the Helena embayment and Belt Basin.

X-RAY Fluorescence (XRF)

Methods

Major and trace element analysis was done on 45 samples collected throughout the field area within the Newland, Chamberlain, and Grayson Formations. Sample amount and locations are as follows: 12 from the Big Snowy Mountains, 5 from Checkerboard, 3 from Belt Creek, 2 from Chamberlain Creek, 10 from Deep Creek, 2 from Miller Gulch, 1 from Sheep Creek, and 3 from Miller Gulch (Appendix A).

Samples were powdered using a shatter box and filtered through a 60 um filter. Samples were placed in a small plastic bag and analyzed using a Thermo Scientific Niton Xl3t™ goldd+ portable XRF machine. Samples were analyzed using the "Geo test all" to capture all elements within the sample, and were analyzed for four minutes per sample. Data was then downloaded in Microsoft Excel™ where elemental concentrations were converted from parts per million to weight percent values. Major elements, trace metals and Si were converted to oxides using the appropriate Stoichiometric Oxide conversation factors (JCU Australia 2015).

The portable -XRF was used to provide semi quantitative results and was standardized base on USGS standards. However, it did not provide reliable REE abundances. REE partitioning of basin sediments, is critical to depicting basin evolution and therefore should be presented in this study. The following REE data are from previously published studies of different formations within the Helena Embayment. They

are the Newland Formation (Schieber, 1989), and the LaHood Formation (Fox, 2017) and have been chondrite normalized.

Harker Diagrams

The weight percent of major element are plotted against SiO_2. All major elements vs. SiO_2 are depleted for the Newland Formation compared to the North American Shale composite (NASC) as seen in (Figure 33). Several major elements had such low abundances that the P-XRF wasn't able to determine their presence and therefore are not presented. Because this correlation of major elements is designed for clastic detritus into a basin, the resulting data appears depleted for all major elements. Depletion across all elements is due to the abundance of precipitated carbonate (calcite or dolomite) along the northern margin and basin center of the Helena embayment compared to the North American Shale Composite. Terrigenous input increases towards the south as seen in the LaHood shale both at Nixon Gulch and Bridger Range (Fox, 2017) and depletes northward (Figure 33).

SiO2 vs. K2O/Na2O ratios have been used to determine the tectonic setting of the basin and reveal that the Newland Formation was sourced from a primarily passive continental margin (Figure 34) (Schieber, 1992). Chromium and nickel can be used to determine the mafic vs. felsic input into the basin. High concentrations of Cr and Ni would suggest a more mafic source and low concentrations would suggest a felsic source. Samples from Swimming Woman Canyon, Decker Gulch and Checkerboard were compared to Taylor and McLennan's (1985) upper continental crust and bulk Archean

crust. Samples of the Newland Formation show an overall low concentration of Cr and Ni and plot close the upper continental crust of Taylor (1982) (Figure 35).

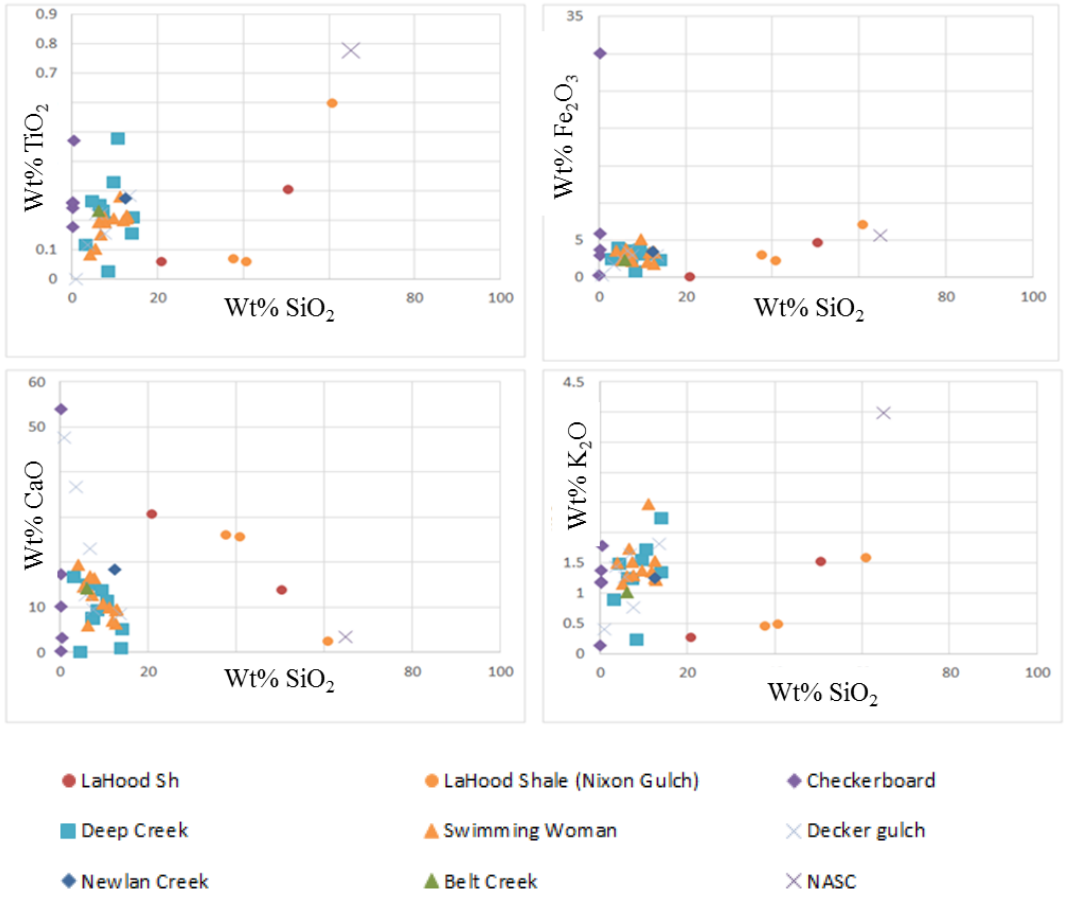


Figure 33. Harker Diagrams shown by location

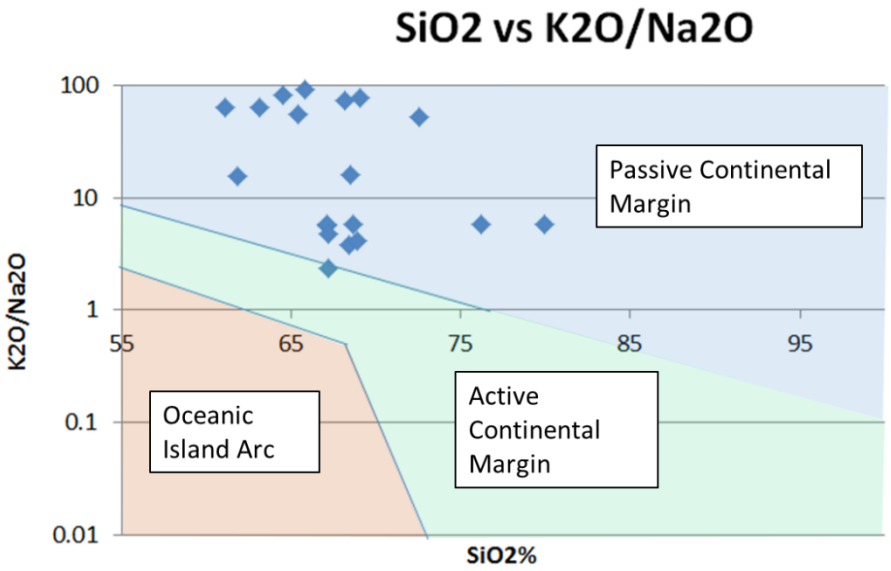


Figure 34. SiO_2 vs. K_2O/Na_2O abundance plot depicting tectonic boundary conditions. Modified from Schieber (1989)

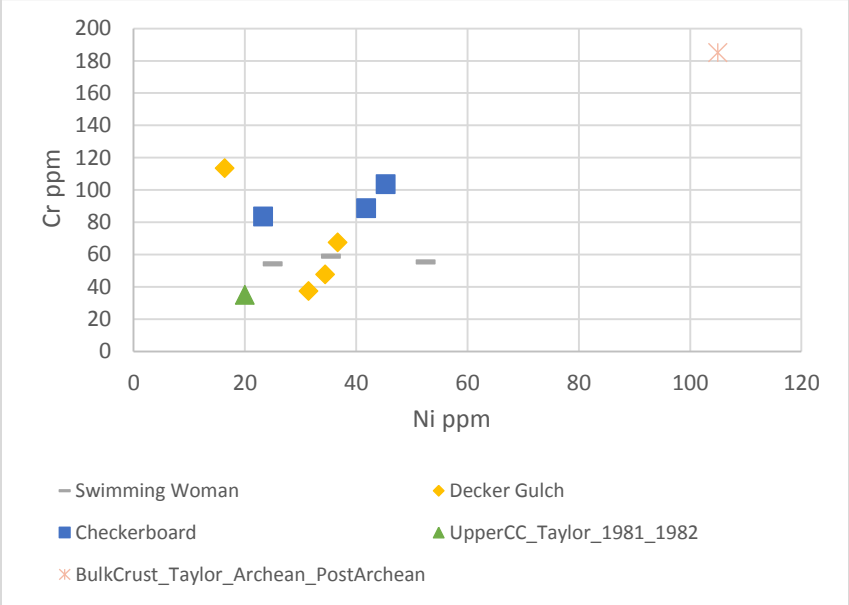


Figure 35. Trace element plot of Cr vs. Ni

Rare Earth Elements

Rare Earth Elements (REE) patterns and trace metal abundance of basin shale can provide critical insight into the source area (Taylor and McLennan, 1985). Source rocks are subject to many weathering processes such as erosion, meteoric fluids, transport and deposition, and diagenesis prior to lithification. Chemical fractionation that occurs within sediments during the weathering processes distinguishes sedimentary rock from the source (Schieber, 1990), although many elements (e.g., REEs) are treated as being "immobile" or refractory and therefore represent the original composition of the source area. Based on the elemental partitioning into natural waters and residence time, Taylor and McLennan (1985) determined that REE can quantitatively be used to determine source rocks.

Results

The average Newland Formation is depleted in both light and heavy REE and it was sourced from evolved upper continental crust due to the enrichment of light rare earth elements (LREE), negative Eu anomaly and depletion of HREE (Figure 36). Data from the Lower and Upper Newland and sandstone packages from Schieber's Newland transition zone (NTZ), Gcs in this study, were chondrite normalized (McDonough and Sun, 1995), and show that the source for all three is relatively the same (Schieber, 1989). LREE, Eu, HREE within the Newland Formation show depleted abundance when compared to PAAS, North American Shale Content (NASC), and European Shale (ES). Depletion within the Newland shale is likely due to low terrigenous input into the basin and increased carbonate production during deposition of the Newland Formation.

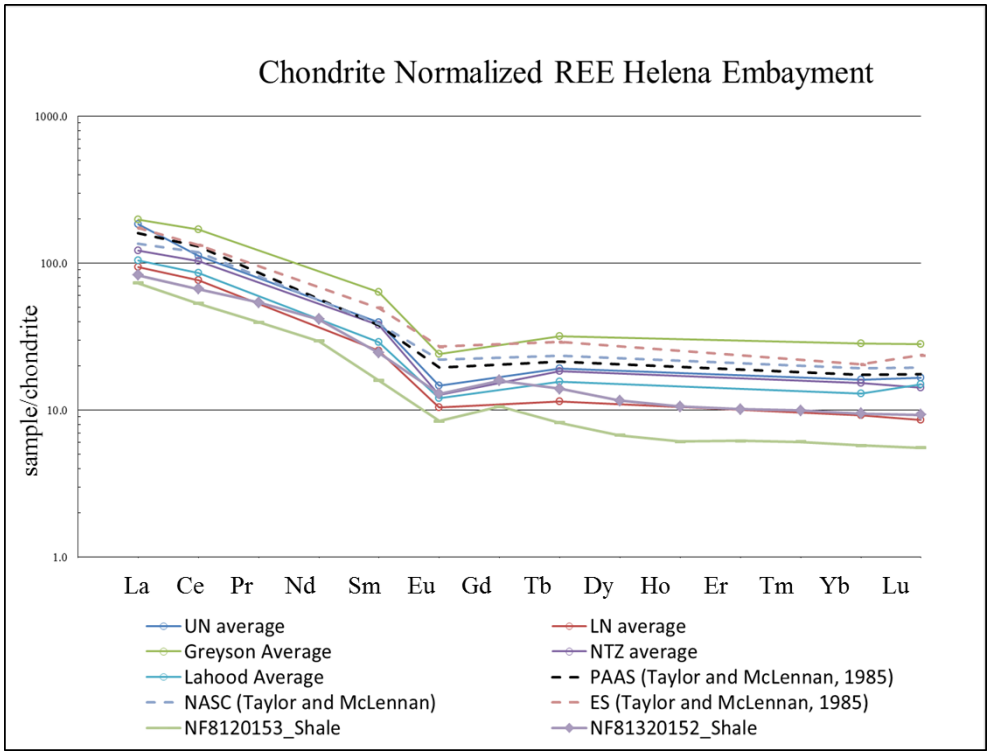


Figure 36. REE spider plot chondrite normalized (McDonough and Sun, 1995) Note that the Upper Newland, Lower Newland, and NTZ show a slight depletion for LREE, EU, and HREE when compared to PAAS or NASC. The patterns are parallel so this may be a dilution effect from restriction of clastics and precipitation of carbonates.

Detrital Zircon Geochronology

Methods

Sample CC-2A was selected for detrital zircon isotopic analysis. CC-2A is from the Gcs lithofacies from the Lower Newland Formation at Carl Creek within the Deep Creek section.

The sample was disaggregated using a jaw crusher and separated using #50 mesh (300 um). The heavy minerals were then concentrated using a Blue Bowl hydraulic separation system to remove lighter minerals such as feldspars and some micas. The heavy mineral concentrate which include zircons accumulate at the bottom of the bowl while the lighter silicate minerals rise in the water and are discarded though the central hole, this step was very dependent on fluid velocity and many of the discarded lighter minerals were processed a second time to collect any potential zircons that were discarded do to water velocity being too high. After blue bowl separation, the sample was left to air dry and separated further using a hand magnet to remove the magnetic minerals.

Further separation and sample prep was done at the University of Florida. Samples were separated using a Frantz Magnetic separator to collect any additional magnetic minerals. After removing the darker magnetic minerals by visual inspection, samples were immersed in Tetrobromethane (TBE). TBE has a density of ~2.96g/cc and therefor further separates the lighter quarts (2.65g/cc) and feldspars (2.56g/cc) from the denser zircons (4.65g/cc).

Zircons were sampled by hand with a microscope from a concentrate and placed in a grid pattern on double sided tape. Epoxy was added in the shape of a puck to secure the zircons in place.

In all 77 zircons were collected from sample CC-2A. Once the epoxy hardened, the tape was removed and the puck polished to expose half of the detrital zircon crystals. With the zircons exposed, a scanning electron microscope (SEM) was used to collect backscatter (BSE) and Cathodo-luminesence (CL) images of the samples (Figure 37). Sampling of U-Pb isotopes was conducted using a New Wave 213µm laser to ablate the center of the zircon crystals. U-Pb abundances were collected using NUPlasma Multi-Collector Inductively Coupled Plasma Mass Spectrometer (MC-ICP-MS) at the University of Florida Geology Department isotope geoscience research facility. No rim data was collected for these samples.

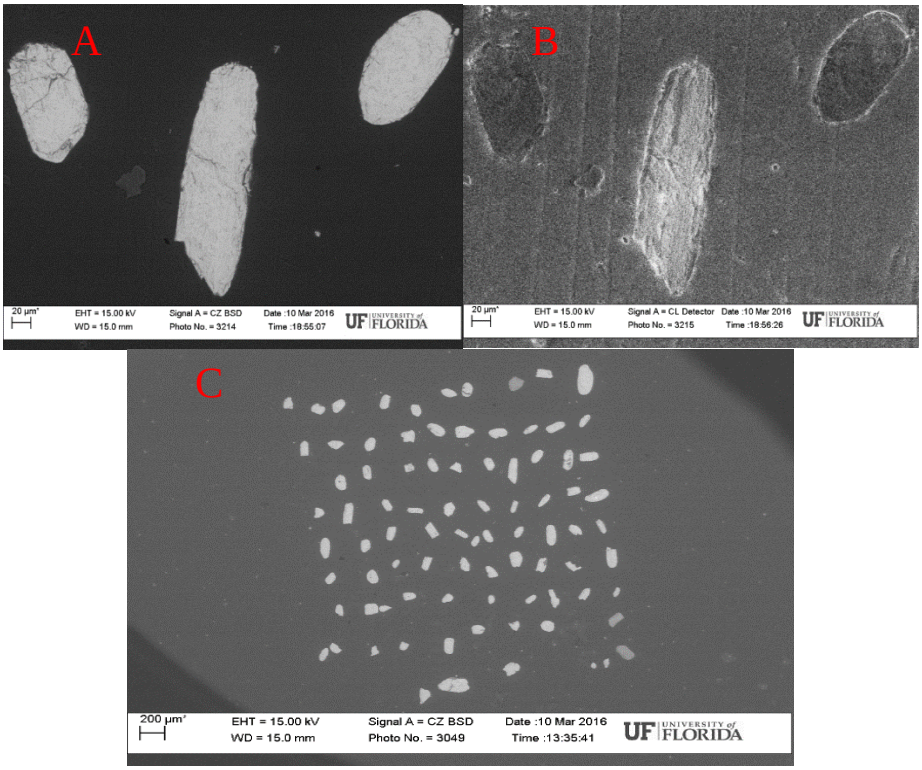


Figure 37. Showing BSE (A) and CL (B) Images of detrital zircons. C) is a BSE image of detrital zircons within the puck.

Results

Of the 59 zircons that display <10% discordance, 35 samples show a primary sedimentary source of 2.45-2.61 Ga. A younger Paleoproterozoic source of 1.79-1.98 and two less prominent Archean sources at 2.61-2.80 and ~3.0-3.2 Ga were also present. Comparing these ages to Ross and Villeneuve (2003), a correlation between the 1.8 and 2.6 to 2.9 Ga ages can be seen (Figure 38). However the primary peak of 2.55 Ga from Deep Creek in the Big Belt Mountains is absent from their data. The 1.8 Ga peak correlates to the GFTZ, which was expected as the Helena embayment is resting directly over the GFTZ and adjacent to the 1.8 Ga Little Belt arc (Foster et al., 2014) and deposition within the Helena embayment likely occurred following the GFTZ (Mueller et

al., 2012). Peaks at 2.6-3.1 Ga are likely sourced from the intra-basinal crystalline basement. The source of the 2.55 Ga peak is less obvious and limited samples of this age have been found within the Belt Basin

Proximal sources in the Wyoming Craton, include the Montana Metasedimentary terrane (3.2-3.5 Ga), the Beartooth Magmatic Zone (2.81 Ga), and the Medicine Hat Block with ages between 2.6-3.2 Ga. (Mueller et al., 2012). Possible distal source include the, Granite Range and Wind River Range of the Wyoming Craton, and the Little Elk Granitic Gneisses (2.55 Ga) (Gosselin et al., 1988) within the Black Hills of South Dakota. The Hearne Province, Sask Craton, and Superior Craton all have ages that could potentially be a source for the primary peek at 2.55Ga (Figure 40).

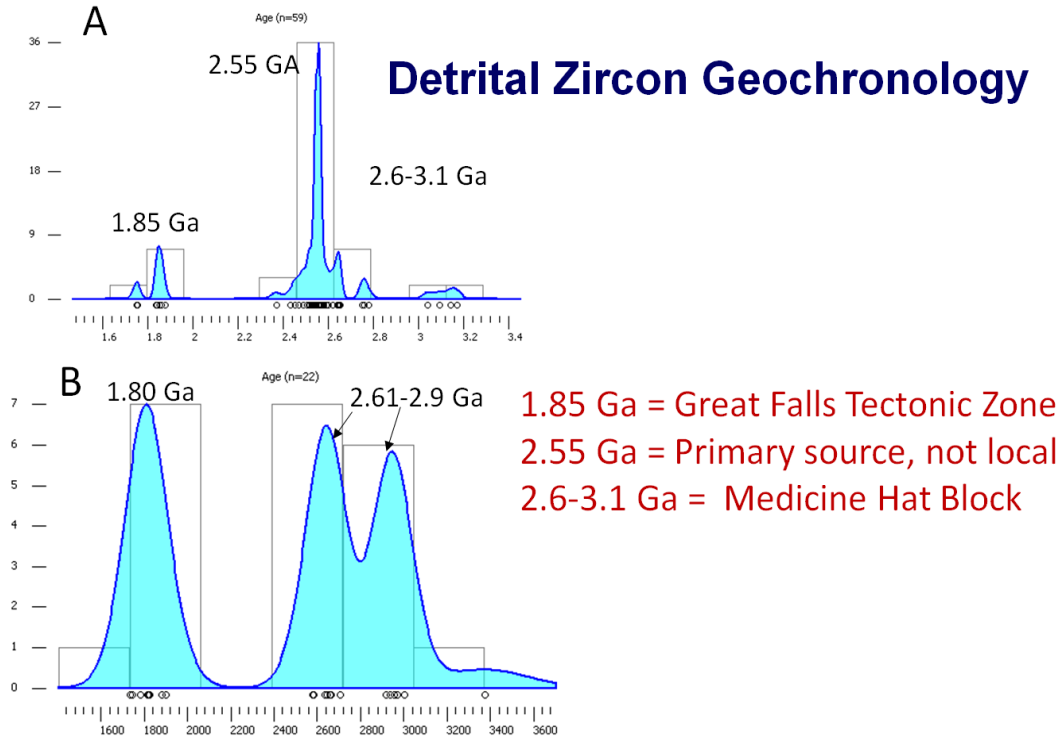


Figure 38. Kernal density plots. A) Sample CC-2A from Deep Creek in the Big Belt Mountains. B) Newland Samples from Ross and Villeneuve (2003).

Discussion

Previous studies have indicated that the source of the Newland Formation was composed of primarily granitic upper continental crust (Schieber, 1986). Three distinct ages were found in this study. Two minor contributors of 1.8 and > 2.6 Ga corresponds to the GFTZ and Medicine Hat Block, which was, expected as they are proximal to the basin. However, the 2.55 Ga age is not typically seen in detrital zircons of Laurentia. Possible sources of the western Belt Basin include Laurentia Archean terrains (>2.55 Ga) of the Hearne, Sask, and Wyoming Cratons, and the Black Hills of South Dakota with more distal sources including the Superior, and Slave provinces (González et al., 2006). Non-Laurentian provenances of 2.55 Ga granitoid events have been linked to Northern

China, India, Antarctica, and the Gawler Craton of Australia (Condie et al., 2009). The only Laurentian source that matches a 2.55Ga source is within the Wyoming Craton. where local occurrences of rocks of this age occur in the North Snowy Block (Mogk et al., 1988); anatectic melts in the Tobacco Root Mountains (Mueller et al., 2004), and the Mount Owen pluton in the Teton Range (Frost et al., 2006).

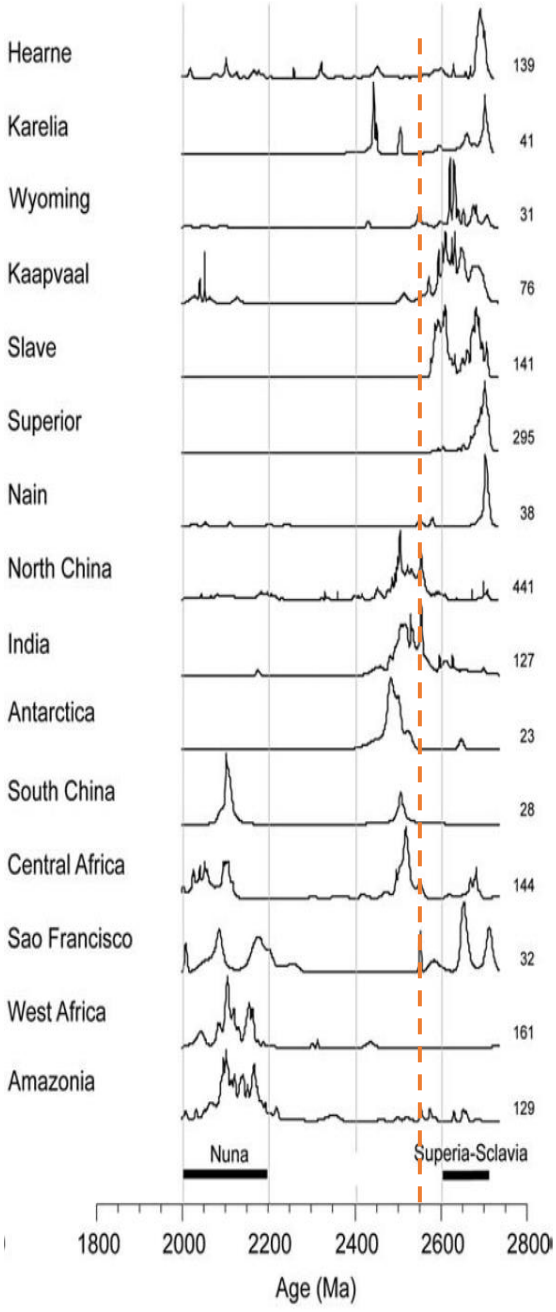


Figure 39. Crustal events that occurred from 2.0-2.8 Ga. The orange dashed line represents the 2.55Ga age found in the Gcs facies in Deep Creek. Based on this graph there is a small peak in the Wyoming province at 2.55Ga. Modified from (Condie, 2009).

Amalgamation of the Wyoming, Hearn and Slave Craton formed the super continent Kenorland by 2.6-2.55 Ga (McComb et al., 2004). 2.55-2.50 Ga magmatism was widespread but of little volume (Mogk et al., 1992). Granitic sills within the Beartooth Mountains and granitic units within the Mirror Lake Shear Zone in the Gallatin Range south west of Bozeman have been dated at 2.55 (Mogk et al., 1992). 2.55 Ga leucosomes in Gallatin Canyon migmatites and partial melts of that age in the Tobacco Roots (personal communication Mogk), as well as the Mt Owen quarts monzonite in the Tetons dated to 2547 ±3 Ma (Zartman and Reed, 1998)

The Wyoming Craton is composed of few proximal primary domains to the Belt Basin and several distal domains (Figure 40). The proximal domains include the Montana Metasedimentary Terrane (MMT) with a principle age of 3.2-3.5 Ga, the Beartooth-Bighorn Magmatic Zone with a primary age of 2.81Ga. Continental arc calc-alkaline Plutons, and GFTZ calc-alkaline arc at 1.81- 1.78 GA (Guerrero et al., 2016). The distal domains include the Black Hills of South Dakota, and the Wind River Mountains, Granite Mountains and Tetons of Wyoming, all of which have granitic intrusive events occurring at 2.55 Ga (Frost, 1998). Within the Black Hills, the Little Elk Granite and Bear Mountain Granite have an age of 2.55Ga. The Wind River Range have several more substantial granitic intrusions at 2.55 Ga which include the Bears Ear Batholith, granite of New Fork Lakes, Middle Mountain Batholith, and South Pass Granite (Figure 41). Within the Granite Mountains the Lankin Dome Granite has been dated to 2.56 Ga (Frost et al., 1997).

The Archean Wyoming Craton- Province has three proximal major domains (MMT, BBMZ, SAT) and one potential distal source (LEG)

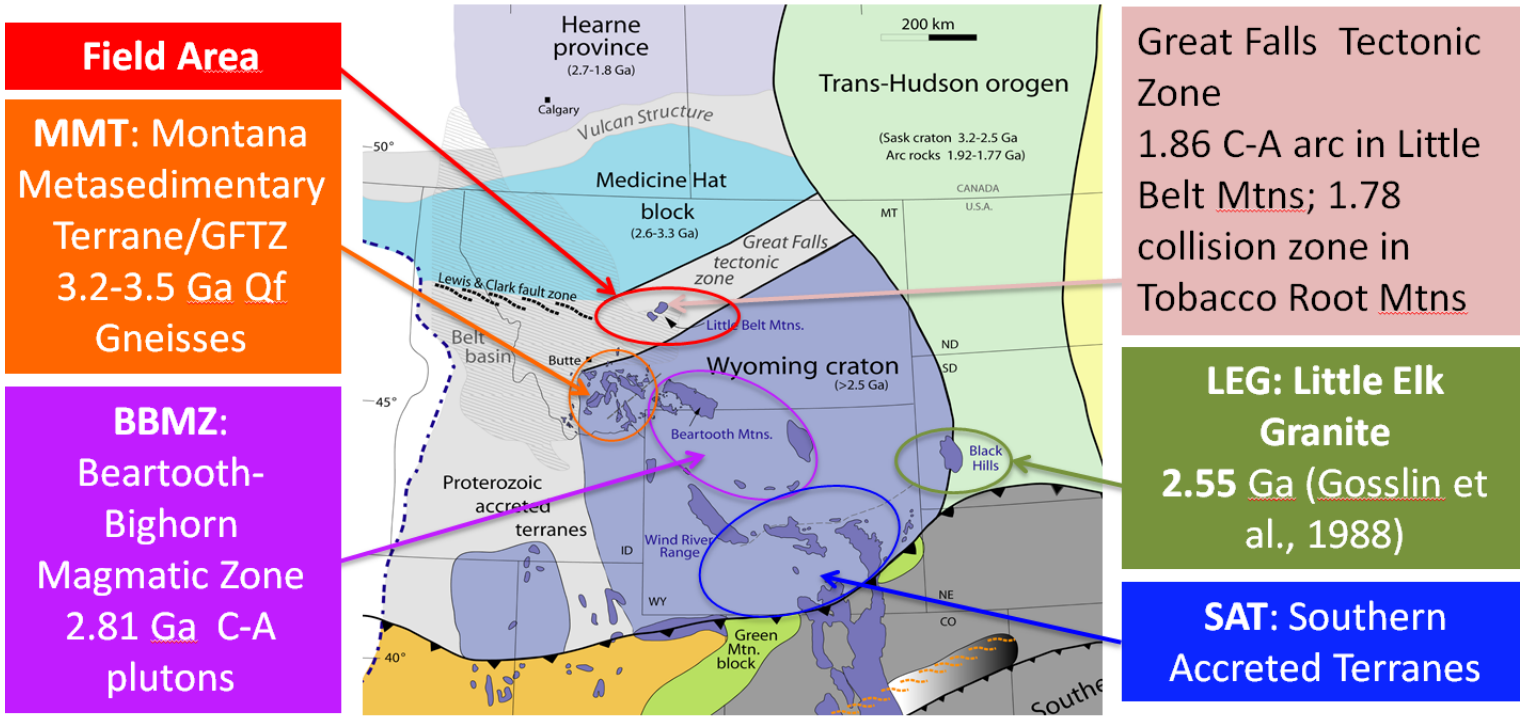


Figure 40. Potential source areas for the Belt Basin. No proximal 2.55 Ga sources are available. Distal sources include the LEG in the Black Hills, the Granite Range and the Wind Rivers Mountains. Modified from (Mueller et al., 2012).

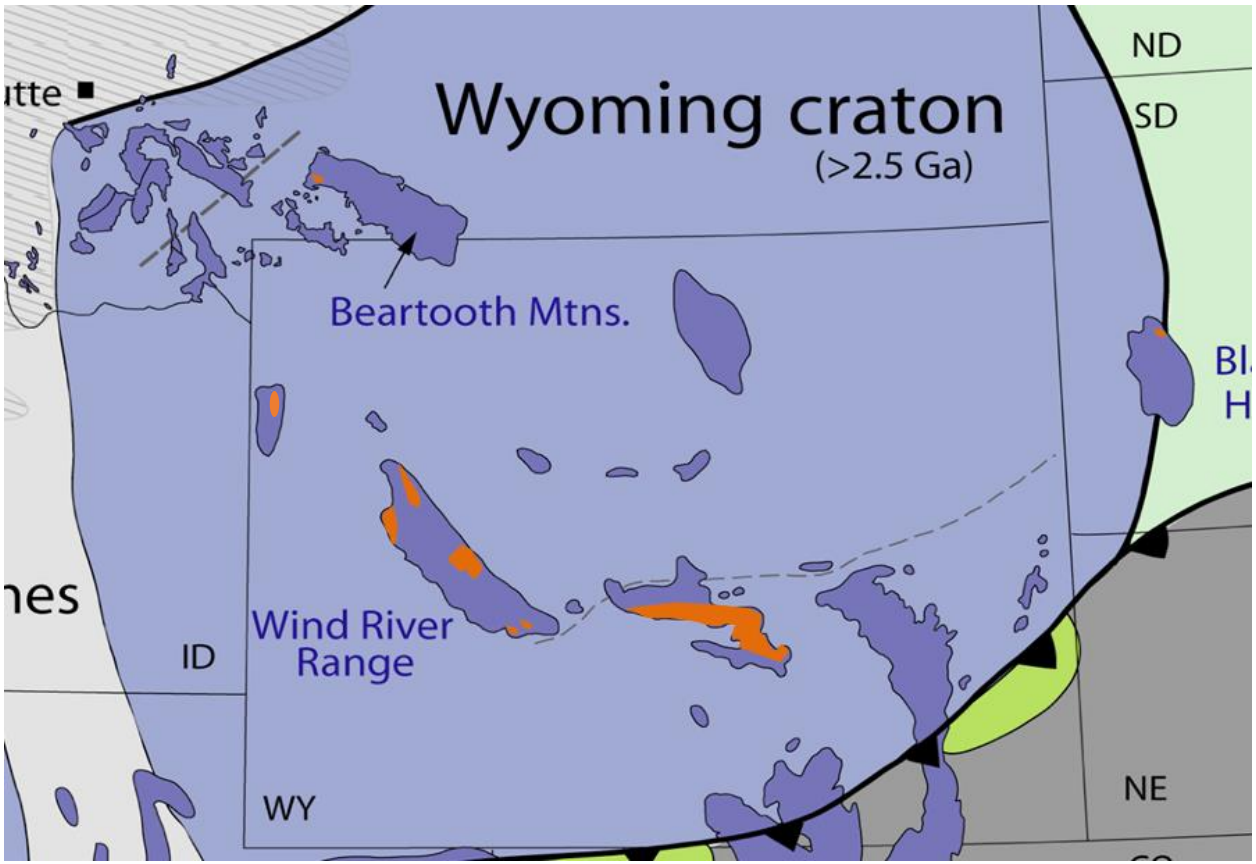


Figure 41. Zoomed in view of the Wyoming Craton. Orange units represent granitic sources of 2.55 Ga. The highest volume of 2.55 Ga source rocks is in the Wind River Mountains and Granite Range of Wyoming. Modified from (Mueller et al 2012) and (Frost, 1998).

Conclusion

Major and trace element comparison support that the Newland Formation was sourced from the upper continental crust. REE element spider plots reveal little change within the Newland Formation but are depleted compared to NASC, ES and PAAS. The depletion of these elements is likely due to the super saturation and large volume of carbonate precipitation, and decreased terrigenous detritus into the basin, specifically along the northern margin.

Though not well represented in the Belt Basin, or at all in in the Helena embayment prior to this study, detrital zircons with an age of 2.55 Ga potentially link the eastern Helena embayment to the main Belt Basin to the west (Table 3). Minor representation of zircons within the 2.55 Ga range are present in the Prichard Formation and the Creston Formation (Canadian Ravalli group). This suggests that the source for the Western Belt may be from the Wyoming Craton or that the Newland Formation had a possible western source possibly from the Australian Gawler Craton.

Based on the volume of 2.55 Ga source rocks within the Wyoming Craton it appears that turbidite deposits may have been sourced from the south. Schieber (1986) proposed that the Lower Newland was widespread prior to deposition of the LaHood Formation. The most likely Laurentian source with an age of 2.55 Ga is from the south. CC-2A was sampled from the lower Newland which supports Schieber's (1990) hypothesis that deposition of the Lower Newland may have occurred prior to faulting along the Perry Line with direct deposition from the south. Further investigation of the

2.55 Ga detrital zircons within the Newland Formation and Western Belt Basin need further analysis to determine if they are from the same source.

Western Belt Basin			
Revett F. (R&V)	Grinnell F. (R&V)	Prichard F. (R&V)	Creston F. (R&V)
1590–1505 1682 1893–1793	1798–1749 (7) 1875–1814 (12) 2682–2599 (4)	1452 (1) 1489 (1) 1611–1540 (16) 1818–1740 (6) 2551–2509 (2)	Discordant array at 1900 2678–2502 (14)
Helena Embayment			
LaHood (Mueller)	LaHood (Fox)	Newland (R&V) 22	Newland (Anderson) 59
Jefferson Canyon 3555 primary	Bridger Range 3220 primary	Big Belts 1800 (9) Primary 2610 (6) 2900 (6) 3390 (1)	Big Belts 2550 (35) Primary 1850 (8) 2600-2800 (12) 3100 (4) 1760 (1)

Table 3. Principle zircon ages from Ross and Villeneuve 2003, and this study. Highlighted ages show a potential link between the Eastern Belt Basin and Western Belt Basin. Initials after formation names show where the data is from (R&V) = Ross and Villeneuve, Mueller 2016, Fox 2016, and this study. Modified from Gonzalez (et al., 2006).

MINERALOGY

Introduction

A series of clay mineral analyses of the Belt Basin, to determine diagenesis from subsidence, was performed by Maxwell and Hower (1967), Ryan (1991), and (Duke and Lewis, 2010). Winston, (1986) proposed the western portion of the Belt Basin reached a burial depth of 16,000 m near superior Montana. In contrast previous studies suggest the eastern Belt Basin outcrops did not exceed 2,000 m of burial depth, or temperatures greater than 80 ^{o}C (Ryan, 1991). In the western portion of the Belt Basin near Rodger's Pass, the Revett Formation experienced burial temperatures up to 400 ^{o}C based on chlorite zones within the greenschist facies (Harrison and Jobin, 1963). Temperatures of 400 ^{o}C correspond to a burial depth of 11,500 m based on the 30 ^{o}C/Km geothermal gradient of a rift system, and average atmospheric temperature of 20 ^{o}C used by Ryan, (1991). This study will look at the transition of diagenetic alteration of illite/smectite across the Helena Salient within the Newland Formation and propose a burial history from the leading edge of the Sevier fold-and-thrust-belt to the Laramide basement involved uplift.

Using powder X-Ray diffractometry the (001) peak in both chlorite and illite can be used to determine metamorphic grade (Eberl, 1989). Kubler (1964) suggested that sharpness of the illite peak can be used to determine diagenesis within low grade metamorphism, and sharpening of the (001) peak along with the breadth of the half height can be used to indicate an increase in temperature or depth of subsidence. The

locations of the (001)/(002) and (002)/(003) illite peaks regardless of intensity can be used to determine the ratio of illite/smectite (Moore and Reynolds, 1989).

Alteration of clay minerals is heavily influenced by hydrothermal alteration and to avoid complications samples were taken at locations devoid of secondary vein intrusion. (Graham et al., 2012) reported that alteration had occurred due to syn-sedimentary hydrothermal fluids, and fluid migration along faults and fractures within the Newland Formation.

Prior to clay mineral analysis, the bulk mineralogy was first addressed in order to identify the presence of clays and general mineralogy.

Bulk Mineralogy

Methods

Eight representative samples collected from the same stratigraphic location spanning the field area were ground and filtered to <60um using a mortar and pestle and added to a 91% alcohol slurry (Table 4. Shows the stratigraphic and geographic locations of the 8 samples used for bulk and clay mineralogy. The slurry was then placed on a slide using an eyedropper and dried using a low temperature hot plate (30 °C). After the samples were prepared a SCINTAG X1 Diffraction System at the Imaging and Chemical Analysis Laboratory (ICAL) at Montana State University was used to perform X-Ray diffraction analysis. Each sample was scanned from 3 to 73^{o} 2θ using a continuous scan of 1 degree/minute, a step size of 0.20^{o} 2θ, and a count time of 1.20 seconds.

Data reduction included background subtraction and peak identification routines in the Scintag software. Search/match functions used the ICDD database to find "best fit" matches of unknown minerals. Peaks were systematically indexed to identify major minerals present (Figure 42).

Unit/Lithofacies	Location	Outcrop
Unit 1 (Ccl)	46 °44’56”N 109 °20’48”W	Swimming Woman Canyon (WF)
Lower Newland (Fcs)	46 °44’22”N 109 °20’31”W	Swimming Woman Canyon (LEF)
Unit 1 (Ccl)	46 °45’11”N 109 °20’26”W	Swimming Woman Canyon (EF)
Unit 4 (Ibs)	46°33’20”N 110 °30’07” W	Checkerboard (CH)
Lower Newland (Fcs)	46°52’20”N 110 °40’30”W	Belt Creek (BC)
Lower Newland (Fcs)	46 °43’40”N 110 °52’04”W	Miller Gulch (MG)
Lower Newland (Fcs)	46 °21’26”N 111 °07’21”W	Deep Creek CC1 (DC)
Unit 1 (Ccl)	46 °19’59”N 111 °15’28W	Deep Creek (DC)

Table 4. Shows the stratigraphic and geographic locations of the 8 samples used for bulk and clay mineralogy.

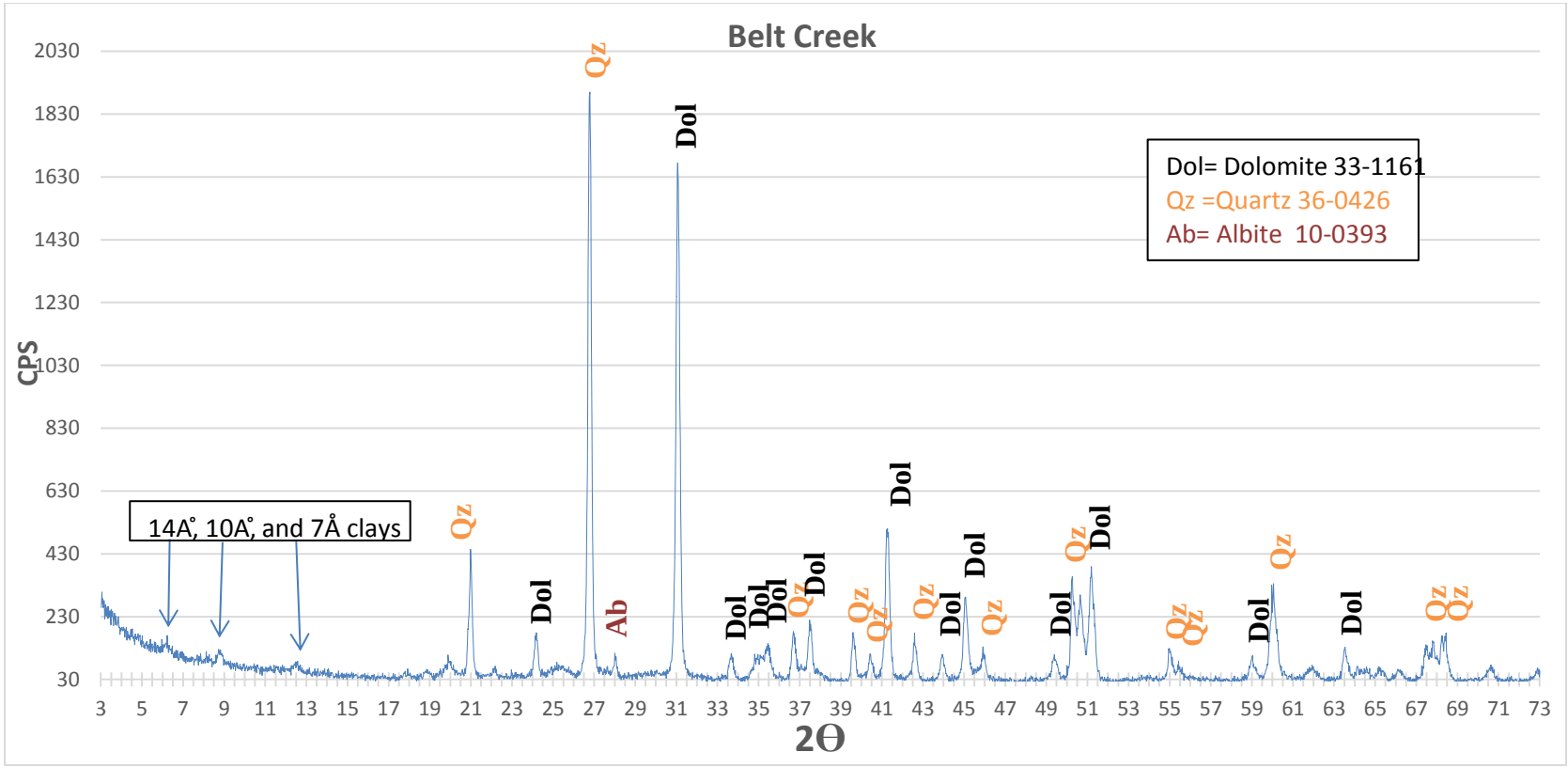


Figure 42. Bulk mineralogy of the Newland Formation from Belt Creek. The number next to the mineral (in upper right corner) represents the index card from the ICDD data base that best fit the peak distribution. The lower peaks <23° 2θ were further scrutinized for subsequent clay mineral identification.

Results

Qualitative mineralogy was performed on eight samples across the field area. Major minerals within the samples include quartz, dolomite, calcite, and 10Å clay identified as illite, with trace amount of albite. Clinochlore is present in several of the samples, and is the Mg rich end member of chlorite as would be expected in a dolomitic carbonate. The modal abundance of the < 2 um clay fraction in these samples is very small, as seen in the 3-23^{o} 2θ portion of (Figure 42). The presence of clinochlore and minor peaks <15 degrees indicate the presence of clays within the bulk mineralogy and need to be examined further through XRD analysis. Bulk mineralogy for each sample and their index cards are presented in Table 5. Raw XRD profiles of all the samples are presented in Appendix B.

Sample/Location	Minerals	Card
Belt Creek	Quartz	33-1161
	Dolomite	36-0426
	Albite (trace)	10-0393
CC1	Dolomite	36-0426
Deep Creek	Quartz	33-1161
	Clinochlore -1MIIB	12-0242
	Albite (trace)	10-0393
Deep Creek	Dolomite	36-0426
	Quartz	33-1161
	Calcite	05-0586
	(10 angstrom clay	07-0025
	Illite/Muscovite)	
EFSW	Dolomite	36-0426
Swimming Woman	Quartz	33-1161
	Calcite	05-0586
	10 angstrom clay	07-0025
	Illite/Muscovite)	12-0242
	Clinochlore -1MIIB	10-0393
	Albite (trace)	
Miller Gulch	Dolomite	36-0426
	Quartz	33-1161
	Calcite	05-0586
	10 angstrom clay	07-0025
	Illite/Muscovite) Albite	10-0393
	(trace)	
SW125	Dolomite	36-0426
Swimming woman	Quartz	33-1161
	10 angstrom clay	07-0025
	Illite/Muscovite) Albite	10-0393
	(trace)	
Ch-6-29 Checkerboard	Dolomite	36-0426
	Quartz	33-1161
	Calcite	05-0586
	10 angstrom clay	07-0025
	Illite/Muscovite) Albite	10-0393
	(trace)	

Table 5. Shows the primary minerals within each sample and the associated index card.

Clay Mineralogy

Illite/Smectite

The ratio of illite to smectite can be directly correlated to pressure and temperature (Moore and Reynolds, 1989). However, debate remains on whether illite and smectite are members of a solid solution, separate phases, interstratified, or a series of phases(Moore and Reynolds, 1997). What is known is that illite is more stable than smectite at higher temperatures and pressures, due to the release of water molecules within the tetrahedral-octahedral-tetrahedral (TOT) stacking of the sheet silicate layers of smectite. Srodon and Eberl (1984) showed a decrease in expandable (smectite) clays with increased temperatures in the Gulf of Mexico coast. Based on (Eberl and Hower, 1976) the reaction from smectite to illite is proposed to be:

potassium-feldspar (detrital) + smectite → illite + chlorite + quartz

This and other previous studies by Eberl and Hower (1976), and Velde et al (1986), show that in the presence of K-feldspar, of the 2<um fraction, almost total alteration of smectite to illite can form at temperatures as low as 80 ^{o}C. Conversely, if K-feldspar is not present then the percent smectite will not likely decrease even at increased temperatures. Ryan, (1991) determined that overburden during Post-Proterozoic did not exceed 1900 m and a temperature of around 80 ^{o}C in the Big Snowy Mountains.

The illite/smectite (I/S) ratio across the Helena Salient from Swimming Woman Canyon to Deep Creek in the Big Belt Mountains will be used as a proxy to determine

temperature of recrystallization. Comparing the I/S ratio from the east to west should allow for direct comparison of burial depth between the two locations.

Chlorite and Corrensite

In a study of the Devonian Orcadian Basin in Scotland, Hillier (1993) found that chlorite authigenesis occurred between dioctahedral clay minerals and dolomite that formed under evaporative conditions (Figure 43).

$$5 \text{ dolomite} + \text{kaolinite} + \text{quartz} + H_2O = \text{chlorite} + 5 \text{ calcite} + 5\ CO_2$$

Or

$$15 \text{ dolomite} + 2 \text{ illite} + 3 \text{ quartz} + 11\ H_2O = 3 \text{ chlorite} + 15 \text{ calcite} + 2K^+ + 2OH^- + 15\ CO_2$$

The above reaction occurs at temperatures around 120 ^oC based on vitrinite reflection measurements from the Devonian Orcadian Basin in Scotland The presence of corrensite within an evaporative carbonate basin suggests diagenetic alteration of >100 ^oC (Hillier, 1993).

Methods

Samples from Deep Creek, Belt Creek, Miller Gulch, Checkerboard, and Swimming Woman Canyon were ground using a mortar and pestle and sieved to <60um to not alter the clay crystallography (personal communication Mogk, 2016). Carbonates were removed using USGS standard protocol of a 1 to 4 dilution of Glacial Acetic Acid at 50-75ml increments until the slurry stopped effervescing (Poppe et al., 2001). After

carbonate was removed from the sample the acetic acid solution was carefully poured off and 300 ml of distilled water was added to the sample. Sodium metahexoaphosphate was added to deflocculate the clay particles and vigorously stirred, using a blender, and dispersed using a sonic probe for 20 seconds. Samples were decanted for 8 hours, allowing suspension of the <2um clay fraction. The suspended particles were then separated through a .45um filter using a vacuum. The filter paper was then rolled onto a slide to create an oriented mount. This was done 4 times for each sample corresponding to the USGS clay mineralogy standard procedures. One more sample was prepared using an eye dropper and a low temperature hot plate to make an un-oriented clay sample for each sample. In all there were 40 slides made for clay analysis of the Newland Formation.

Following USGS clay mineralogy standard protocol, each sample was air dried, heated to 400^{o}C, heated to 550^{o}C, and heated to 60-70^{o}C in an ethyl glycol (EG) glass baking dish for at least 4 hours. X-Ray diffractometry was performed using three individual 2 theta scanning increments ranging from: 3-23 $^{o}2\theta$, 26-28 $^{o}2\theta$, and 59-61$^{o}\theta$ using a SCINTAG X1 Diffraction System at ICAL. The first scan from 3-23 $^{o}2\theta$ was used to determine the type of clays present within the samples by examining the effects of ethyl glycol and heating to determine the presence of swelling clays (Figure 43). The second scan from 26-28^{o} 2θ was performed to determine the presence of SiO_2 within the clay fraction for each sample. The third scan was done to determine the crystal form of illite if present in the sample by looking at the (060) peak. Ideally, illite should have a peak at 1.52 Å while glauconite will have a peak at 1.5 Å. See Appendix B.

Moore and Reynolds, (1989) concluded that the percent of illite/smectite (I/S) and chlorite/smectite (C/S) can be determined through XRD peak location (Table 6). When determining the portion of illite/smectite within an interstratified clay, the location of the (001)/(002) or (002)/(003) (Figure 44 or the (002)/(002) and (004)/(005) %C/%S peak of the Ethyl-Glycolated treated sample can be used (Moore and Reynolds, 1989). The first step in this process is to examine the ethyl glycol treated sample and look for a peak in 5.2^{o} 2θ area. A Peak in the 5.2^{o} 2θ area suggests the presence of smectite, giving a non-swelling clay/smectite interstratified clay. This is further supported by a peak in the ~9^{o} 2θ and ~16^{o} 2θ. A peak at 11.2^{o} 2θ is a diagnostic characteristic for corrensite (trioctahedral C/S) (Moore and Reynolds 1989). However, the deviation of the 50/50 C/S ratio by as little as 2-3% will sharply diminish the peak. Exact peak locality of the $002_{chl}/002_{sm}$ peak can then be used to determine the C/S ratio within a sample. Based on the presence of a 5.2^{o} 2θ peak, the I/S percentages have been determined for samples containing smectite, and samples containing peaks at 11.2^{o} 2θ support the presence of corrensite and are discussed below.

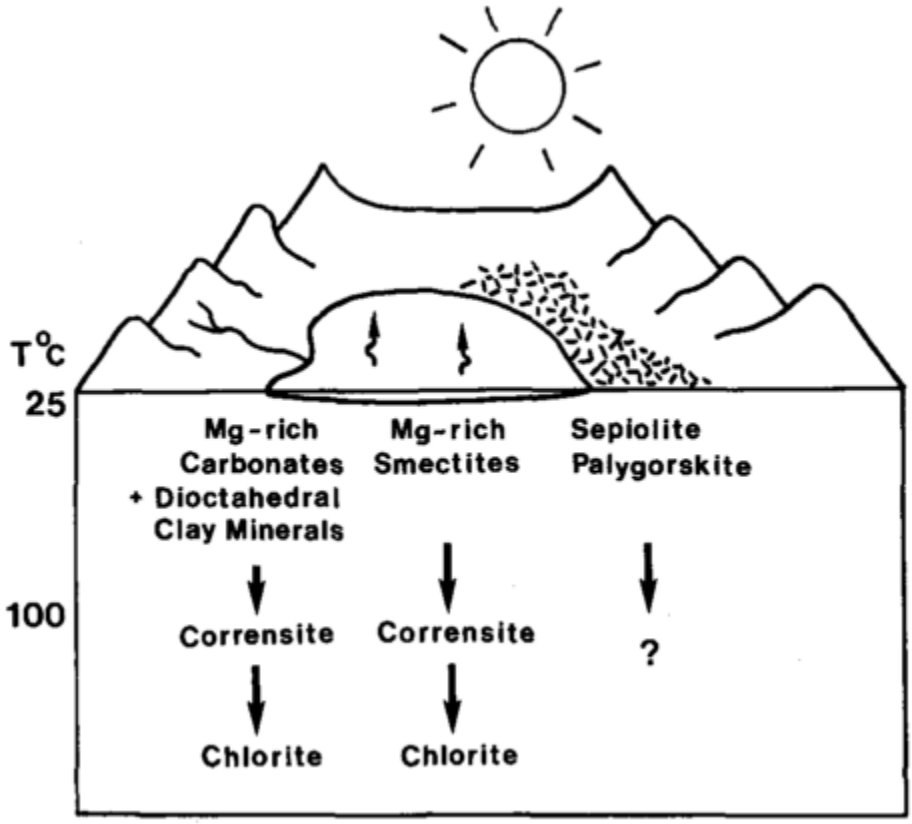


Figure 43. Schematic interpretation or corrensite and chlorite pathways within an evaporate-carbonate basin. From Hillier (1993)

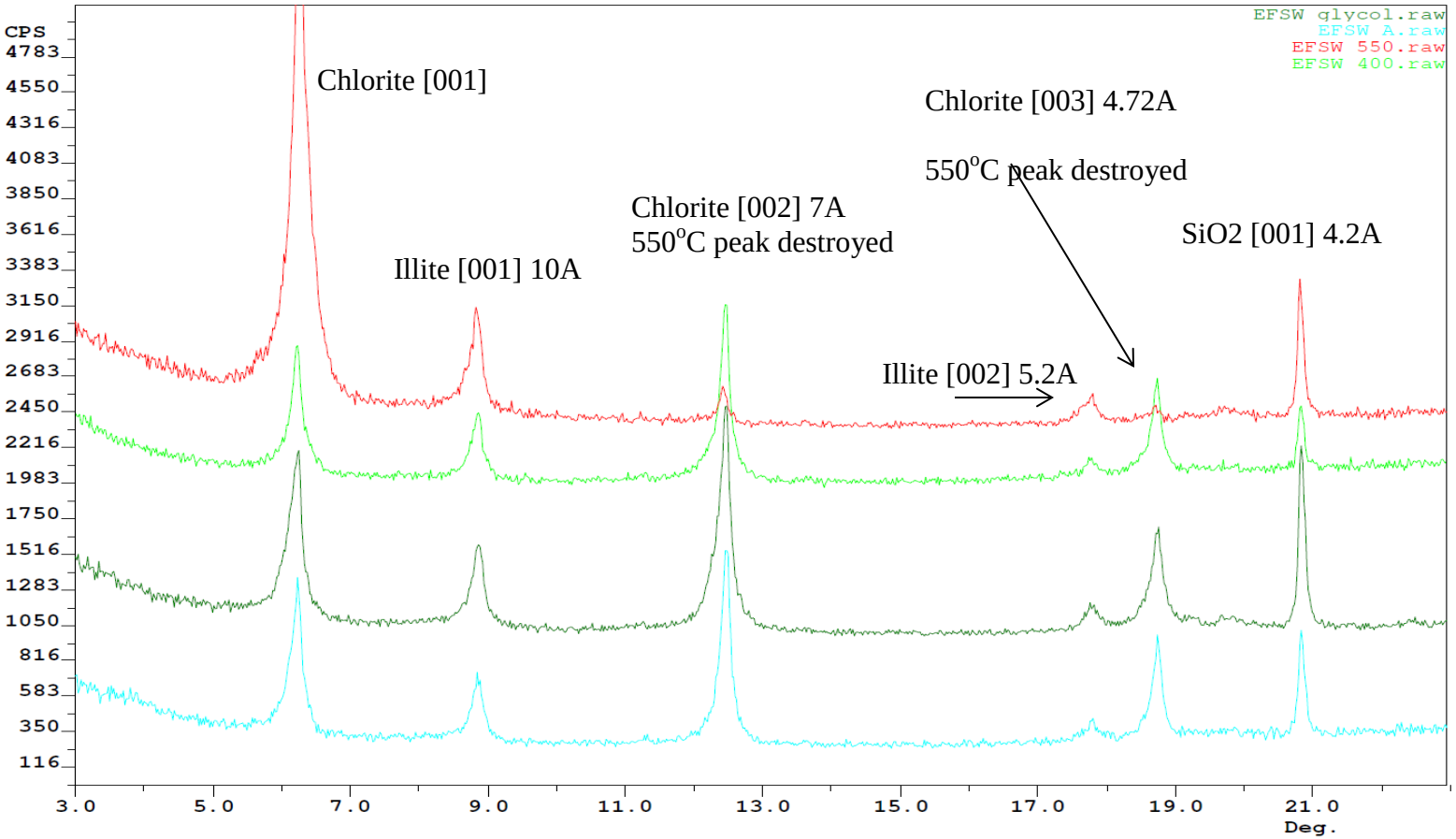


Figure 44. Four treatments of air dried (blue), ethyl glycol (dark green), baked at 400°C (light green), and baked at 550 °C (red) from Swimming Woman Creek locality. Chlorite is represented by 14 Å , 7 Å , 4.7 Å , while illite is represented by 10 Å , 5.2 Å peaks, 4.2 Å peak is <2um SiO_2. Peak collapse at 7 Å and 4.72 Å is associated with iron bearing chlorites (Reynolds, 1997)

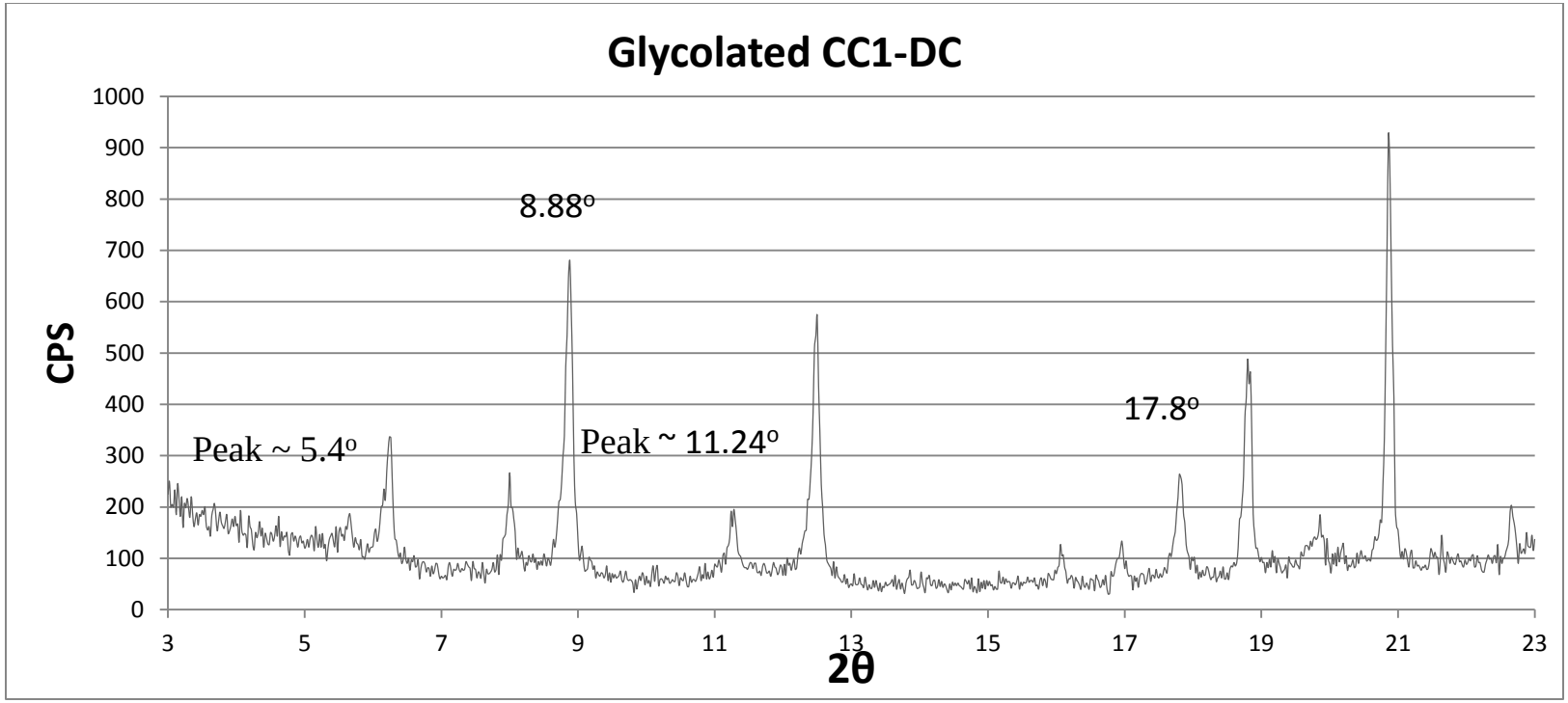


Figure 45. Ethyl glycol treated sample from the Deep Creek locality. A peak at 5.4° 2θ indicates the presence of smectite. The 001/002 illite/smectite peak is at 8.88 ° 2θ and the 002/003 illite/smectite peak is at 17.8° 2θ. The presence of an 11.24 2 theta peak suggests the presence of corrensite (trioctahedral chlorite/smectite) is present.

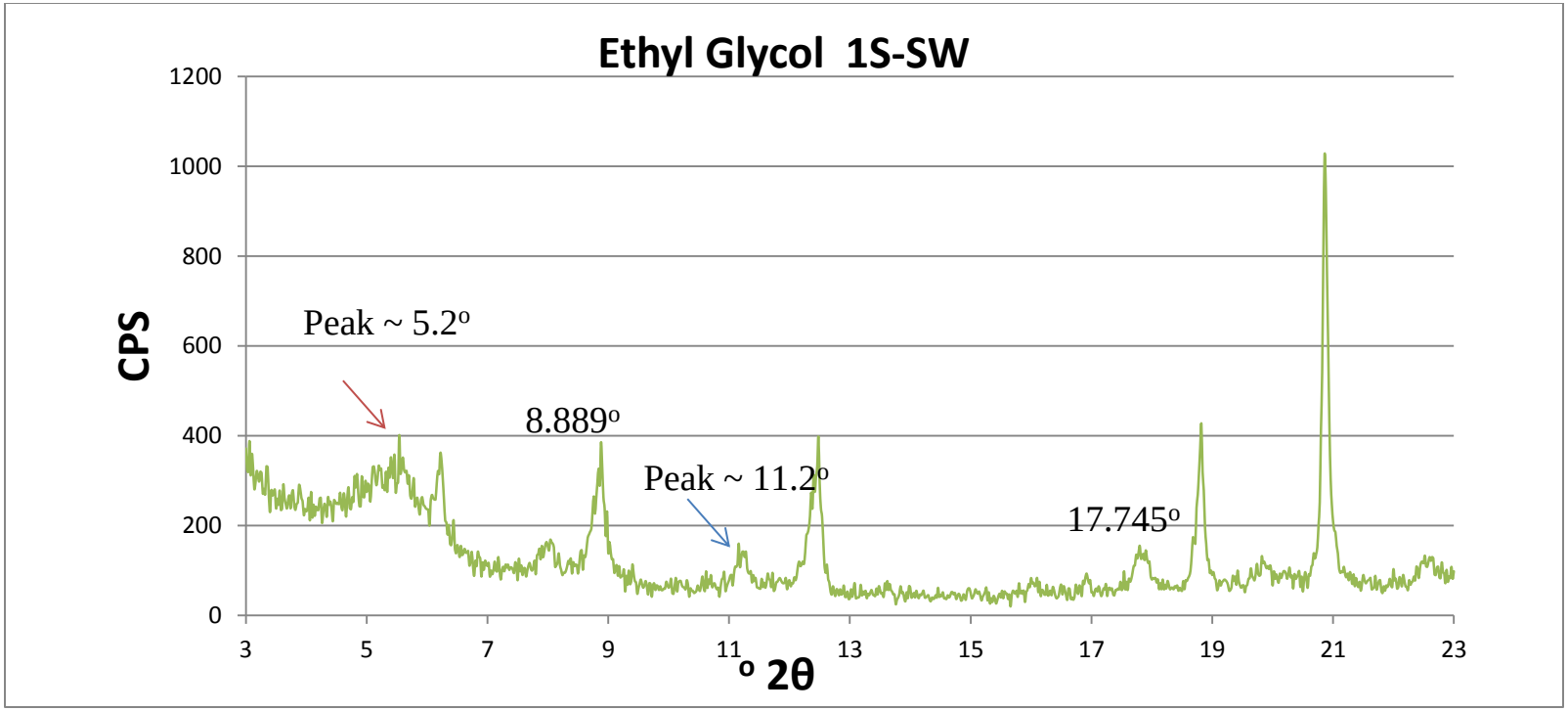


Figure 46. Ethyl glycol treated sample from Swimming Woman Canyon. A peak at 5.2° 2θ indicates the presence of smectite. The 001/002 illite/smectite peak is at 8.889 ° 2θ and the 002/003 Illite/Smectite peak is at 17.745° 2θ. The presence of an 11.2 peak suggests the presence of corrensite (trioctahedral chlorite/smectite) is present. However, 2-3% difference in the 50/50 stacking of chlorite/smectite shows up as a weak peak in X-ray diffraction and the exact location of the peak must be used to determine the ratio of interstratified chlorite/smectite.

% Illite	001/002 d(Å)	001/002 °2θ	002/003 d(Å)	002/003 °2θ	oΔ2θ
10	8.58	10.31	5.61	15.80	5.49
20	8.67	10.20	5.58	15.88	5.68
30	8.77	10.09	5.53	16.03	5.94
40	8.89	9.95	5.50	16.11	6.16
50	9.05	9.77	5.44	16.29	6.52
60	9.22	9.59	5.34	16.60	7.01
70	9.40	9.41	5.28	16.79	7.38
80	9.64	9.17	5.20	17.05	7.88
90	9.82	9.01	5.10	17.39	8.38

Table 6. Position of peak reflections for estimating percent illite/smectite from (Moore and Reynolds 1989)

Results

Using the USGS Clay Mineral Identification workflow, the most likely clay minerals for each sample were determined (Table 7 and Appendix B). Major clay minerals within the Newland Formation include illite, chlorite, and interstratified I/S and C/S, and corrensite. Samples in The Big Snowy Mountains and Big Belt Mountains have a greater than 95% I/S ratio. Illite polytypes vary systematically based on diagenetic grade while chlorite polytypes do not. 1MD→1M→$2M_1$ illite polytype conversion occurs with increased metamorphic grade (Ryan 1991)and the presence of 1MD and 1M illite polytype in the Newland Formation across the Helena embayment is indicative of low grade metamorphism. Ryan, (1991) found that such low grade metamorphism occurred in the Big Snowy Mountains.

Samples from the Big Snowy Mountains and Big Belt Mountains have a peak at ~11.2 Å indicating the presence of corrensite. The (004)/ (005) peak of the C/S is not displayed in the 3-23° analysis used in this study and therefore the C/S data needs to be

approached with caution. Ryan, (1991) interpreted the C/S ratio of the Newland Formation in Swimming Woman Canyon as being 6% smectite. I/S ratios of the samples from east to west show no change or a very minor decrease in smectite occurring to the west. Based on Maxwell and Hower, (1967) illite polytype identification can be performed by dividing the 3.74 Å peak by the 2.54 Å peak. Illite polytype identification was attempted on the bulk mineralogy sample because dehydration efforts using a very low temperature 40^{o} C hot plate of the 2um fraction did not result in a randomly oriented sample. Determining the 1M and 2M polytypes of illite requires a very pure sample as the difference in 1M-2M peaks are as minor as 0.15 ^{o} 2θ (Moore and Reynalds, 1989). Illite polytype identification for each sample was not diagnostic.

The I/S ratio of the Deep Creek CC1 and Swimming Woman Canyon 1S-SW, which spans the entire field area, shows a minor decrease in smectite to the west. Sample IS-SW has a (001)/ (002) peak at 8.88 ^{o} 2θ, and a (002)/ (003) peak at 17.74 ^{o} 2θ (Table 8). Sample CC1 has a (001)/ (002) peak of 8.88 ^{o} 2θ, and a (002)/ (003) peak at 17.78 ^{o} 2θ (Figure 45). Peak location of both CC1 and 1S-SW support an illite to smectite ratio greater than 90%. The presence of corrensite suggests that strata in Swimming Woman Canyon was subjected to burial temperatures of >120 ^{o}C. Samples from Deep Creek with diagenetic chlorite and corrensite also suggest a burial temperature of >120 ^{o}C.

Air dried	Ethyl Glycol	Heated to 400°C	Heated to 550°C	060 peak (randomly oriented)	Mineralogy
14 Å	No change	No change	increase in intensity		Chlorite or Dioctahedral Chlorite
~10 Å	No change	No change	No change		Illite and or mica or Glauconite
~7 Å	No change	No change	Destroyed		Chlorite or Dioctahedral Chlorite
~4.2 Å	No change	No change	No change	Peak at 1.50	<2um SiO_2

Table 7. Clay Mineralogy from the east fork of Swimming Woman Canyon was identified as Chlorite or dioctahedral chlorite and illite.

Sample	001/002 °2θ	002/003 °2θ	% Illite	%Smectite
1S-SW	8.88	17.74	>90	<10
Checkerboard	8.88	17.78	>90	<10
DCU1	8.78	17.76	>90	<10
EFSW	8.84	17.78	>90	<10
Miller Gulch	9.04	18.02	>90	<10
WFSW	9.14	18.1	>90	<10
Belt Creek	8.88	17.78	>90	<10
DC CC1	8.88	17.78	>90	<10

Table 8. Percent illite found in each sample.

Conclusion

Qualitative bulk mineralogy along the northern margin of the Helena embayment identified the primary mineralogy as quartz and dolomite for all samples. Illite was present in all samples except Belt Creek and CC1 in Deep Creek, calcite was present in Deep Creek, EFSW, Miller Gulch, and Checkerboard. Clinochlore 1MIIB is present in Fcs lithofacies in Deep Creek and EFSW. Clinochlore is a form of chlorite and based on the destruction of the 002 and 003 peaks in the clay analysis, it is enriched in Mg (Moore and Reynolds, 1989). This study concurs with previously published X-ray Powder Diffraction data from Ryan, (1991), Feedback, (1997) and Ambrose, (2005) who also looked at the Chamberlain and Wallace Formations, supporting homogenetic characteristic of the Belt Basin shales.

In a study on the variability of illite to smectite within the Gulf of Mexico(Freed and Peacor 1989) concluded that diagenesis of shales are a function of local geology, and should not be interpreted as being diagnostic of anything other than the specific sample. Looking at the samples individually from east to west a low (<10%) smectite is present in the <2um fraction in the Big Belt Mountains in the west and the Big Snowy Mountains to the east, suggesting a similar subsidence history across the Helena salient.

Subsidence history of the Newland Formation has been proposed to have a maximum burial temperature of 80 ^{o}C (Ryan 1991) and a burial depth of 2,000m based on illite and chlorite polytypes. This study used the %illite/%smectite ratios to look at degree of alteration and proposes the amount of burial diagenesis from east to west within the Helena embayment, and concluded they are not distinguishable. In a study of the Gulf

Coast Freed and Peacor, (1989) determined that the onset of smectite to illite transition begins at 58 ^{o} to 92 ^{o}C, and the completion of >80% illite occurs between 88 ^{o}C and 142 ^{o}C. XRF analysis in this study across the Helena salient suggests >90% illite of the clays. According to Hillier's reaction, the presence of corrensite is a reliable indicator of diagenetic alteration at temperatures >100 ^{o}C and the presence of IIB chlorite found in Ryan's (1991) study suggest a minimum temperature of 120 ^{o}C for both the Big Snowy Mountains and Big Belt Mountains. Using the geothermal gradient of rift system of 30 ^{o}C/K and an average atmospheric temperature of 20 ^{o}C suggests a depth of 3.33 km of burial death was reached by the Newland Formation. Ryan (1991) states that conodonts from the Snowy Range Formation 300 m above the Newland Formation have a color index of alteration of 1. This suggests that temperatures between 50 ^{o} and 80 ^{o}C were reached in the Phanerozoic. Alteration of clays in this study imply burial diagenesis occurred during the Proterozoic, as Cambrian strata directly above only experienced temperature up to 80 ^{o}C. Clay alteration of I/S and the presence of chlorite and corrensite within the Helena embayment increase the previously proposed burial depth by more 1300 m to burial depth of at least 3300 m.

SUMMERY AND CONCLUSIONS

The Newland Formation was deposited below wave base prior to block faulting along the Proterozoic Buttress fault. The Newland Formation has two distinct provenances including the primary granitic source based on major and trace elemental analysis, and REE analysis. Detrital zircon geochronology indicates the presence of the primary 2.55Ga source from the Wyoming craton. The Provenance for the Gcs lithofacies in Deep Creek was located to the south in the Beartooth Mountains, Wind River Mountains, Gravely Mountains, or Black Hills to the East. Suggesting The Lower Newland may have extended beyond the southern Perry Line prior to LaHood deposition (Schieber, 1990).

Clay mineralogy of illite/smectite and the presence of chlorite and corrensite from Deep Creek in the west to Swimming Woman Canyon in the east indicates the Newland Formation was buried to a depth of 3,300 m, increasing the previously proposed burial depth of 2,000 m by 1,300 m. Clay mineralogy of the Fcs facies of the Lower Newland suggests the western portion of the Helena embayment experienced roughly the same burial diagenesis or depth as the eastern Helena embayment.

Newland stratigraphy within Swimming Woman Canyon correlates to the transition from primarily deposition of Fcs lithofacies of the Lower Newland and the onset of Ccl deposition. Lithofacies Sgc transitions into Ccl and Gcs and Rls are also present, and have interpreted as basin floor or basin center and suggest a deep water depositional environment for the eastern most autochthonous Belt rocks. Because the deepest depositional environment is also the eastern most outcrops we can infer using

Walther's Law that the landward lithofacies (Gms, Lm, Fs, Sm, Sr) were present during deposition and the Belt Basin extended further east.

Several contrasting hypotheses for the displacement of the Belt Supergroup exist (Hildebrand, 2015 and Sears, 2007). The presence of para-authochonous Newland Formation in Swimming Woman Canyon of the Laramide uplifted Big Snowy Mountains pins the Belt Basin to cratonic North America. This research supports Sears's (2007) interpretation of clockwise rotation of the entire Belt Supergroup rather than thousands of kilometers of right lateral translation during the Sevier and Laramide as proposed by Hildebrand (2013).

Future Work

Future work to better understand the eastern extent of the Helena embayment needs to be done. Proprietary wells east of Swimming Woman Canyon could connect the stratigraphy of the Lower Belt Basin along Cat Creek and further east. Though detrital zircon geochronology was done and provided evidence for a southern provenance and potential link to the Prichard Formation in the Western Belt Basin, further work needs to be done from other units with the Newland Formation to further connect the southern boundary and possible southern and eastern provenances to the Newland Formation. Elemental composition and isotopic signatures from detrital zircons within the Newland and other lower belt Formations would provide critical data regarding the composition of the source rocks from which the zircons crystalized, placing further restraints on the multiple 2.55 sources within the Wyoming craton.

REFERENCES CITED

Adam, Zachary Robert. 2014. “MICROFOSSIL PALEONTOLOGY AND BIOSTRATIGRAPHY OF THE EARLY MESOPROTEROZOIC BELT SUPERGROUP, MONTANA.” Montana State University.

Ambrose, Rachele B. 2005. “A Petrrologic Study of Hte Chamberlain Carbonate, the Newland Limestone, the Helena Formation,and the Wallace Formation of Hte Middle Proterozoic Belt Supergroup, Montana.”

Anderson, Colter, Cody Bodman, Julian Stahl, and Nicholas Fox. 2015. “Shifting Depo-Centers and Structural Compartmentalization of the Mesoproterozoic Belt-Purcell Supergroup, Western Montana.” *Montana State University Earth Sciences Colloquium*, no. 1986: 2015.

Boggs, Sam Jr. 2012. *Principles of Sedimentology and Stratigraphy*. Edited by Crissy Dudonis and Michelle White. 5th ed. Upper Saddle River: Pearson Prentice Hall.

Chandler, F.W. 2000. “The Belt-Purcell Basin as a Low-Latitude Passive Rift; Implications for the Geological Environment of Sullivan Type Deposits.” http://geoscienceworld.org/georef/2004-052653.

Condie, Kent C., Elena Belousova, W. L. Griffin, and Keith N. Sircombe. 2009. “Granitoid Events in Space and Time: Constraints from Igneous and Detrital Zircon Age Spectra.” *Gondwana Research* 15 (3–4): 228–42. doi:10.1016/j.gr.2008.06.001.

Dalrymple, robert. 2010. *Facies Models 4*. Edited by Noel James and Robert Dalrymple. Fourth edi. Geological Association of Canada, St. John’s Newfoundland, fourth edition. GEOtext 6.

Duke, Edward F., and Reed S. Lewis. 2010. “Near Infrared Spectra of White Mica in the Belt Supergroup and Implications for Metamorphism.” *American Mineralogist* 95 (7): 908–20. doi:10.2138/am.2010.3281.

Eberl, D. D. and Velde B. 1989. “Beyond the Kubler Index.” *Clay Minerals* 24 (4): 571–77. doi:10.1180/claymin.1989.024.4.01.

Eberl, Dennis, and John Hower. 1976. “Kinetics of Illite Formation.” *Bulletin of the Geological Society of America* 87 (9): 1326–30. doi:10.1130/0016-7606(1976)87<1326:KOIF>2.0.CO;2.

Evans, David A.D. 2013. “Reconstructing Pre-Pangean Supercontinents.” *Bulletin of the Geological Society of America* 125 (11–12): 1735–51. doi:10.1130/B30950.1.

Feedback, Derek. 1997. “Stratigraphy and Sedimentation of the Chamberlain Formation-Newland Formation Boundry, Lower Belt Supergroup (Middle Proterozoic), Central Montana.”

Foster, David A, Paul A Mueller, James J Vogl, Jennifer N. Gifford, and David W Mogk. 2014. “The Little Belt Arc of the Great Falls Orogen.” In *GSA Rocky Mountain (66th Annual) and Cordilleran (110th Annual) Joint Meeting*, Paper No. 9-6. Bozeman.

Fox, Nicholas. 2017. “Sedimentary Tectonics of the Mesoproterozoic Lahood Formation Southwest, Montana.”

Frank, Tracy D., and Timothy W. Lyons. 1998. “Molar-Tooth Structures: A Geochemical Perspective on a Proterozoic Enigma.” *Geology* 26 (8): 683–86. doi:10.1130/0091-7613(1998)026<0683:MTSAGP>2.3.CO;2.

Freed, R. L., and D.R. Peacor. 1989. “Variability in Temperature of the Smectite/Illite Reaction in Gulf Coast Sediments†.” *Clay Minerals* 24 (2): 171–80. doi:10.1180/claymin.1989.024.2.05.

Frost, B Ronald, Carol D Frost, Mary Cornia, Kevin R Chamberlain, and Robert Kirkwood. 2006. “The Teton – Wind River Domain: A 2.68–2.67 Ga Active Margin in the Western Wyoming Province.” *Canadian Journal of Earth Sciences* 43 (10): 1489–1510. doi:10.1139/e06-102.

Frost, C. 1998. “The Late Archean History of the Wyoming Province as Recorded by Granitic Magmatism in the Wind River Range, Wyoming.” *Precambrian Research* 89 (3–4): 145–73. doi:10.1016/S0301-9268(97)00082-X.

Frost, Carol D, and Don Winston. 1987. “Nd Isotope Systematics of Coarse- and Fine-Grained Sediments : Examples from the Middle Proterozoic Belt-Purcell Supergroup Author (S): C . D . Frost and Don Winston Source : The Journal of Geology , Vol . 95 , No . 3 (May , 1987), Pp . 309-327 Publis” 95 (3): 309–27.

Gifford, Jennifer N. (Montana State University). 2013. “PRECAMBRIAN CRUSTAL EVOLUTION IN THE GREAT FALLS TECTONIC ZONE.” University of Florida.

Gifford, Jennifer N., Paul A. Mueller, David A. Foster, and David W. Mogk. 2014. “Precambrian Crustal Evolution in the Great Falls Tectonic Zone: Insights from Xenoliths from the Montana Alkali Province.” *The Journal of Geology* 122 (5): 531–48. doi:10.1086/677262.

Godlewsk, D, and Gerald A. Zieg. 1984. “Stratigraphy and Depositional Setting of the Precambrian Newland Formation.” *Montana Bureau of Mines and Geology Special Publication 90* 90: 2–4.

González-Álvarez, Ignacio, Monika Agnieszka Kusiak, and Robert Kerrich. 2006. “A Trace Element and Chemical Th-U Total Pb Dating Study in the Lower Belt-Purcell Supergroup, Western North America: Provenance and Diagenetic Implications.” *Chemical Geology* 230 (1–2): 140–60. doi:10.1016/j.chemgeo.2005.12.004.

Goodge, J. W., J. D. Vervoort, C. M. Fanning, D. M. Brecke, G. L. Farmer, I. S. Williams, P. M. Myrow, and D. J. DePaolo. 2008. "A Positive Test of East Antarctica-Laurentia Juxtaposition Within the Rodinia Supercontinent." *Science* 321 (5886): 235–40. doi:10.1126/science.1159189.

GOSSELIN, DAVID C, JAMES J PAPIKE, ROBERT E ZARTMAN, ZELL E PETERMAN, and J C LAUL. 1988. "Archean Rocks of the Black Hills, South Dakota: Reworked Basement from the Southern Extension of the Trans-Hudson Orogen." *GSA Bulletin* 100 (8): 1244–59. http://dx.doi.org/10.1130/0016-7606(1988)100%3C1244:AROTBH%3E2.3.CO.

Graham, Garth, Murray W H Itzman, and Jerry Zieg. 2012. "Geologic Setting, Sedimentary Architecture, and Paragenesis of the Mesoproterozoic Sediment-Hosted Sheep Creek Cu-Co-Ag Deposit, Helena Embayment, Montana." *Economic Geology* 107 (6): 1115–41. doi:10.2113/econgeo.107.6.1115.

Guerrero, Juan Carlos, Paul Mueller, and David Mogk. 2016. "Provenance Study and Geochemical Analysis of the LaHood Formation of the Bridger Range." *Geological Society of America, Abstracts with Programs* 47 (6): 41.

Hall, Susan M., and Ján Veizer. 1996. "Geochemistry of Precambrian Carbonates: VII. Belt Supergroup, Montana and Idaho, USA." *Geochimica et Cosmochimica Acta* 60 (4): 667–77. doi:10.1016/0016-7037(95)00424-6.

Halpin, Jacqueline A., Torsten Jensen, Peter McGoldrick, Sebastien Meffre, Ron F. Berry, John L. Everard, Clive R. Calver, Jay Thompson, Karsten Goemann, and Joanne M. Whittaker. 2014. "Authigenic Monazite and Detrital Zircon Dating from the Proterozoic Rocky Cape Group, Tasmania: Links to the Belt-Purcell Supergroup, North America." *Precambrian Research* 250. Elsevier B.V.: 50–67. doi:10.1016/j.precamres.2014.05.025.

Harrison, Jack E., Allan B. Griggs, and John D. Wells. 1974. "Tectonic Features of the Precambrian Belt Basin and Their Influence on Post-Belt Structures." *Geological Survey Professional Paper* 866.

Harrison, Jack E., and D.A. Jobin. 1963. "Geology of the Clark Fork Quadrangle, Idaho-Montana." *Geological Survey Bulletin* 1141. http://pubs.usgs.gov/bul/1141k/plate-1.pdf%5Cnhttp://pubs.er.usgs.gov/thumbnails/usgs_thumb.jpg%5Cnhttp://ngmdb.usgs.gov/Prodesc/proddesc_20869.htm%5Cnhttp://pubs.usgs.gov/bul/1141k/plate-2.pdf%5Cnhttp://pubs.usgs.gov/bul/1141k/report.pdf.

Hildebrand, Robert S, and Planetary Sciences. 2013. "Dimemberment and Northward Migration of the Cordilleran Orogen: Baja_BC Resolved." *GSA Today* 25 (11): 4–11. doi:10.1130/GSATG255A.1.Figure.

Hillier, S. 1993. “Origin, Diagenesis and Minerolgoy of Chlorite Minerals in Devonian Lacustriane Mudrocks, Orcadian Basin , Scottland.” *Clays and Clay Minerals* 41 (2): 240–59.

Himes, M. D, and Peterson E.U. 1990. “Geological and Mineralogical Characteristics of Hte Sheep Creek Copper-Cobalt Sediment Hosted Stratabound Sulfied Deposits, Meagher County, Montana.”

Karlstrom, Karl E., Stephen S. Harlan, Michael L. Williams, James McLelland, John W. Geissman, and Karl Inge Åhäll. 1999. “Refining Rodinia: Geologic Evidence for the Australia-Western U.S. Connection in the Proterozoic.” *GSA Today* 9 (10): 2–7.

Lageson, David R., James G. Schmitt, Brian K. Horton, Thomas J. Kalakay, and Bradford R. Burton. 2002. “Influence of Late Cetaceous Magmatism on the Sevier Orogenic Wedge, Western Montana.” *Geology* 29 (8): 723–26. doi:10.1130/0091-7613(2001)029<0723:IOLCMO>2.0.CO;2.

Lindesy. 1980. “Reconnaissance Geologic Map of the Big Snowy Wilderness and Contiguous Rare II Study Areas, Fergus, Golden Valley, and Wheatland Counties, Montana.” *U.S. Geological Survey*.

Lydon, J. 2005. “Synopsis of the Belt-Purcell Basin.” *Geological Survey of Canada, Open File Xxx*. http://scholar.google.com/scholar?hl=en&btnG=Search&q=intitle:SYNOPSIS+OF+THE+BELT-PURCELL+BASIN#1.

Maxwell, Dwight T., and John Hower. 1967. “High-Grade Diagenesis and Low-Grade Metamor-Phism of Illite in the Precambrian Belt Series.” *The American Mineralogist* 52 (1955): 843–57.

McDonough, W.F., and S. -s. Sun. 1995. “The Composition of the Earth.” *Chemical Geology* 120: 223–53.

McMannis, William J. 1963. “LaHood Formation—A Coarse Fades of the Belt Series in Southwestern Montana.” *Geological Society of America Bulletin* 74 (4): 407–36. doi:10.1130/0016-7606(1963)74.

Miall, A.D. 2010. *Facies Models 4*. Edited by N.P. James and Dalrymple R.W. Geological Association of Canada, St. John’s Newfoundland, fourth edition. GEOtext 6.

Mogk, D. W., P. A. Mueller, J. L. Wooden, and D. R. Bowes. 1992. “The Northern Wyoming Province: Contrasts in Archean Crustal Evolution.” *International Basement Tectonics Association Publication No. 8*, no. 8: 283–97. http://scholar.google.com/scholar?hl=en&btnG=Search&q=intitle:The+northern+Wyoming+Province:+contrasts+in+Archean+crustal+evolution#8.

Mogk, David, Paul Mueller, and Joseph Wooden. 1988. *Archean Tectonics of the North Snowy Block, Beartooth Mountains, Montana*. *Journal of Geology*. Vol. 96. doi:10.1086/629205.

Moore, D M, and R C Reynolds. 1989. *X-Ray Diffraction and the Identification and Analysis of Clay Minerals*. Oxford University Press.

Moore, Duane M, and Robert C Reynolds. 1997. "X-Ray Diffraction and the Identification and Analysis of Clay Minerals,." *Oxford University Press, Oxford, New York*, 373.

Mueller, P.A., H.R. Burger, J.L. Wooden, A.L. Heatherington, D.W. Mogk, and K. D'Arcy. 2004. "Age and Evolution of the Precambrian Crust of the Tobacco Root Mountains, Montana." *Precambrian Geology of the Tobacco Root Mountains, Montana*, 181. doi:10.1130/0-8137-2377-9.181.

Mueller, Paul A., Ann L. Heatherington, Dawn M. Kelly, Joseph L. Wooden, and David W. Mogk. 2002. "Paleoproterozoic Crust within the Great Falls Tectonic Zone: Implications for the Assembly of Southern Laurentia." *Geology* 30 (2): 127–30. doi:10.1130/0091-7613(2002)030<0127:PCWTGF>2.0.CO;2.

Nelson, W John. 1993. "Cat Creek Anticline : Tectonic History and Petroleum." *Montana Geological Society Energy and Mineral Resources of Central Montana*, 105–14.

Nilson, Tor and Arthur, Sylvester. 1995. *Tectonics of Sedimentary Basins*. Edited by Cathy Busby and Raymond Ingersoll. Blackwell Science, 425-56 Ltd.

O'Neill, J. Michael, and David A. Lopez. 1985. "Character and Regional Significance of Great Falls Tectonic Zone, East-Central Idaho and West-Central Montana." *American Association of Petroleum Geologists Bulletin* 69 (3): 437–47. doi:10.1306/AD462506-16F7-11D7-8645000102C1865D.

Patchett, P.J., G. Bylund, and B.G.J. Upton. 1978. "Palaeomagnetism and the Grenville Orogeny: New Rb-Sr Ages from Dolerites in Canada and Greenland." *Earth and Planetary Science Letters* 40 (3). Elsevier: 349–64. doi:10.1016/0012-821X(78)90159-0.

Poppe, L, V Paskevich, and J Hathaway. 2001. "A Laboratory Manual for X-Ray Powder Diffraction." *U.S. Geological Survey Open File Report*. https://pubs.usgs.gov/of/2001/of01-041/index.htm.

Price, R. A. 1964. "The Precambrain Purcell System in The Rocky Mountains of Southern Alberta and British Columbia." *Bulletin of the Canadian Petroleum Geology* 12 (August): 399–426.

Reeves, Frank. 1931. “GEOLOGY OF THE BIG SNOWY MOUNTAINS M0NTANA.” *United States Departmetn of Interior, Geological Survey,*.

Ross, Gerald M., Randall R. Parrish, and Don Winston. 1992. “Provenance and UPb Geochronology of the Mesoproterozoic Belt Supergroup (Northwestern United States): Implications for Age of Deposition and Pre-Panthalassa Plate Reconstructions.” *Earth and Planetary Science Letters* 113 (1–2): 57–76. doi:10.1016/0012-821X(92)90211-D.

Ross, Gerald M., and Mike Villeneuve. 2003. “Provenance of the Mesoproterozoic (1.45 Ga) Belt Basin (Western North America): Another Piece in the Pre-Rodinia Paleogeographic Puzzle.” *Bulletin of the Geological Society of America* 115 (10): 1191–1217. doi:10.1130/B25209.1.

Ryan, Peter. 1991. “Structural Variations in Illite and Chlorite in the Belt Supergroup Western Montana and Northern Idaho.”

Schieber, Jürgen. 1989. “Facies and Origin of Shales from the Mid-Proterozoic Newland Formation, Belt Basin Montana.” *Sedimentology* 36: 203–19.

Schieber, Jürgen. 1990. “Distribution of REE in the Eastern Belt Supergroup (Montana, U.S.A.): Implications for Stratigraphic Correlations and Basin Evolution.” *Chemical Geology* 81 (1–2): 83–98. doi:10.1016/0009-2541(90)90040-E.

Schieber, Jürgen. 1992. “A Combined Petrographical—geochemical Provenance Study of the Newland Formation, Mid-Proterozoic of Montana.” *Geological Magazine* 129 (2): 223. doi:10.1017/S0016756800008293.

Schieber, Jürgen. 1998. “Possible Indicators of Microbial Mat Deposits in Shales and Sandstones: Examples from the Mid-Proterozoic Belt Supergroup, Montana, USA.” *Sedimentary Geology* 120 (1–4): 105–24. doi:10.1016/S0037-0738(98)00029-3.

Schieber, Jürgen, and Brooks B Ellwood. 1993. “Determination of Basinwide Paleocurrent Patterns in a Shale Succession from Anisotropy of Magnetic Susceptibility (AMS); a Case Study of the Mid-Proterozoic Newland Formation, Montana.” *Journal of Sedimentary Research* 63 (5): 874–80. doi:10.1306/d4267c30-2b26-11d7-8648000102c1865d.

Schieber, Jürgen Juergen. 1986. “Stratigraphic Control of Rare-Earth Pattern Types in Mid-Proterozoic Sediments of the Belt Supergroup, Montana, U.S.A.: Implications for Basin Analysis.” *Chemical Geology* 54 (1–2). Elsevier: 135–48. doi:10.1016/0009-2541(86)90077-X.

Sears, J. W., and R. A. Price. 2000. “New Look at the Siberian Connection: No SWEAT.” *Geology* 28 (5): 423–26. doi:10.1130/0091-7613(2000)28<423:NLATSC>2.0.CO;2.

Sears, James W. 2007. “Belt-Purcell Basin : Keystone of the Rocky Mountain Fold-and-Thrust Belt , United States and Canada.” *Geological Society of America Special Paper* 433 (7): 147–66. doi:10.1130/2007.2433(07).

Sims, P.K., J.M. O’Neill, V. Bankey, and E. Anderson. 2004. “Precambrian Basement Geologic Map of Montana - an Interpretation of Aeromagnetic Anomalies.” *Scientific Investigations Map* 2829: 80225.

Taylor, S.R., and S.M. McLennan. 1985. *The Continental Crust: Its Composition and Evolution*. Blackwell Scientific, Oxford.

Velde, B., T. Suzuki, and E. Nicot. 1986. “Pressure-Temperature-Composition of Illite/Smectite Mixed-Layer Minerals: Niger Delta Mudstones and Other Examples.” *Clays and Clay Minerals* 34 (4): 435–41. doi:10.1346/CCMN.1986.0340410.

Vuke, S. M., K.W. Porter, J.D. Lonn, and D.A. Lopez. 2009. “Geologic Map of Montana Field Notebook: Montana Bureau of Mines and Geology Geologic Map 62-E.”

Walcott, Charles D. 1899. “Pre-Cambrian Fossiliferous Formations.” *Bulletin of the Geological Society of America* 10: 199–244.

Walcott, Charles D. 1916. “Cambrian Geology and Palentology.” *Smithsonian Micellaneous Collections* 64 (5): 100–130 and 273.

Warren, Shepard. 1987. “Geology and Economis Potential of Montana Aulocogen.” *AAPG Bulletin*.

Weed, Walter Harvey, and Louis Valentine Pirsson. 1896. “Geology of the Castle Mountain Mining District, Montana.” *Bulletin of the United States Geological Survey*, no. 139: 163.

Winston, Don. 1986a. “Sedimentation and Tectonics of the Middle Proterozoic Belt Basin and Their Influence on Phanerozoic Compression and Extension in Western Montana and Northern Idaho.” *AAPG Memoir* 41: 87–118.

Winston, Don 1986b. “Sedimentology and Tectonics of the Middle Proterozoic Belt Basin and Their Influance on Phanerozoic Coompression and Extention in Western Montana and Northern Idaho.” *Belt Symposium*.

Winston, Don, Robert J Horodyski, and James W. Whipple. 1989. *Middle Proterozoic Belt Supergroup, Western Montana: Field Trip Guidebook T334*. 28th Inter. American Geophyscial Union.

Wu, Jonathan E., Ken McClay, Paul Whitehouse, and Tim Dooley. 2009. “4D Analogue Modelling of Transtensional Pull-Apart Basins.” *Marine and Petroleum Geology* 26 (8). Elsevier Ltd: 1608–23. doi:10.1016/j.marpetgeo.2008.06.007.

Zartman, Robert E., and John. C. Reed. 1998. “Zircon Geochronology of the Webb Canyon Gneiss and the Mount Owen Quartz Monzonite, Teton Range, Wyoming: Signigicance to Dating Late Archean Metamorphism in the Wyoming Craton.” *The Mountain Geologist* 35 (2): 71–77.

Zieg, Gerald A. 1981. “Stratigraphy, Sedimentology, and Diagenesis of the Precambrian Upper Newland Limestone, Central Montana.”

Zieg, Jerry, Vince Scartozzi, Nathan Chutas, Doyl Albers, Kevin Gostomski, and Jennifer Jones. 2013. “Zieg Black Butte Copper Deposit.pdf.” *The Journal of the Tobacco Root Geological Society*.

APPENDICES

APPENDIX A:

GRAPHIC LOGS

Stratigraphic sections created in SedLog are provided in this supplemental file: Anderson_AppendixC.pdf.

1. Swimming Woman Canyon east
2. Swimming Woman Canyon Lower
3. Swimming Woman Canyon west
4. Checkerboard
5. Sc12-112 (core log)

APPENDIX B:

BULK MINERALOGY

The following Xrd graphs were taken from 3 to 73^{o}θ using a continuous scan of 1 degree/minute, a step size of 0.20^{o}, and a count time of 1.20 seconds. The Mineral identification for each sample can be found in Chapter 5 (Table X)

Checkerboard

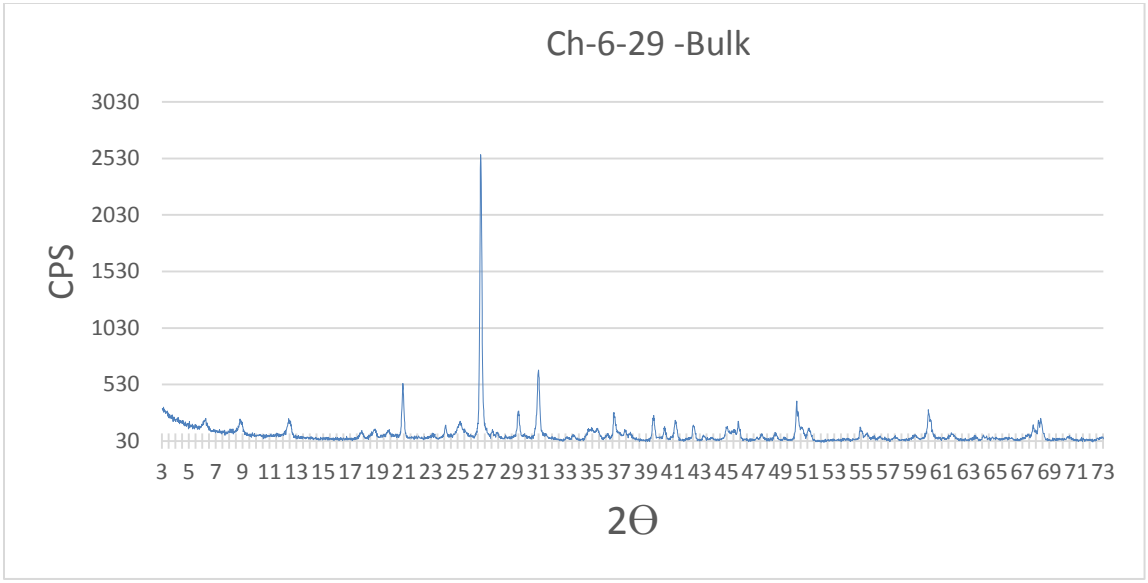


Figure 47. Xrd profile of Ch-6-29

1S-SW

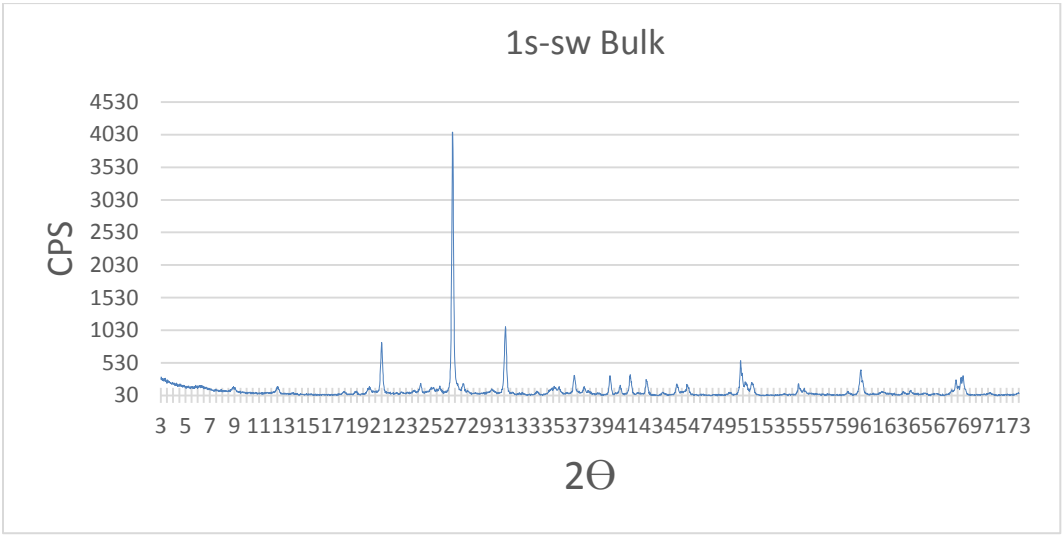


Figure 48. Xrd profile of 1S-SW

Belt Creek

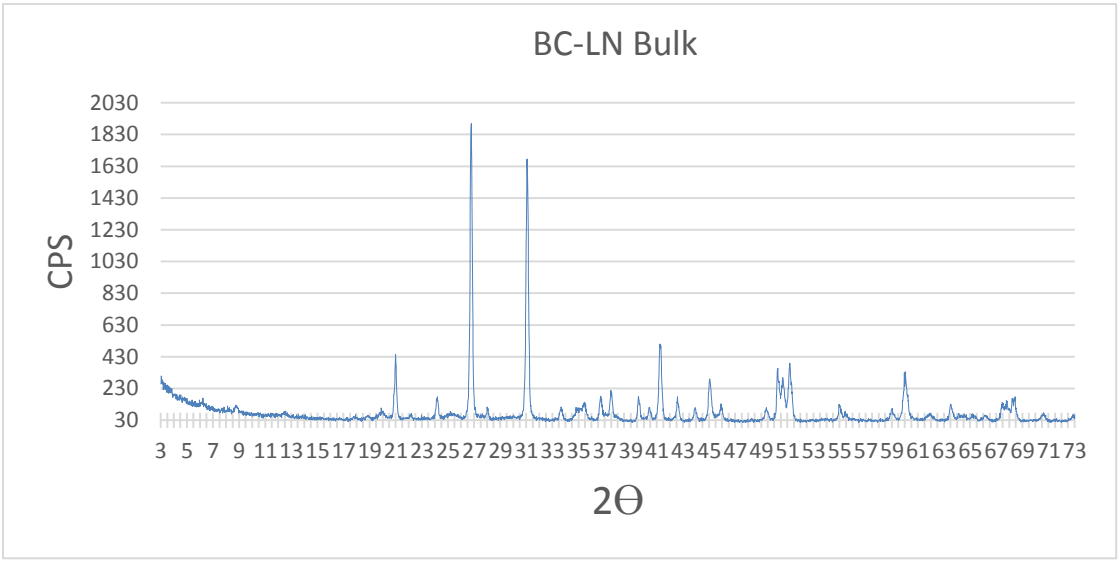


Figure 49. Xrd profile of Belt Creek

Deep Creek

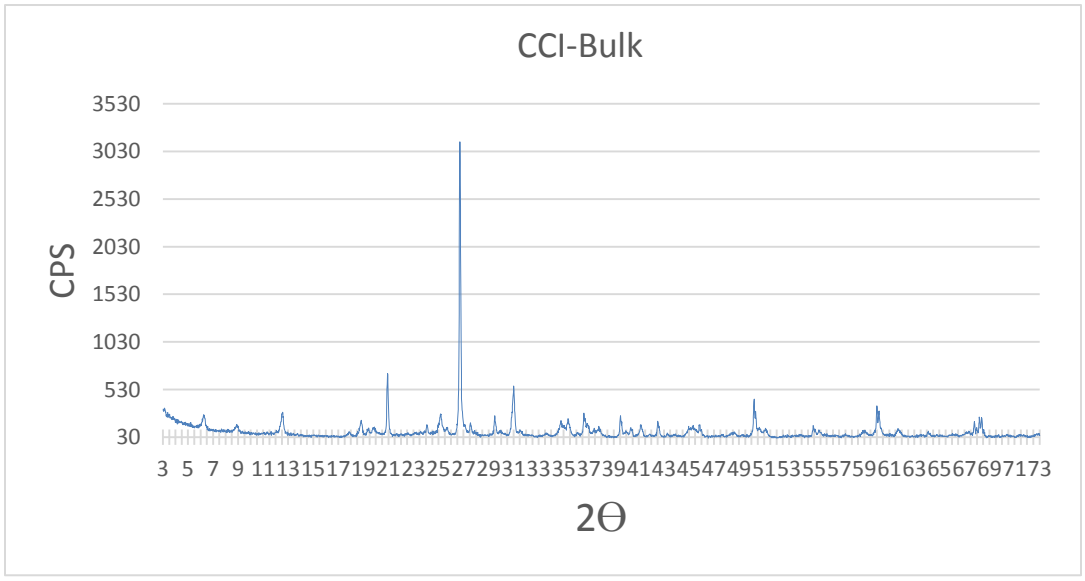


Figure 50. Xrd profile of Deep Creek

Deep Creek Unit 1

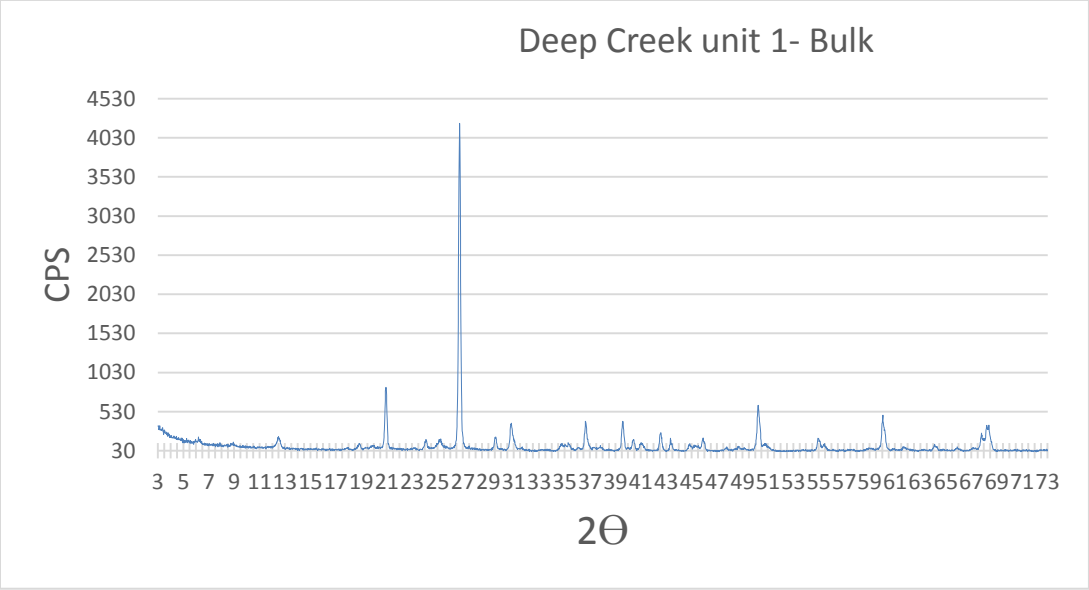


Figure 51. Xrd profile of Deep Creek Unit 1

EFSW

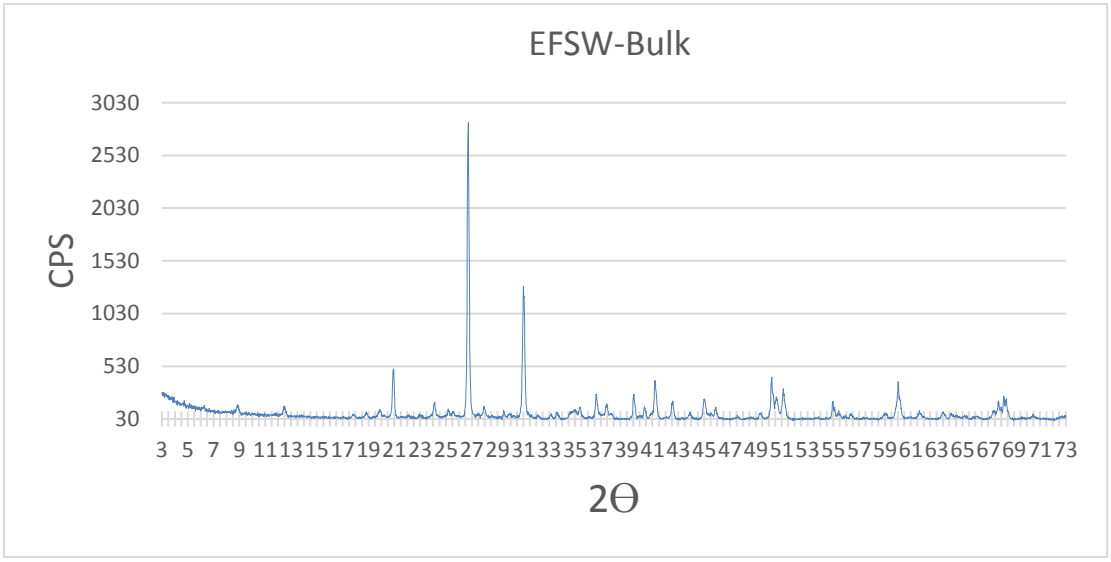


Figure 52. Xrd Profile of EFSW Swimming Woman Creek

Miller Gulch

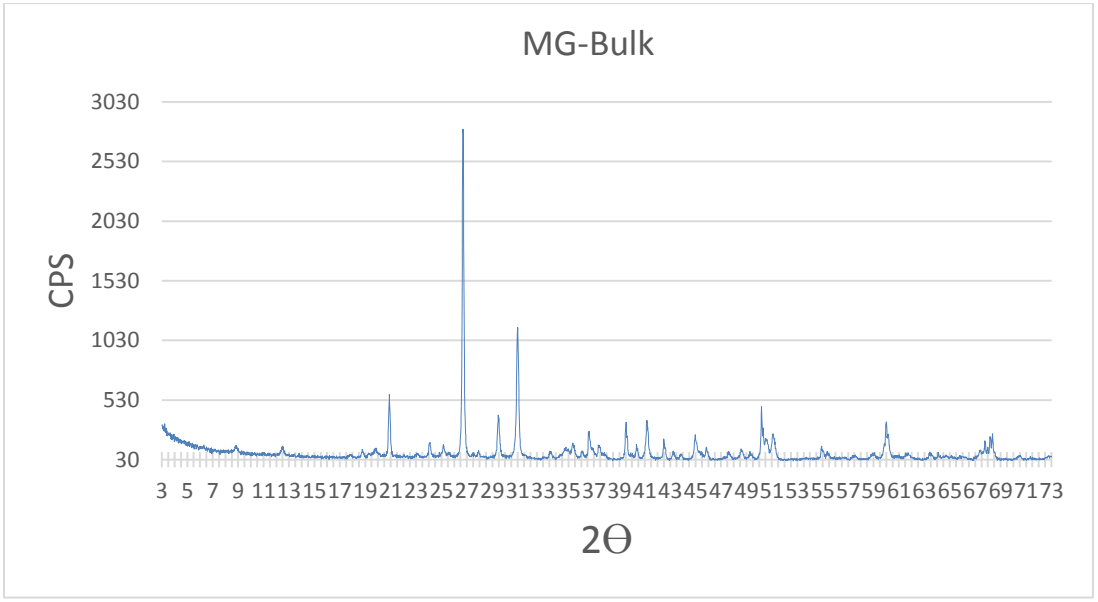


Figure 53. Xrd Profile of Miller Gulch

West Fork Swimming Woman Creek

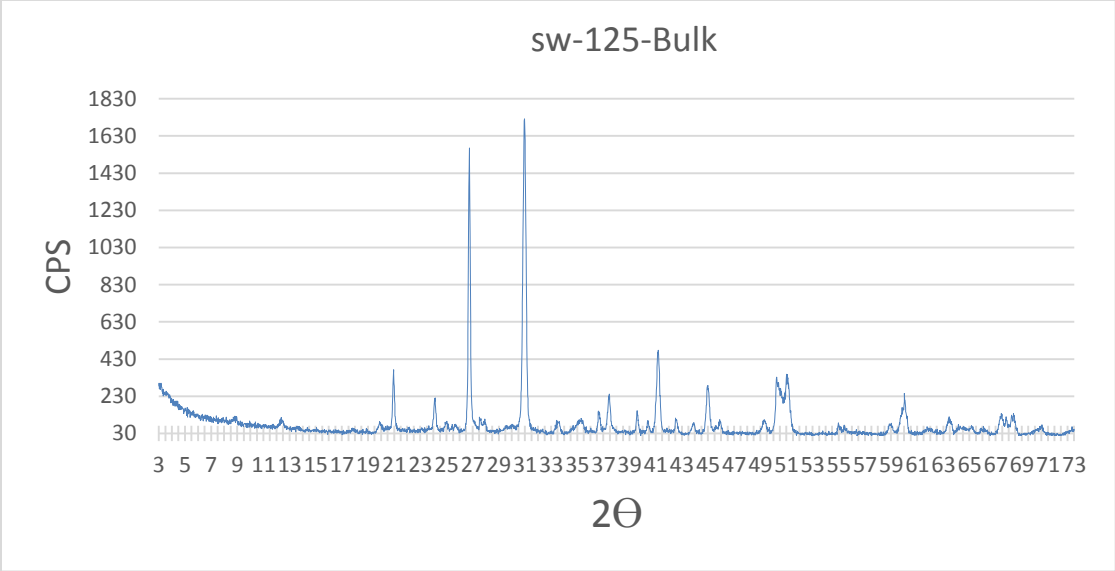


Figure 54. Xrd profile of Sw-125

APPENDIX C:

CLAY MINERALOGY

The following figures and tables show the clay mineralogy from 3-23$^{o}\theta$. Each graph has Air dried, Ethyl Glycol treated, heated to 400 ^{o}C, and heated to 550 ^{o}C. Samples were prepared using USGS standard procedures which can be found at the following link https://pubs.usgs.gov/of/2001/of01-041/htmldocs/methods.htm. Using the USGS flow diagram which can be found at the following link (https://pubs.usgs.gov/of/2001/of01-041/htmldocs/images/flow.gif). The probable clay mineralogy for each sample was determined and is presented in the following tables below each graph. Further analysis of each sample was done to determine illite/smectite ratio and the presence of chlorite and corrensite as discussed in the Chapter 5 and is also presented below.

1S-SW

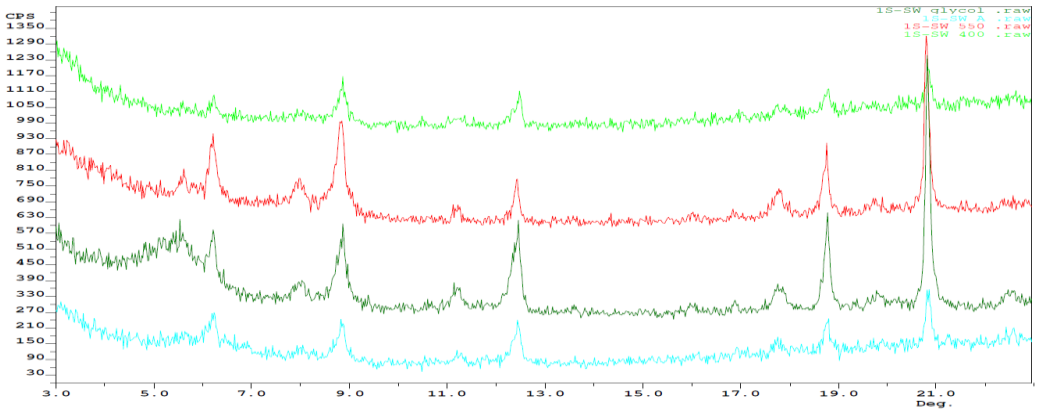


Figure 55. Clay mineralogy of 1s-sw from Swimming Woman Creek. Each sample was air dried (blue), treated with ethyl glycol (Dark Green), baked to 400 oC (Light Green) and baked to 550 oC (Red). Range is 3-23 degrees.

Air dried	Ethyl Glycol	Heated to 400°C	Heated to 550°C	060 peak (randomly oriented)	Mineralogy
14 Å	No change	No change	increase in intensity		Chlorite or Dioctahedral Chlorite
~10 Å	No change	No change	No change		Illite and or mica or Glauconite
~7 Å	No change	No change	Destroyed		Chlorite or Dioctahedral Chlorite
~5 Å	No change	No change	No change		
~4.2 Å	No change	No change	No change	Peak at 1.50	<2um SiO_2

Table 9. Clay Identification of 1S-SW

Checkerboard

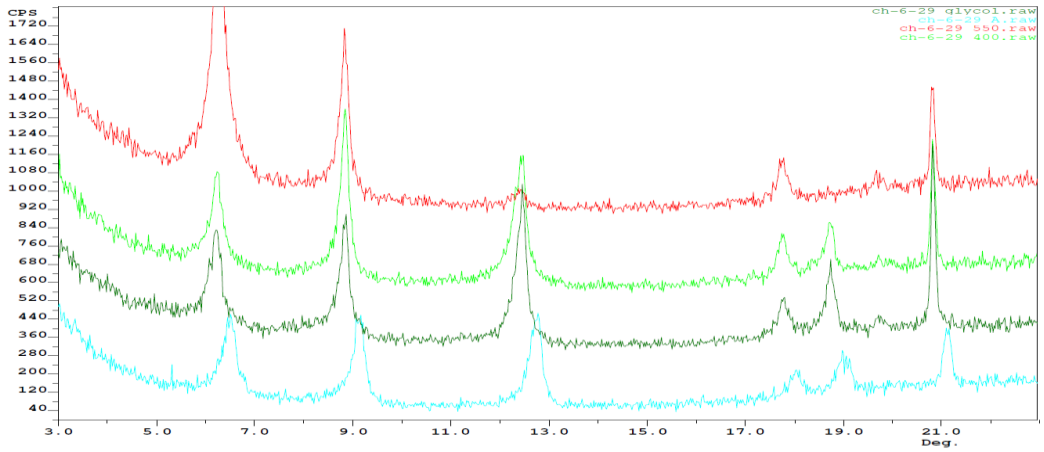


Figure 56. Clay mineralogy of ch-6-29 from checkerboard. Each sample was air dried (blue), treated with ethyl glycol (Dark Green), baked to 400 ^{o}C (Light Green) and baked to 550 ^{o}C (Red). Range is 3-23 degrees.

Air dried	**Ethyl Glycol**	**Heated to 400^{o}C**	**Heated to 550^{o}C**	**060 peak (randomly oriented)**	**Mineralogy**
10-14 Å	No change	No change	Slight increase in intensity		Randomly interstratified illite – chlorite
~10 Å	No change	No change	No change		Illite and or mica or Glauconite
~7 Å	No change	No change	Destroyed		Chlorite
~4.2 Å	No change	No change	No change	Peak at 1.50	<2um SiO_2

Table 10. Clay identification of Ch-6-29 from checkerboard outcrop

Deep Creek Unit 1

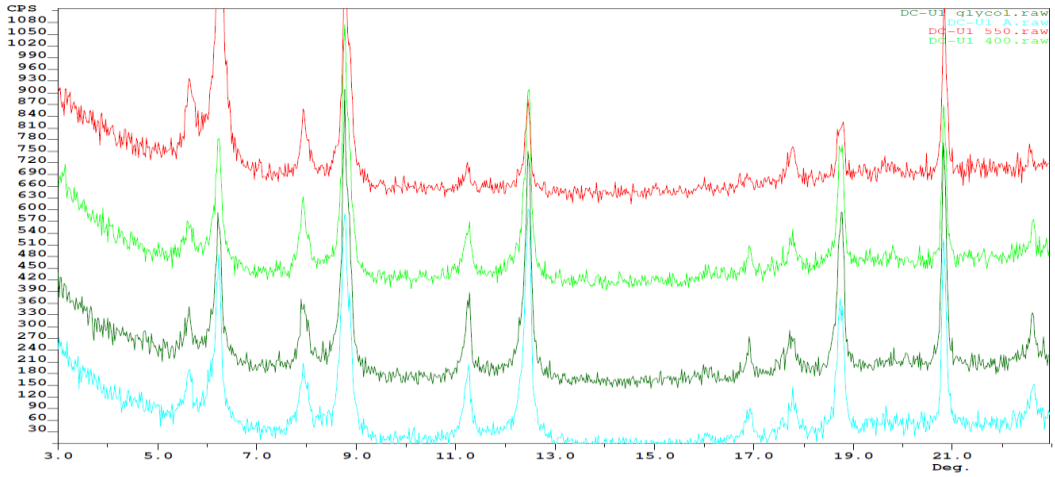


Figure 57. Clay mineralogy of DC-U1 from Deep Creek. Each sample was air dried (blue), treated with ethyl glycol (Dark Green), baked to 400 oC (Light Green) and baked to 550 oC (Red). Range is 3-23 degrees.

Air dried	Ethyl Glycol	Heated to 400°C	Heated to 550°C	060 peak (randomly oriented)	Mineralogy
10-14 Å	No change	No change	Slight increase in intensity		Randomly interstratified illite – chlorite
~10 Å	No change	No change	No change		Illite and or mica or Glauconite
~7 Å	No change	No change			Chrysotile or antigorite
~4.2 Å	No change	No change	No change	Peak at 1.50	<2um SiO_2

Table 11. Clay identification of Deep Creek Unit 1

East Fork Swimming Woman Creek

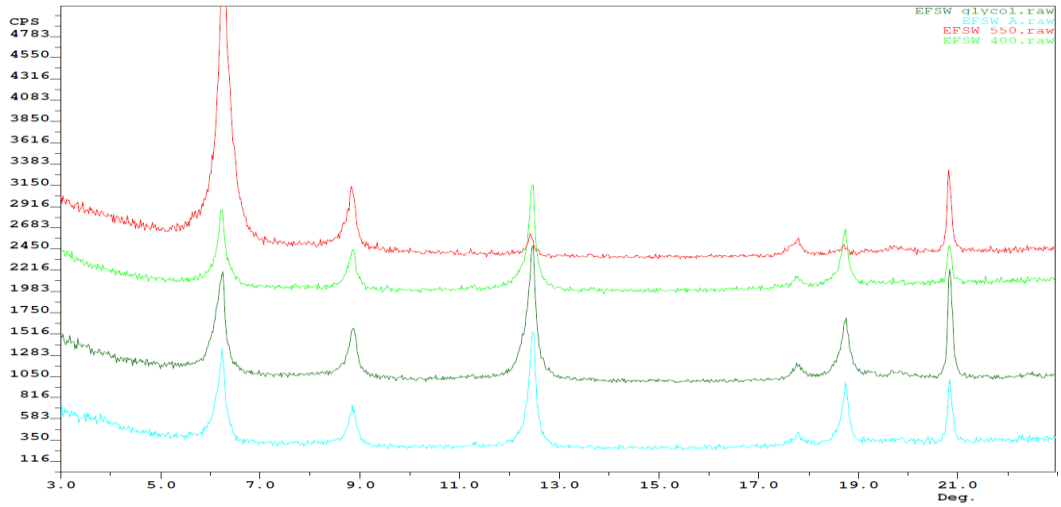


Figure 58. Clay mineralogy of EFSW from Swimming Woman Creek. Each sample was air dried (blue), treated with ethyl glycol (Dark Green), baked to 400 ^{o}C (Light Green) and baked to 550 ^{o}C (Red). Range is 3-23 degrees.

Air dried	Ethyl Glycol	Heated to 400^{o}C	Heated to 550^{o}C	060 peak (randomly oriented)	Mineralogy
14 Å	No change	No change	increase in intensity		Chlorite or Dioctahedral Chlorite
~10 Å	No change	No change	No change		Illite and or mica or Glauconite
~7 Å	No change	No change	Destroyed		Chlorite or Dioctahedral Chlorite
~4.2 Å	No change	No change	No change	Peak at 1.50	<2um SiO_2

Table 12. Clay identification of East Fork Swimming Woman Creek

Miller Gulch

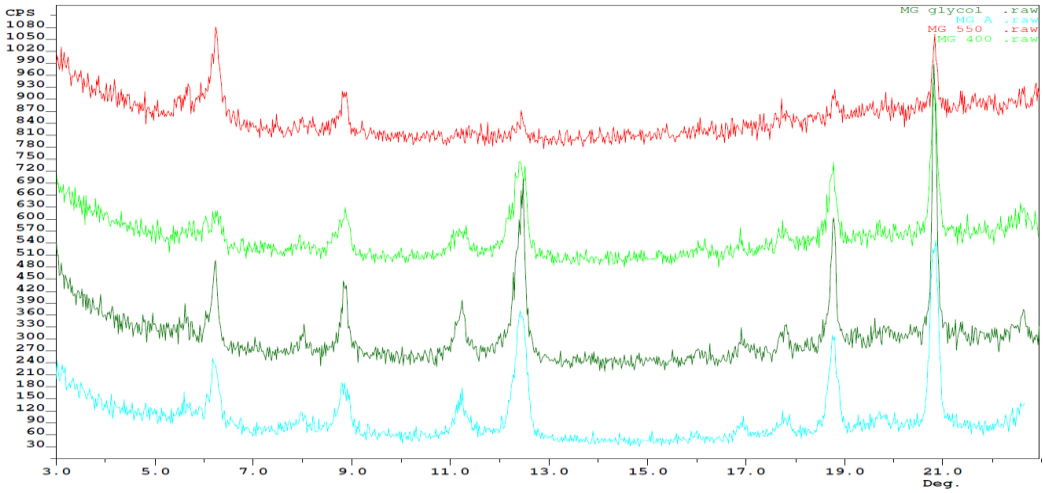


Figure 59. Clay mineralogy of Lower Newland form Miller gulch. Each sample was air dried (blue), treated with ethyl glycol (Dark Green), baked to 400 ^{o}C (Light Green) and baked to 550 ^{o}C (Red). Range is 3-23 degrees.

Air dried	**Ethyl Glycol**	**Heated to 400^{o}C**	**Heated to 550^{o}C**	**060 peak (randomly oriented)**	**Mineralogy**
14 Å	No change	No change	Increase intensity		Chlorite or Dioctahedral Chlorite
~10 Å	No change	No change	No change slight decrease in intensity		Illite and or mica or Glauconite
~7 Å	No change	No change	Destroyed		Chlorite or Dioctahedral Chlorite
~5 Å	No change	No change	Destroyed		
~4.2 Å	No change	No change	No change	Peak at 1.50	<2um SiO_2

Table 13. Clay identification of Miller Gulch

West Fork Swimming Woman Canyon

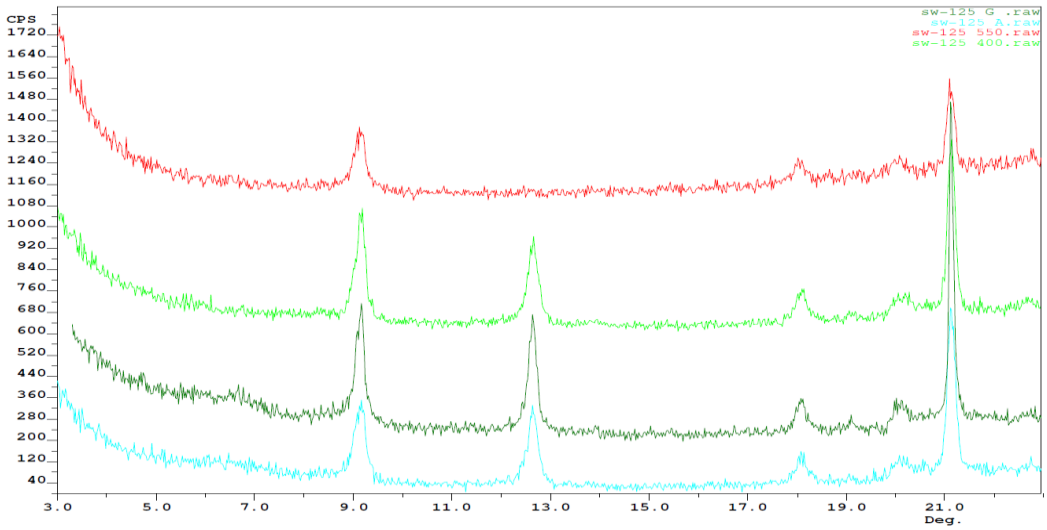


Figure 60. Clay mineralogy of the West Fork Swimming Woman Canyon

Air dried	Ethyl Glycol	Heated to 400°C	Heated to 550°C	060 peak (randomly oriented)	Mineralogy
14 Å	No change	No change	increase in intensity		Chlorite or Dioctahedral Chlorite
~10 Å	No change	No change	No change		Illite and or mica or Glauconite
~7 Å	No change	No change	Destroyed		Chlorite or Dioctahedral Chlorite
~5 Å	No change	No change	No change		
~4.2 Å	No change	No change	No change	Peak at 1.50	<2um SiO_2

Table 14. Clay identification of West Fork Swimming Woman Canyon

Belt Creek

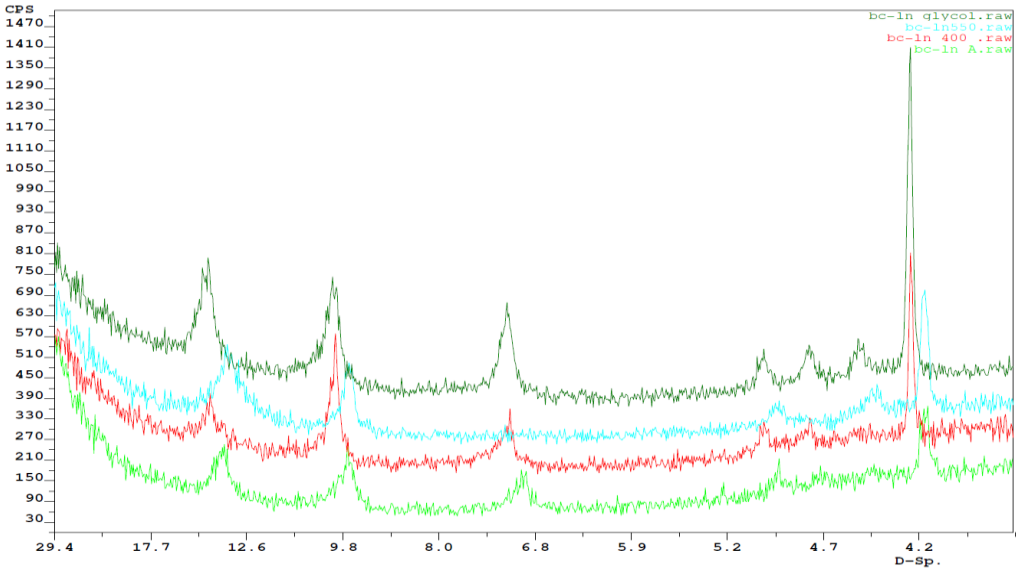


Figure 61. Clay mineralogy of Belt Creek Sample

Air dried	**Ethyl Glycol**	**Heated to 400°C**	**Heated to 550°C**	**060 peak (randomly oriented)**	**Mineralogy**
>10-14 Å	No change or slight increase in intensity	No change	Slight increase in intensity	Near 1.54 Å	Regularly interstratified illite-chlorite
~10 Å	Slight shift to larger D-Sp.	Slight sharpening of the peak	Peak does not collapse but is not a sharp as 400 °C	Variable	Interstratified illite-montmorillonite or illite-vermiculite
~7 Å	No change	No change	Destroyed	Peak near 1.54 Å	Chlorite
~4.2 Å	No change	No change	No change	Peak at 1.50	<2um SiO_2

Table 15. Clay Identification of Belt Creek

Deep Creek CC1

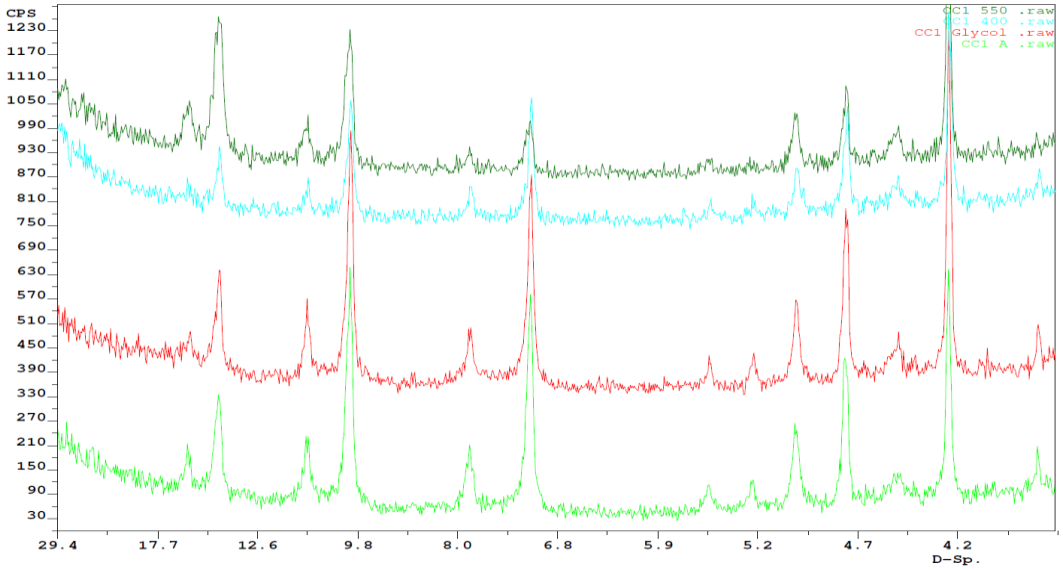


Figure 62. Clay mineralogy of CC1

Air dried	Ethyl Glycol	Heated to 400°C	Heated to 550°C	060 peak (randomly oriented)	Mineralogy
10-14 Å	No change	No change	Slight increase in intensity		Randomly interstratified illite – chlorite
~10 Å	No change	No change	No change		Illite and or mica or Glauconite
~7 Å	No change	No change	No change		Chrysotile or antigorite
~4.2 Å	No change	No change	No change	Peak at 1.50	<2um SiO_2

Table 16. Clay identification for Deep creek CC1

Ethyl Glycol Treatment

Based on the location of the 001/002 and 002/003 peaks of Illite the % illite/%smectite can be determined. Using Moore and Reynalds 1997 table of %Illite (Table 17) the following percentages of I/S were found for each sample, and the Ethyl Glycol treated graphs show the position of 001/002 and 002/003 peaks of illite.

% Illite	001/002 d(Å)	001/002 °2θ	002/003 d(Å)	002/003 °2θ	oΔ2θ
10	8.58	10.31	5.61	15.80	5.49
20	8.67	10.20	5.58	15.88	5.68
30	8.77	10.09	5.53	16.03	5.94
40	8.89	9.95	5.50	16.11	6.16
50	9.05	9.77	5.44	16.29	6.52
60	9.22	9.59	5.34	16.60	7.01
70	9.40	9.41	5.28	16.79	7.38
80	9.64	9.17	5.20	17.05	7.88
90	9.82	9.01	5.10	17.39	8.38

Table 17. Position of (CuKά) of Useful reflections for estimating percent Illite/smectite from (Moore and Reynalds 1997)

1S-SW

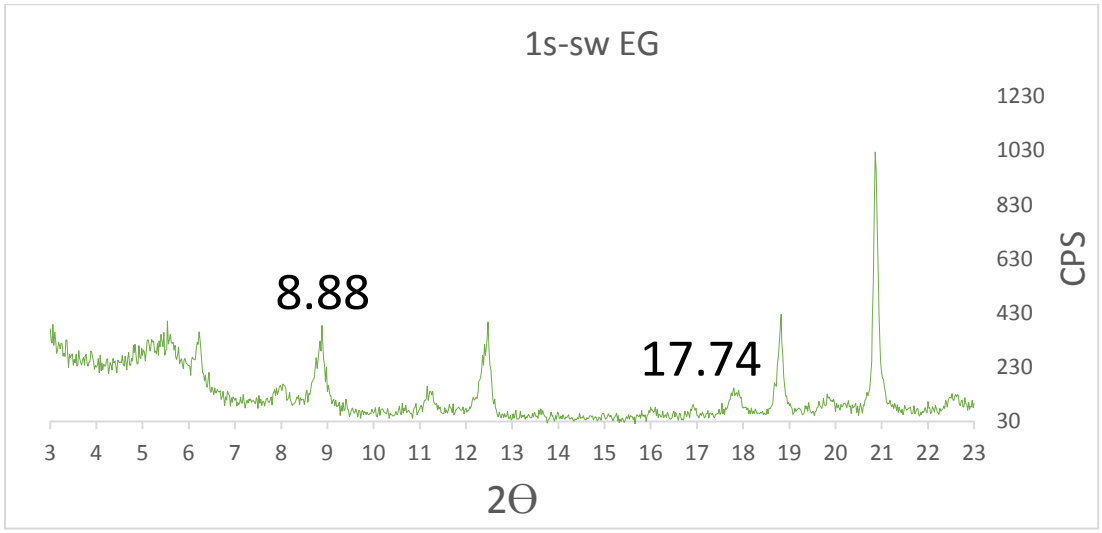


Figure 63. 1S-SW Ethyl Glycol treatment

Checkerboard

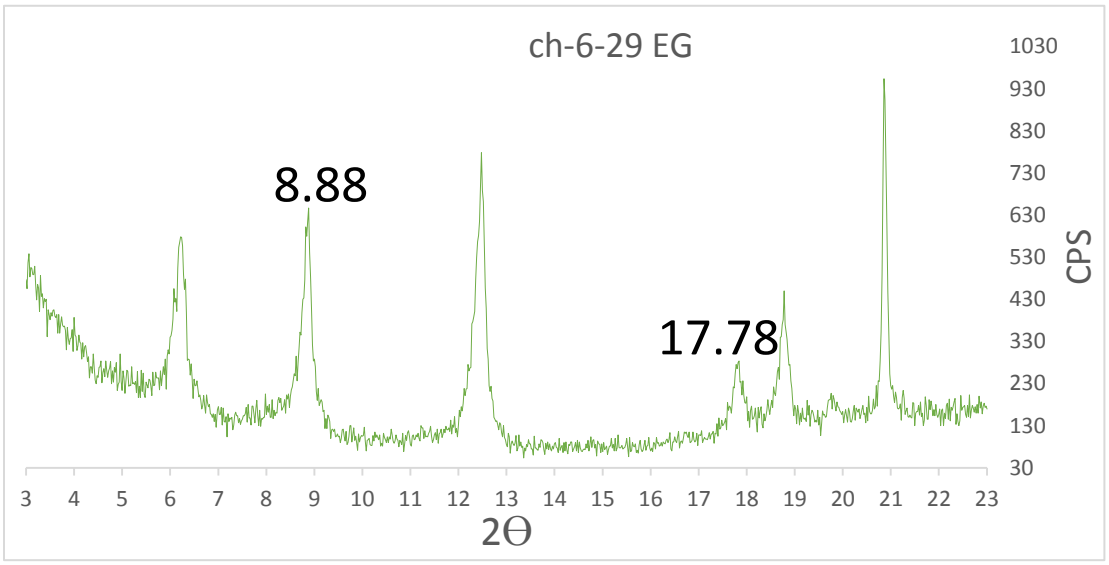


Figure 64. Ch-6-29 Ethyl Glycol treatment

Deep Creek Unit 1

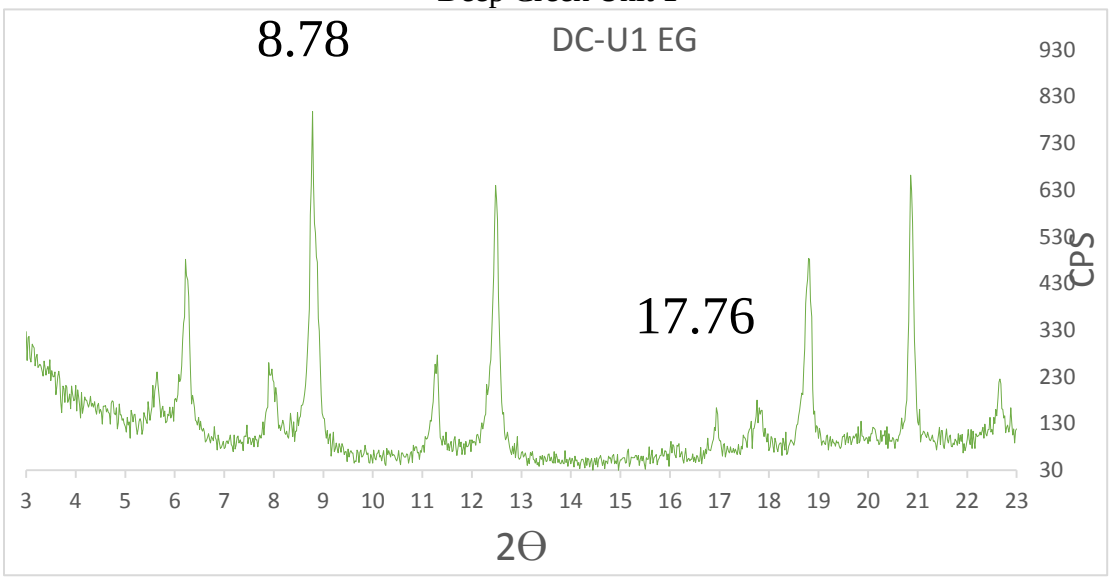


Figure 65. DC-U1 Ethyl Glycol treatment

East Fork Swimming Woman Creek

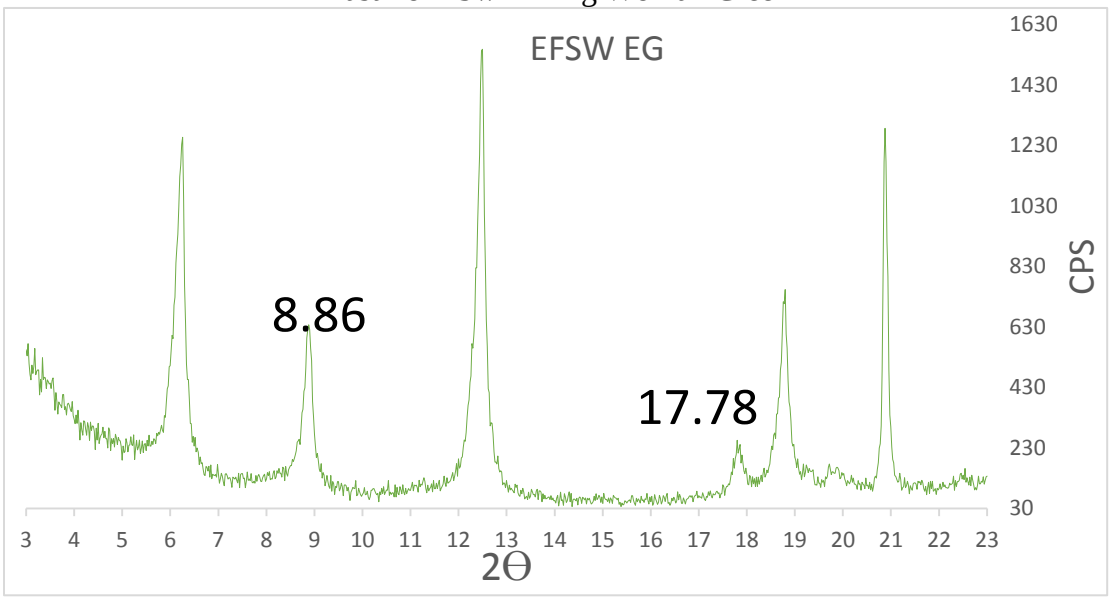


Figure 66. EFSW Ethyl Glycol treatment

Miller Gulch

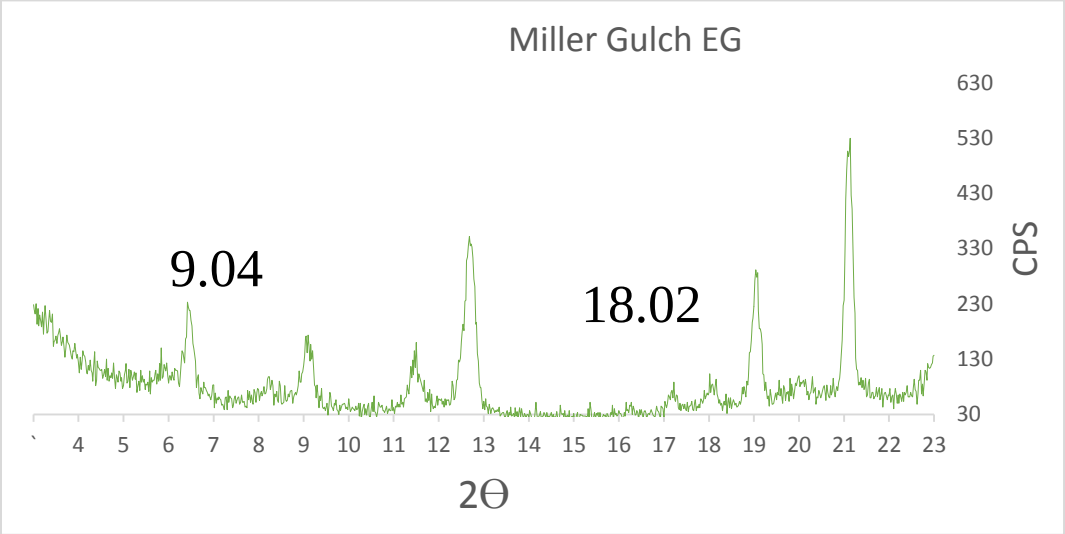


Figure 67. Miller Gulch Ethyl Glycol treatment

West Fork Swimming Woman Creek

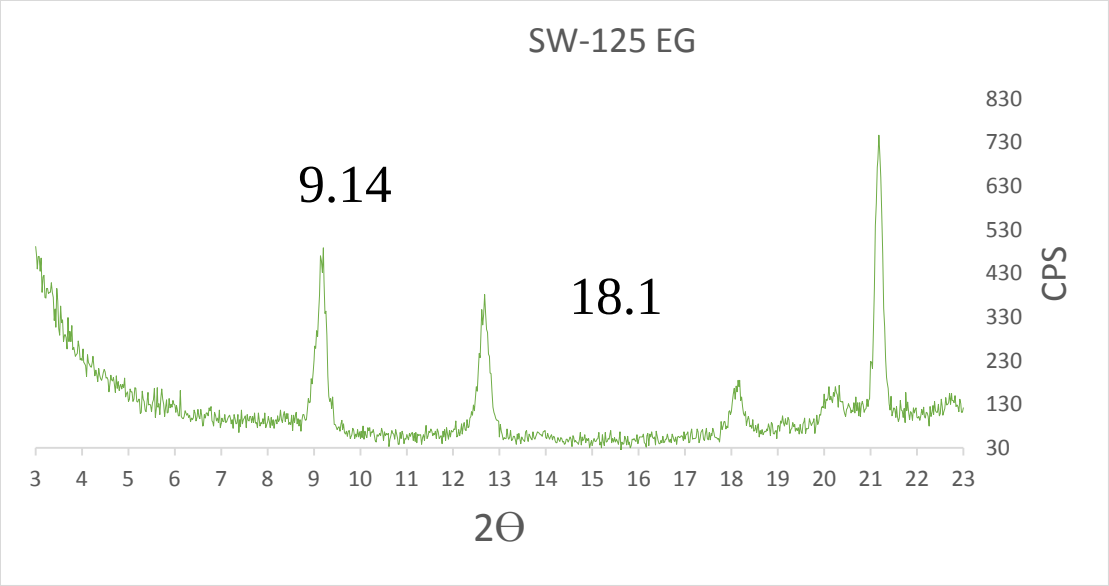


Figure 68. SW-125 Ethyl Glycol treatment

Belt Creek

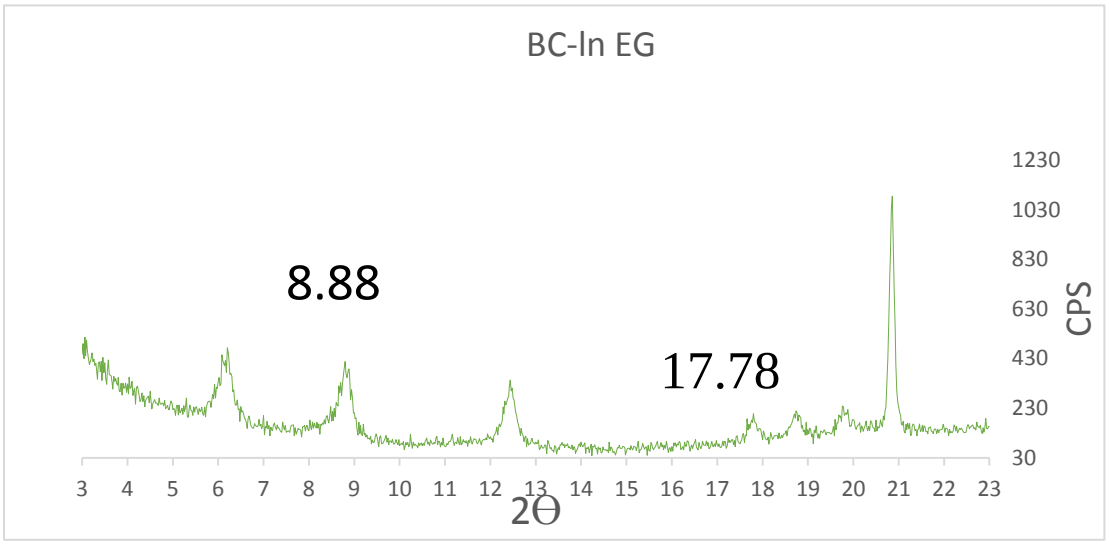


Figure 69. BC-ln Ethyl Glycol treatment

Deep Creek CC1

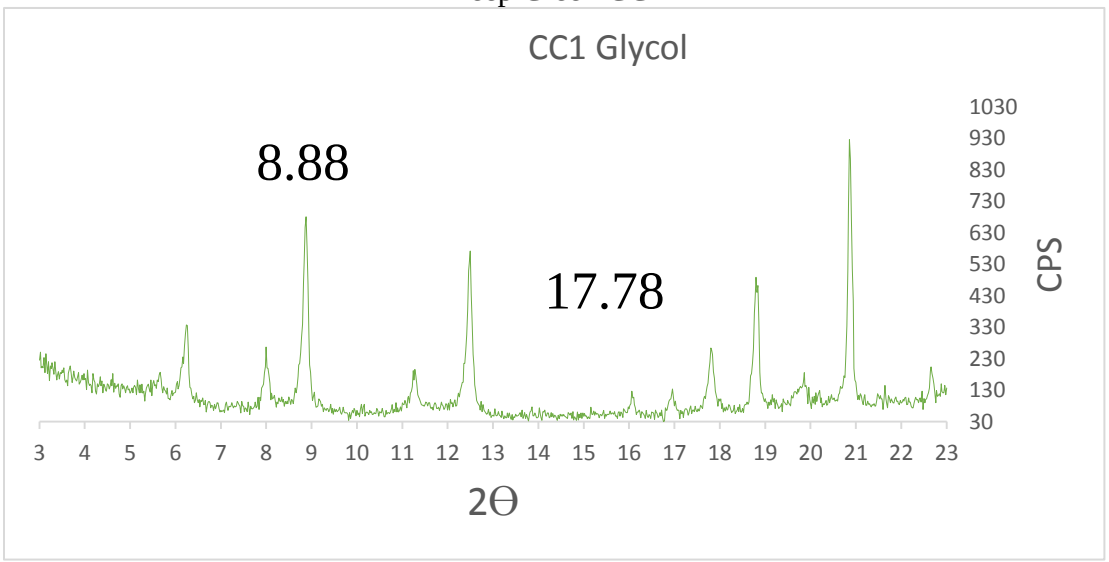


Figure 70. CC1 Ethyl Glycol treatment

Sample	001/002 °20	002/003 °20	% Illite	%Smectite
1S-SW	8.88	17.74	>90	<10
Checkerboard	8.88	17.78	>90	<10
DCU1	8.78	17.76	>90	<10
EFSW	8.84	17.78	>90	<10
Miller Gulch	9.04	18.02	>90	<10
WFSW	9.14	18.1	>90	<10
Belt Creek	8.88	17.78	>90	<10
DC CC1	8.88	17.78	>90	<10

Table 18. Percent illite found in each sample